INAUGURAL-DISSERTATION

zur
Erlangung der Doktorwürde
der
Naturwissenschaftlich-Mathematischen Gesamtfakultät
der
Ruprecht-Karls-Universität Heidelberg

vorgelegt von

Dipl.-Phys. Thomas J. Rivinius

aus Mannheim

Tag der mündlichen Prüfung: 2. Dezember 1998

Nature and Activity of the Be Star μCentauri

Gutachter:

Herr Prof. Dr. Bernhard Wolf
Herr Prof. Dr. Peter Ulmschneider

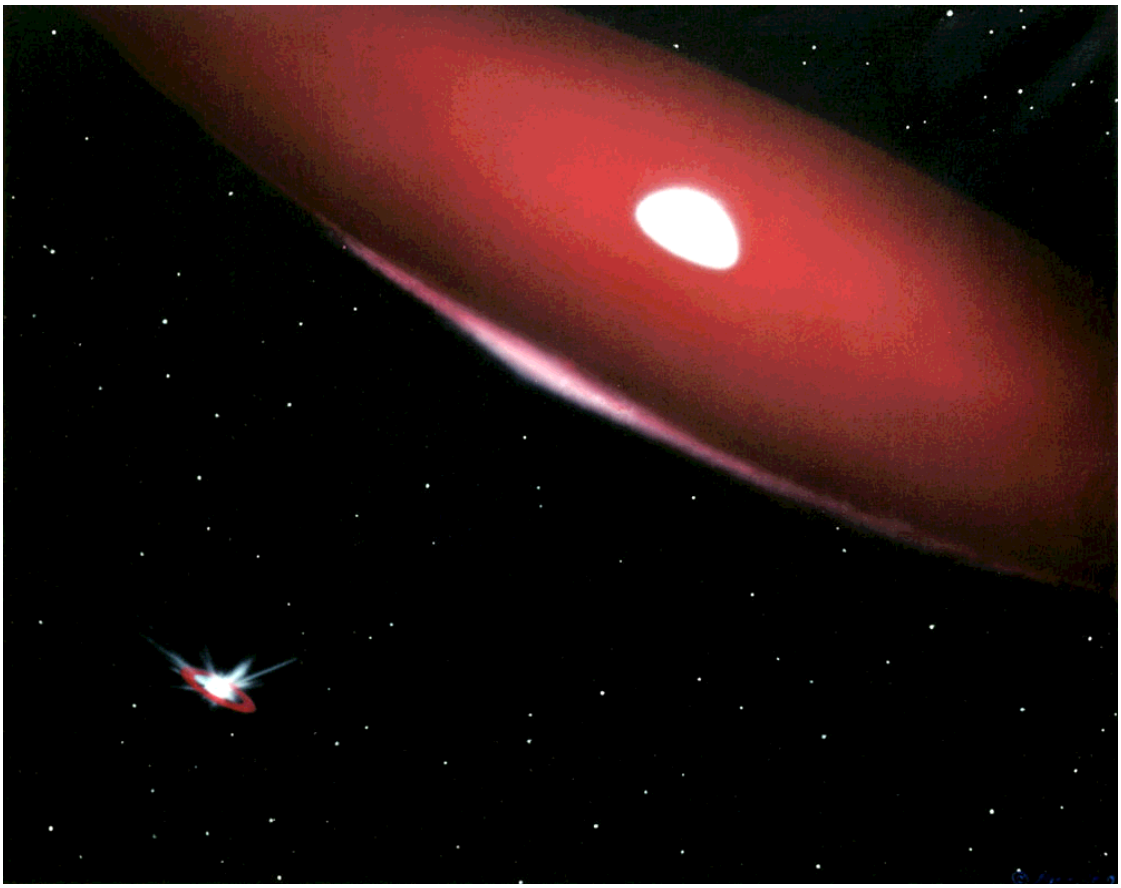

“It was hoped that the analysis of this simple spectrum would assist in the study of more complicated cases” (Curtiss, 1916, on the Be star γ Cas)

Previous page:
The artist's depiction of the Be/sdO binary φ Persei. Image credit: Bill Pounds, AURA/STScI

Zusammenfassung

Natur und Aktivität des Be Sterns μ Centauri: Mit insgesamt 408 Echelle Spektren, in 6 Beobachtungkampagnen über 355 Nächte innerhalb von vier Jahren, aufgenommen mit HEROS (Heidelberg Extended Range Optical Spectrograph), der einen Wellenlängenbereich von 3450 bis 8620 Å bei einem Auflösungsvermögen von 20 000 besitzt, basiert diese Arbeit auf einer der ausgedehntesten homogenen Beobachtungskampagnen der Variabilität eines Be Sterns. Während der Beobachtungsperiode wurden zahlreiche Linienemissionsausbrüche festgestellt. Ein detailliertes, allgemeines Schema des Verlaufs eines Ausbruchs wurde aufgestellt. Um die photosphärische Variabilität zu untersuchen, wurde eine Zeitserienanalyse an den Radialgeschwindigkeiten zweier Gruppen von Linien durchgeführt. Eine Periodensuche mit iterativer Periodenentfernung ergab sechs Perioden, die über den gesamten Beobachtungszeitraum kohärent blieben. Vier dieser Perioden liegen nahe bei der zuvor veröffentlichten 0.505 Tage Periode. Die beiden anderen sind nahe 0.28 Tagen. Innerhalb einer Periodengruppe ist das Variationsmuster ununterscheidbar, während es von Gruppe zu Gruppe deutlich unterschiedlich ist. Dies zeigt, daß es ebenso zwei unterschiedliche Oberflächenmuster mit beiden Gruppen verknüpft sind. Diese wurden als nichtradiale g Moden niedriger Ordnung modelliert. Mit Hilfe des Schwebungsmusters der längerperiodischen Gruppe kann eine Ausbruchsephemeride erhalten werden. Ausbrüche finden zu Zeiten maximaler Amplitude statt. Die Ergebnisse werden zu einem Bild des Be Sterns μ Cen vereint.

Abstract

Nature and activity of the Be star μ Centauri: With a total of 408 echelle spectra obtained with HEROS (Heidelberg Extended Range Optical Spectrograph) during 6 observing runs covering 355 nights in 4 years and the spectral range from 3450 to 8620 Å at a resolving power of 20 000, this study is based on one of the most extensive homogeneous observational records of the variability of any Be star. During the monitoring period numerous line emission outbursts were observed. A detailed generalized pattern of an outburst cycle is derived. To investigate the photospheric variability separate time series analyses were performed for the mean radial velocities of two groups of lines. A period search with iterative pre-whitening revealed six periods which maintained phase coherence over the entire time interval covered. Four of them are close to the previously reported 0.505-day period. The other two periods are near 0.28 day. Within either group of periods, the line-profile variability patterns are indistinguishable from one another whereas the difference between the two groups is highly significant. This implies that there are also two different stellar surface patterns associated with the two groups. They have been modelled by means of non-radial low order g-modes. The beating pattern of the longer period grioup can be used to derive an outburst ephemeris. Outbursts occur at times of maximal amplitude. The results are assembled into a picture of the Be star μ Cen.

Contents

List of Figures

List of Tables

1. Introduction

Since the very first discovery of stellar line emission in γ Cas by Secchi (1867), Be stars have been subject to disputes about the origin of their numerous spectral peculiarities (Slettebak, 1976; Jaschek & Groth, 1982; Underhill & Doazan, 1982; Slettebak & Snow, 1987; Balona et al., 1994). Only in the past decade could the geometry of the circumstellar envelopes by interferometric methods (Stee et al., 1995; Quirrenbach et al., 1997) be directly observed to be disk-like. Still ongoing discussions focus intensely on the physical mechanism leading to the formation of the circumstellar disk (Lamers & Pauldrach, 1991; Bjorkman & Cassinelli, 1993; Owocki et al., 1996) and on the nature of the short-term variability of the stellar absorption lines and the integral light (Smith, 1989; Baade & Balona, 1994). The primary candidates for the periodic component of the rapid variability are nonradial pulsation and corotating active areas or star spots.

Not considering the apparently required rapid rotation (Slettebak, 1982; Hanuschik, 1989, e.g.), which however is not *sufficient* as a defining criterion, the Be phenomenon covers a large parameter space, in the Hertzsprung-Russell diagram as well as in metallicity (Galaxy; LMC: Kjeldsen & Baade 1994; SMC: Grebel et al. 1992) and variability patterns. There are stars whose Balmer line emission is stable over decades, and there are others with variability on a time scale of hours, like μ Cen. It is therefore possible that there is more than one way for a B star to become a (classical) Be star.

With $V = 3.47\,\mathrm{mag}$ μ Cen (= HR 5193 = HD 120 324; B2IV-Ve) is one of the apparently brightest and with a HIPPARCOS distance of 162 ± 18 pc (Perryman et al., 1997) also most nearby Be stars so that it ought not to be too exotic an object of its kind. From high-signal-to-noise (S/N) echelle spectroscopy a projected rotational velocity, $v \sin i$, of $130\,\mathrm{km\,s^{-1}}$ has been derived (Brown & Verschueren, 1997). This relatively low value (as compared with the statistically established high mean equatorial rotation velocity, v, of Be stars – cf., e.g., Slettebak 1982, Hanuschik 1989, $< v \sin i >= 230 \ldots 270\,\mathrm{km\,s^{-1}}$) as well as the shape of the Hα emission during phases, when it has significant strength (Hanuschik, 1989; Hanuschik et al., 1996), both imply an intermediate value of 30-45 degrees for the inclination angle, i, of the rotation axis.

1.1 Emission Variability

The most enigmatic Be-star variations are the line emission outbursts. Up to now, a stringent definition of an outburst has not been given, and any significantly faster and stronger than average increase in the Balmer emission line strength has been called an outburst. Accordingly, the associated parameter space is again quite large and ranges from the slow (1-2 years) but spectacular outbursts of γ Cas in the 1930's (cf. Doazan et al. 1980, Hummel 1998) via drops in equivalent width (the general convention is adopted that an equivalent width is the more negative the stronger the emission is) by $\leq$0.1 Å within 1-3 days (Peters, 1988, e.g.) to even faster glitches that take place within hours (Oudmaijer & Drew, 1997).

Usually, all outbursts are thought to be events or periods of enhanced mass transfer to the disk. Attempts to find a link between the rapid periodic variability in the photosphere and the episodic mass loss usually did not exceed the level of conjectures or gave negative results (Smith, 1989, e.g.). However, Kambe et al. (1993a) find weak evidence for the amplitude of the stellar line

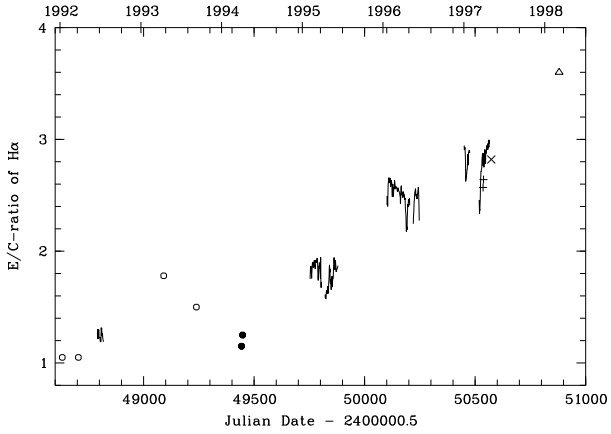

Figure 1.1: The Hα-emission peak height (relative to the local continuum) from 1992 to 1998. Lines show the measurements of this study, open symbols ($\circ$) were taken from Hanuschik et al. (1996), and filled symbols ($\bullet$) from Peters (1995). Crosses mark unpublished spectra taken by M. Thaller (+) and C. Aerts (x), the 1998 data ($\triangle$) was taken by the author at Mt. Stromlo, Australia in March 1998. The numerous narrow dips are not due to measuring errors but mostly correspond to the onset of line emission outbursts (cf. Sect. 3.2.2)

profile variability being larger than average close to the time of an outburst. In no case (excluding some binaries) has a convincing scheme for the temporal occurrence of outbursts been established which *apparently* happen at random. The best known examples of stars exhibiting frequent, rapid small or intermediate outbursts are λ Eri (Smith, 1989; Smith et al., 1991) and μ Cen.

1.1.1 History of μ Cen

μ Cen was first reported to exhibit Hβ emission by Fleming (1890). Since then it has been observed during numerous campaigns. The star is known to have lost its emission entirely for two times, once around 1918 for nearly ten years, and the second time from 1977 through 1989. Summaries of this behaviour were given by Peters (1979) and Hanuschik et al. (1993). In the 1977-1989 interval, μ Cen exhibited only flickering emission (Baade et al., 1988; Hanuschik et al., 1993). This activity strengthened after 1989. Although the emission-peak height thereafter rose temporarily up to values around 2 in units of the local continuum (Peters, 1995), it still decayed at least twice (1992 and 1994) to close to unity between two emission episodes. Since 1995, there has been a steady increase in the ratio of the emission peak height to the ambient continuum (E/C ratio) from ~ 1.8 in 1995 to 2.4 in 1996, 2.9 in 1997, and finally to 3.6 in March 1998. It seems, therefore, that μ Cen is indeed building up a new persistent envelope, as reported by Stahl et al. (1995a) and Hanuschik et al. (1996). The run of the Hα-peak height from 1992 to 1997 is shown in Fig. 1.1.

1.2 Stellar Line Profile Variability

Together with ζ Oph (Vogt & Penrod, 1983) μ Cen was the first Be star in which rapid variability on a scale of 1/10 of the full width at half maximum (FWHM) of the stellar line profiles was noticed (Baade, 1984a; Baade, 1987a). It also shows, often with high amplitude, the large-scale asymmetry variability of the absorption lines which seems to be typical of most Be stars (Baade, 1987b).

Part of this study in particular addresses the ambiguities (Baade, 1984a; Harmanec, 1987; Baade, 1987b) in the characterization of the low-order line-profile variability in the time domain: cyclic vs. periodic, one-third of a day vs. one-half of a day, singly periodic vs. multiply periodic, etc. The published photometric results (Cuypers et al., 1989; Dachs & Lemmer, 1991) have only increased rather than lessened the confusion.

The restriction to low-order line-profile variations is imposed by the limited resolving power of the FLASH/HEROS and Boller&Chivens spectra. On the other hand, the large number of spectral

lines contained in the wavelength coverage of the FLASH/HEROS spectrographs (3450-8620 Å) offers major multiplexing and differentiation advantages.

1.3 Nonradial Pulsation

The most promising hypotheses for the periodic photospheric varaibility are nonradial pulsation (*nrp*) and rotational modulation (*rm*). For the recent works advocating either the one or other mechanism see e.g. Baade (1998), Balona (1998), and Baade & Balona (1994).
With the public availability of new models capable to calculate even relatively rapid rotating g-mode pulsators under consideration of real intrinsic profiles, it became possible to model a pulsating star individually for different spectral lines. The previously published grids (Schrijvers et al., 1997, e.g.) are i.e. not suitable for slow g-mode pulsations, neither do they use intrinsic line profiles instead of approximating Gaussians.
Also it was possible to calculate photometric variations with respect to temperature, geometric surface, and geometric normal vector pertubations instead of the first two, or sometimes even only the first, alone. As it will be shown, taking into account all three pertubations is crucial in understanding the zero detection of photometric variability with the pulsational periods in this Be star.

1.4 Goal and Structure of this Work

The scientific purpose of this work was to decide the long lasting discussion about the nature of the rapid periodic variability of Be stars. In the data obtained for this task it would be furthermore possible to look for photospheric variability that could be connected to circumstellar emission activity, and thus to give clues on the mechanism responsibe for the formation of the circumstellar disk; still being an open problem since the first sighting of Be star emission by Secchi (1867).
To achieve this, spectroscopic data of southern Be stars, i.e. μ Cen, η Cen, ω CMa, and FW CMa over observing runs lasting for months during several season was secured. In almost all runs the ESO 50cm telescope was used together with the spectrograph HEROS. The instrument and the particulars of the observations and data reduction are presented in Chapter 2, together with the description of additional datasets provided by D. Baade and S. Štefl (Sect. 2.2, Boller&Chivens at the ESO 1.52m data, and Sect. 2.3, CAT/CES data).
Sighting the data in an early stage of the work I decided to concentrate on μ Cen, which was the most active of all observed stars. Chapter 3 lists the observed circumstellar variability for this star, and defines an Hδ activity criterion that seems arbitrary at first look, but will prove useful in determining consistent dates for the beginning of outbursts (Fig. 3.3). In Sect. 3.1 I extract the common features of the emission outbursts but also discuss their heterogeneity, while the individual phases of the emission outburst are described in detail for various groups of representative spectral lines in Sect. 3.2. These phases were named relative quiescence (Sect. 3.2.1), precursor phase (Sect. 3.2.2), the outburst proper (Sect. 3.2.3), and relaxation (Sect. 3.2.4). The analysis of accompanying V/R variations is presented in Sect. 3.3 and examples of transient absorption components appearing in connection with the outbursts in Sect. 3.4.
An analysis of the spectral lines of photospheric origin is given in Chapter 4. Sect. 4.1 presents time series analyses (TSA's) of various scalar parameters of the stellar line profiles. The large temporal extent of the FLASH/HEROS+CAT/CES observations is the basis for the analysis of radial velocities at high frequency resolution (Sects. 4.1.1 and 4.1.2). The Boller&Chivens (Sect. 4.1.3) data are complementary in that they only cover a short time interval but at very high sampling and, moreover, at the time of a line emission outburst (cf. Chapter 3). A TSA of the full line profiles

in slices of constant width in velocity, which therefore exploits the entire spectral and temporal information simultaneously, is performed in Sect. 4.2. Only in a non-parametric analysis does the cyclical occurrence of narrow absorption features at fixed positions within the photospheric profiles becomes apparent. They are strongly enhanced during outbursts (Sect. 4.3).
The interpretation and modelling of the periodic variability found in the photospheric lines is subject of Chapter 5.
Chapter 6 finally introduces a simple scheme, by which, based on the photospheric period analysis results, the timing of the circumstellar outburst events cannot only be reconstructed within the HEROS-dataset, but also for other previous datasets up to twelve years ago. Even a prediction of the activity in summer 1997, that was submitted for publication in spring, could be confirmed (Rivinius et al., 1997d; Rivinius et al., 1998e).
Chapter 7 summarizes the findings for μ Cen in Sect. 7.1 and compares the behaviour and properties of μ Cen with those of other Be stars, partially published earlier, or found in our own extensive Be star spectral database in Sect. 7.2. The found periods are not easy to distinguish from their 1 cycle per day aliases, special care is taken not only on possible mimicking of multiperiodicity by aliasing problems, but also on the values of the periods themselves. Therefore, Sect. 7.3 carefully tests and critically discusses the reality of the periods found.
The observations and analyses are assembled into a picture of the Be star μ Cen in Chapter 8. The variability of photospheric origin (Sect. 8.1) is reviewed with respect to a number of proposed explanations of the various observed phenomena. The nonradial pulsations are put into the context of the current theoretical framework in Sect. 8.2 and possible mechanisms that could result in mass ejections are outlined. In Sect. 8.4, I attempt to give a generalized qualitative and mostly kinematic description of an outburst. Finally, Sect. 8.5 summarizes secondary and future projects stimulated by this work.
The content of this thesis has been published in the European Journal Astronomy & Astrophysics (Rivinius et al., 1998a; Rivinius et al., 1998b), in the Be Star Newsletter (Rivinius et al., 1997d; Rivinius et al., 1998e), presented on meetings (Rivinius et al., 1997a; Rivinius et al., 1997b; Rivinius et al., 1998c; Rivinius et al., 1998d; Rivinius et al., 1998f), or is currently being prepared for publication in Astronomy & Astrophysics in one more paper.

2. Instrumentation, Observations and Data Reduction

This work is based on eight spectroscopic observing runs at ESO's La Silla observatory and also incorporates three sets of previous observations (Baade, 1991). The resolving powers range from 2 500 with the Boller&Chivens spectrograph at the ESO 1.52-m telescope (Sect. 2.2) over 20 000 with the Heidelberg FLASH and HEROS spectrographs and fibre link to the ESO 0.5 or 1.52 meter telescopes (Sect. 2.1) and finally to $\geq$60 000 with the Coudé Echelle Spectrometer (CES) and the ESO 1.4-m Coudé Auxiliary Telescope (CAT) (Sect. 2.3). A summarizing journal of observations and technical parameters characterizing the spectra is provided in Table 2.1. The particulars of the raw data and the reduction procedures applied to them are described in the following subsections. For the Boller&Chivens data the standard reduction and calibration techniques were used as implemented in ESO-MIDAS (1995). For the FLASH and HEROS data, a customized version of the ESO-MIDAS echelle context was developed (Stahl et al., 1995b). Note that throughout the entire thesis Modified Julian Date (MJD $\equiv$ JD-2 400 000.5) is used.

2.1 FLASH/HEROS Observations

2.1.1 The Instrument

The fiber-linked echelle spectrograph HEROS (**H**eidelberg **E**xtended **R**ange **O**ptical **S**pectrograph, Kaufer 1998) is an upgrade of the FLASH-spectrograph described by Mandel (1994) and Stahl et al. (1995b). In HEROS, a dichroic beam splitter is used to divide the light beam into two channels after the echelle grating. Each channel has its own cross-disperser, camera, and detector. The blue one covers the range from 3450 Å to 5560 Å, and the red one from 5820 Å to 8620 Å. The spectral resolving power in both channels is $\lambda/\Delta\lambda \approx 20\,000$. The link to the telescope was provided by a 10 m long glass fiber.

In 1996 the blue CCD system manufactured by Wright Instruments Ltd. (1024x1024 22μ pixel) was replaced by a backthinned CCD by SiTe (2000x800 15μ pixel) connected to a controller by Instruments SA. The Signal-to-noise ratio S/N improved dramatically not only in the UV region, but even in the optical range around 4800 the value increased by 20 %. However it was necessary to create own software based on a routine library by Instruments SA, since the utility provided by the manufacturer was not optimized for astronomical purposes. The software written is an easy-to-use command line based program for exposing and writing an image in the Flexible Image Transfer Standard (FITS) format to disk. The program was also given to the Skinkakas observatory, Crete, and the Astronomical Institute in Potsdam, who have implemented such CCD sytems since then and wanted to perform tests. Since the software is taylored to the needs of HEROS, it is however not well suited for general astronomical use. A secondary display program was written to allow quality checks and inspection of the data immediately after an exposure.

The stability of the wavelength calibration of the red channel was assessed by Kaufer et al. (1997). They found the telluric water vapour lines in a time series of β Ori of 84 spectra over 104 nights to be stable to within 0.35 $\mathrm{km\,s^{-1}}$ rms, with a peak-to-peak range of 1.7 $\mathrm{km\,s^{-1}}$. The standard deviation corresponds to 1/10 of a 22 μ pixel and is caused by the shift of the lines of the ThAr-lamp between subsequent calibration exposures, which were typically taken every two hours. Schmutz et al. (1997) tested the blue channel using the interstellar Ca IIλ3934 line in ϵ Cap.

Table 2.1: The μ Cen observing campaigns

Observing season	Telescope	No. of spectra/ No. of Nights	Instrument	Typical exposure time	Typical S/N	Resolving power	Spectral range
1985 June/July	CAT	81/10	CES+Reticon	20 min	≥ 500	80 000	6650-6700 Å
1986 April	CAT	111/10	CES+Reticon	20 min	≥ 500	80 000	6650-6700 Å
1987 April	CAT	119/10	CES+Reticon	20 min	≥ 500	80 000	6650-6700 Å
1992 June/July	ESO 0.5m	28/28	FLASH	15-30 min	104	20 000	4050-6750 Å
1995 Feb.-May	ESO 0.5m	96/118	HEROS	20 min	110	20 000	3450-8620 Å
1995 June	ESO 1.52m	348/8	Boller&Chivens	1.5-6 min	250-350	2 500	3450-5100 Å
1995 June	CAT	27/4	CES+CCD	15-20 min	320	60 000	4537-4563 Å
1996 Jan.-April	ESO 0.5m	87/103	HEROS	30 min	135	20 000	3450-8620 Å
1996 May/June	ESO 0.5m	115/27	HEROS	30 min	165	20 000	3450-8620 Å
1997 Jan.&Mar.	ESO 0.5m	64/68	HEROS	20-30 min	160	20 000	3450-8620 Å
1997 April	ESO 1.52m	18/11	HEROS	4 min	184	20 000	3450-8620 Å

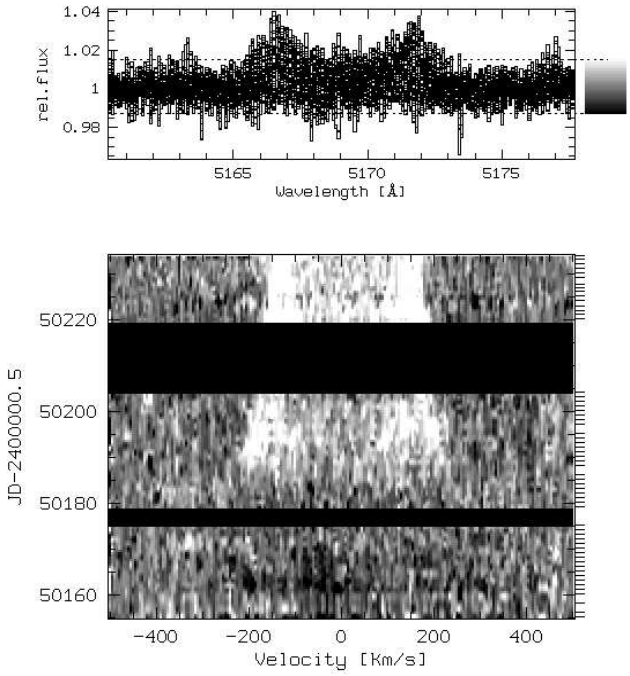

Figure 2.1: The dynamical spectrum of the Fe IIλ5169 emission line from April to June, 1996. Grey-scale values represent the continuum-normalized flux of the spectra; the scale is shown on the right side of the upper panel. Horizontal black stripes are due to major time gaps, which were not interpolated across. Tickmarks on the right side mark the times of exposure of the original spectra. Above the grey-scale picture, all actual line profiles are overplotted to give an idea of the variability and the noise. The appearance of the emission from date MJD 50 183 on coincides with a major outburst. Note the variation of the velocities of the emission peaks

Since however ϵ Cap has a variable photospheric contribution to this line and the S/N is not as high as in β Ori, their rms value of $0.5\,\mathrm{km\,s^{-1}}$ for the blue channel is to be regarded as a lower stability limit.

2.1.2 Data Reduction

After the extraction and merger of the echelle orders, a wavelength dependent ripple became apparent at the order boundaries. It is noticeable at both ends of the blue channel, namely from 3450 Å to 3600 Å and from 5100 Å to 5560 Å where towards either end of the detector the peak-to-valley amplitude reaches 5 %. At all other wavelengths, including the whole red channel, the ripples are of the order of 1 % or less.

FLASH, the predecessor of HEROS, had the same spectral resolution, but only one channel, covering the wavelength range from 4050 Å to 6750 Å.

The signal-to-noise ratio (S/N; for some typical values see Table 2.1) was measured for both the FLASH and the HEROS data as the inverse of the rms (in units of the continuum) in the wavelength range 4760-4800 Å. In May 1996 the more sensitive CCD was implemented in the blue channel of HEROS. This is reflected by the increase of the typical S/N at comparable exposure times. For the later runs of 1997 a new fiber link was implemented. The improved throughput permitted from then on the exposure times to be shortened by one third without losing in S/N.

The standard reduction, extraction, and visualization of the data is described in detail by Stahl et al. (1995b). To represent the large amount of data we display the spectra as dynamical spectra (cf. Fig. 2.1), i.e. time (or phase)-vs.-velocity grey-scale pictures around the rest wavelength of the spectral line.

2.2 Boller&Chivens Observations

During 8 consecutive nights in 1995 June, low-resolution spectra were obtained with the Boller & Chivens spectrograph attached to the ESO 1.52-m telescope. On a 2048-pixel CCD, the spectra

Table 2.2: Modified Julian dates (MJD ≡ JD-2 400 000.5) and numbers of observations obtained in the observing nights with the Boller&Chivens spectrograph on the ESO 1.52-m telescope and the CAT/CES. One B&C observation yielded one 'upper' and 'lower' spectrum each (cf. Sect. 2.2)

Modified Julian Date	No. of observations	
	B&C	CAT/CES
49 890	28	
49 891	36	
49 892	34	3
49 893	51	8
49 894	56	8
49 895	51	8
49 896	35	
49 897	57	

covered approximately the range from 3400 to 5100 Å. The resolving power as deduced from the helium and argon lines of the comparison spectra, which were taken 3 - 5 times per night, is 2 500. The typical rms of a third-order polynomial fitted to 35-40 HeAr comparison lines is $3\,\mathrm{km\,s^{-1}}$.
In order to approximately equalize the detected signal over the observed range in wavelength, a BG-24 filter was inserted into the beam. The primary purpose of the observations was the monitoring of rapid Balmer jump variations the results of which will be reported elsewhere (Štefl, Baade, Cuypers in preparation). Since at this short wavelength atmospheric dispersion would normally strongly compromise the spectrophotometric fidelity of the data, the telescope was drastically defocussed in order to scramble the atmospheric spectra on the entrance slit. The amount of defocussing was chosen such as to stay in the linear regime of the detector and to keep the exposure times in the range between 90 and 120 seconds where scintillation effects are of no importance. Only at times of poor sky transparency was it necessary to increase the exposure time (up to 6 minutes); this concerned 19% of all observations.
Since the observations were more nearly of the telescope pupil than of the stellar image, the resulting 'long-slit' spectra featured two maxima along the slit axis. This permitted the extraction of two spectra (hereafter called 'lower' and 'upper') per exposure.
Inspecting the data, a systematic radial velocity difference between 'upper' and 'lower' spectra became apparent, which decreases linearly from $30\,\mathrm{km\,s^{-1}}$ at 3500 Å to $13\,\mathrm{km\,s^{-1}}$ at 4500 Å and from there on remains constant. The explanation for this difference is that, as RV measurements were not among the original aims of the observations, the arc spectrum was only extracted at the center of the slit but used to calibrate both the 'lower' and 'upper' spectra. The arc spectra were also taken relatively infrequently.
Because the exposure levels were high and particle events were few in number, no signal-to-noise optimized extraction procedure was applied. The typical S/N per extracted spectral pixel is between 250 and 350 and very nearly identical for both upper and lower spectra.
The total database accumulated in this way consists of 348 'upper' and 'lower' spectra each. A statistical overview is given in Table 2.2.

2.3 CAT/CES Observations

The CES is a pre-dispersed (as opposed to cross-dispersed) spectrograph so that only part of one order can be observed at a time. It is fed by the ESO 1.4-m Coudé Auxiliary Telescope (CAT).
In 1995, the wavelength region from 4537-4563 Å was chosen to monitor the Si III line at 4553 Å. At a resolving power of 60 000 the point spread function was sampled by 3.6 pixels. A second order polynomial fitted to the positions of 15-20 thorium lines had a standard deviation of 0.02-0.025 Å. An optimal extraction technique was applied to remove particle hits from the data.
However, this wavelength range turned out to be heavily contaminated by double peaked Fe II emission lines which reached up to three percent of the continuum level. The average of the FLASH spectra from 1992, when the emission was weak even in the Balmer lines, was used to obtain the uncontaminated absorption line profiles and to improve the continuum rectification. By subtracting these profiles from the CAT/CES spectra it was possible to isolate the emission line spectrum. The emission lines proved to have been constant over the four days of observations to within the noise. Accordingly, the remaining variability is intrinsic to the photospheric Si III λ4553 line. This was confirmed by comparison with the variability of the residuals of the Si III λ4568 line, part of which was covered at the very edge of the wavelength range.
Profiles of several lines that were obtained (see also Baade 1991) from 1983 to 1990 with the CAT/CES equipped with a Reticon detector prior to 1990 and with a CCD from 1990 on have been kindly provided by D. Baade.
Besides the data already listed in Table 2.1, these are profiles of He I λ6678 (March 1984, 8 spectra over 3 nights; Feb. 1987, 3/3; and March 1990, 8/3), He I λ4471 (June 1983, 20/14; March 1984, 8/8; and July 1985, 5/2), Si III λ4553 (March 1984, 3/3), and Hα (June 1985, 4/15; Jan. 1986, 4/4; April 1986, 13/10; Feb. 1987, 3/3; and April 1987, 9/10). The usage of a Reticon resulted in a S/N which in almost all cases exceeded 500, often quite substantially, but at exposure times of 15-20 minutes. The resolving power is 80 000-100 000.

2.4 Data of other Be Stars

Besides μ Cen, also other Be stars were observed with FLASH/HEROS (see Table 2.3). Most of these stars have been observed only once or for a few times in a single season. However, more extensive campaigns were carried out for a few stars, e.g. 28 Cyg (Tubbesing, 1998). These datasets will not be reviewed in detail in this thesis, but for at least some of the findings it can be proven that they are a quite general property of Be stars rather than an unusual phenomenon found in μ Cen only.

Table 2.3: A complete list of Be stars observed by the Heidelberg Hot Star Group with HEROS and FLASH. If a campaign took place over new years eve, the whole campaign is noted for the year in which the major part of the observations were taken. For each season the number of spectra is given. The observations were performed at La Silla, Calar Alto, Tautenburg, and the Königstuhl

		1990	1991	1992	1995	1996	1997	Remarks
BN Gem	O8V:pevar	1	12	–	–	–	–	7
γ Cas	B0IVe	–	–	–	–	1	–	7
FR CMa	B1Vpe	–	–	–	1	–	–	2
η Cen	B1.5Vne	–	–	–	46	294	80	1,4
59 Cyg	B1.5Vnne	12	–	–	–	1	1	5,7
κ CMa	B1.5IVne	–	–	–	–	–	4	7
μ Cen	B2Vnpe	–	–	28	96	202	82	1
FW CMa	B2Vne	–	–	–	–	8	48	1
φ Per	B2Vpe	–	–	–	–	–	7	5,7
χ Oph	B2Vne	–	–	–	1	–	–	2
ω CMa	B2IV-Ve	–	–	–	–	99	128	1
λ Eri	B2IVne	–	–	–	–	–	8	1
δ Cen	B2IVne	–	–	–	–	1	–	7
ζ Tau	B2IV	1	–	–	–	–	1	5,7
28 Cyg	B2.5Ve	–	–	–	–	–	98	1
48 Per	B3Ve	–	–	–	–	–	1	7
ϵ Cap	B3V:p	–	–	–	6	61	–	1,4
α Eri	B3Vpe	–	–	–	–	4	–	7
48 Lib	B3IVe	–	–	–	1	8	–	2,5,6
ω Ori	B3IIIe	–	–	–	–	–	14	1
PP Car	B4Vne	–	–	–	1	–	–	2
λ Cyg	B5Ve	–	–	–	–	1	–	7
θ CrB	B6Vnne	–	130	1	–	–	–	3
κ Dra	B6IIIpe	–	195	1	–	–	–	3,5
ϵ PsA	B8Ve	–	–	38	–	1	–	7
Pleione	B8IVevar	2	39	–	–	–	4	5,7
ω Car	B8IIIe	–	–	–	1	10	7	4
ν Pup	B8III	–	–	–	1	8	7	4
51 Oph	A0V	–	–	–	1	–	–	2

1: Search for multiperiodicity and outbursts (in coll. with D. Baade and S.Štefl)

2: ASTRO-2 & WUPPE support observations (in coll. with K. Bjorkman)

3: Search for high order line profile variability (Stumpf, 1992)

4: Quasi emission bump (Baade, 1989a; Baade, 1989b) monitoring (in coll. with D. Baade and S.Štefl)

5: V/R variability – polarimetry – interferometry connection (in coll. with D. McDavid and Ph. Stee)

6: Search for narrow optical absorption components (Hanuschik & Vrancken, 1995; Hanuschik & Vrancken, 1996) (in coll. with R. Hanuschik)

7: Test observations

Note that only the main collaborators are given in this list.

3. Circumstellar Emission Variability

3.1 Commonalities and Different Appearances of Outbursts

Fig. 3.1 illustrates that the variability of the equivalent width of Hα, Pa$_{15}$, and Fe IIλ5169 is very complex. Similarly to the photometric variability of Be stars (Štefl et al., 1995; Štefl & Balona, 1996, e.g.), it can be understood as composed of variations on 2 or 3 different time scales. Long-term season-to-season variations of the Hα equivalent width become easily apparent from the comparison of the mean emission level in the individual sub-panels of Fig. 3.1 and are assumed to be connected with changes of the total disk mass. The outburst-like variations discussed below are at the short end of the time scales. In addition, there may be links to trends on a time scale of months.

There are indications that the Boller & Chivens (Sect. 3.3.2) and some of the CAT (Sect. 3.3.3) observations were obtained during outbursts. Only in systematic long-term monitoring data from HEROS one can unambiguously recognise and follow the entire development of the emission outbursts. In the period 1995–1997, 11 outbursts of different strengths were detected. In Table 3.1 their dates and strengths are listed.

Rather than commenting on individual events it is attempted here to abstract and describe typical states and patterns which may ultimately form the basis for the physical understanding of the observations. Fig. 3.1 represents a schematic picture of μ Cen's line-emission outbursts. It needs to be understood that this scheme is not representative of any particular outburst, although a few outbursts with such a course of the Hα equivalent width were observed in 1995. Rather, Fig. 3.1 is typical in the sense that it combines all main phases of the outburst as they appear in equivalent width, E/C ratio, emission wing strength and peak separation at different levels of the quiescent emission. The four primary phases of an outburst cycle are (i) periods of (relative) quiescence, (ii) sudden, short (5–13 days) drops in strength of all circumstellar emission lines (termed 'precursor' phase below), (iii) subsequent rapid increase (within 2–15 days) of the emission strength, which henceforth will be called outburst for brevity, and (iv) the transition phase which after the outburst eventually evolves into relative quiescence (10–35 days) and for which the term relaxation was chosen. The details of the main phases are provided in Sect. 3.2.

Already from this coarse description it is clear that a single scalar quantity such as the often used equivalent width or also the E/C ratio cannot adequately describe the temporal run of an outburst. Only based on the variability of the entire line profile this is possible. Particularly the initial phases of an outburst can look significantly different if monitored in different spectral lines or at different levels of the quiescent emission and also if recorded as equivalent widths or E/C ratios. For instance, at low emission levels, the equivalent width is not a sensitive indicator of the onset of an outburst. So long as the underlying absorption profile is not filled in, the decrease of the emission peak height can be compensated by the enhanced emission wings. Therefore the total equivalent width may remain about constant, whereas the outburst can already be well recognised in the E/C ratio. This happened during the outbursts observed in 1995. Similarly, exclusive usage of the E/C ratio cannot overcome this problem either, since the peak height increases only after the extended emission wings have appeared.

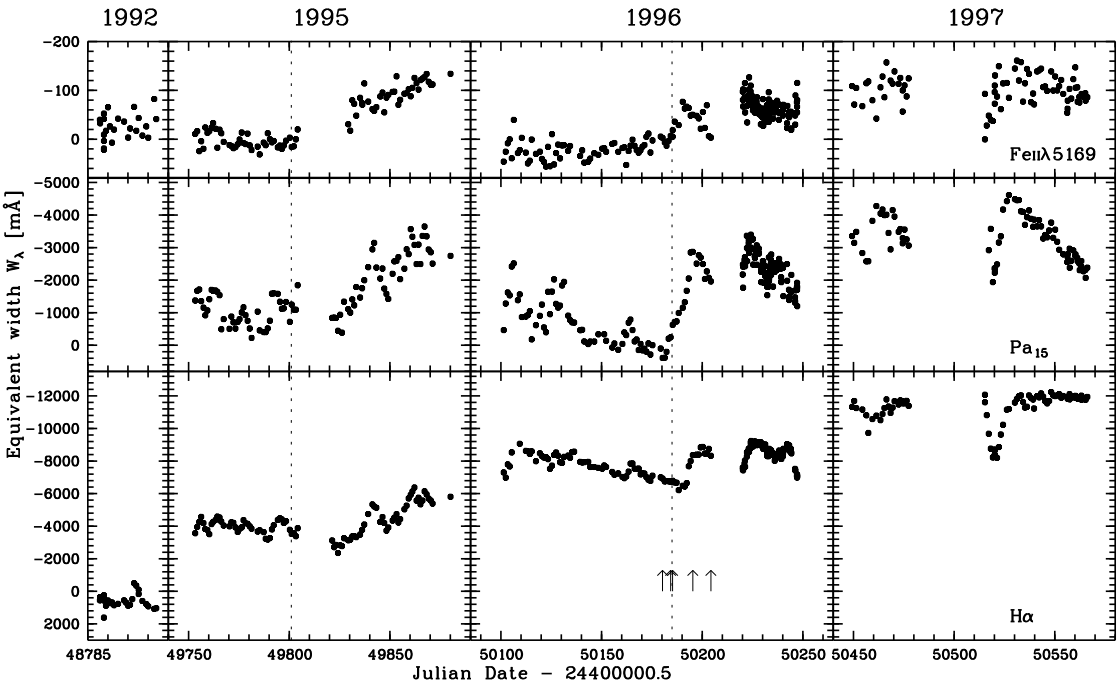

Figure 3.1: Equivalent widths of emission lines of Fe IIλ5169 (top), Pa_{15} with Ca IIλ8542 (middle), and Hα (bottom) during the HEROS monitoring period. The typical measuring error is 20 mÅ. The offset from 1995 to 1996 in the Fe IIλ5169 line is caused by a somewhat different echelle ripple pattern (cf. Sect. 2.1). The lines mark special events discussed in Sect. 3.2.3, and the arrows point at the dates of the spectra plotted in Fig. 3.4

The problem of a suitable scalar quantity concerns not only the full description of the outburst, but also the choice of the criterion which defines the moment when the outbursts starts. The analysis shows that the emission in the wings of higher Balmer lines, mainly Hδ, is a reliable indicator at all quiescent emission levels covered by the monitoring. An example is given in Fig. 3.3. The strengths of the wing was measured by fitting a Gaussian to the complete line profile. Due to emission in the line core, the derived equivalent widths are systematically wrong in their absolute value, but their gradient is high just at the beginning of the outburst (see Fig. 3.1). The method is not influenced by a missing precursor phase in equivalent width and/or E/C variations and was also used in order to determine the outbursts dates in Table 3.1.

In many actual outbursts some of the phases listed above may appear missing. The apparent lack of a precursor phase, when the mean emission is weak and if only equivalent widths are measured, was already mentioned. A corresponding threshold in Hα may be $W_\lambda \approx -4 \ldots -6$ Å, $E/C \approx 1.5$–2. A corresponding limit can be presumed for the Paschen lines but it would fall in phases of relative quiescence not covered by the observations. The precursor phase is getting more conspicuous with increasing average strength of the emission. Then, the initial drop in emission strength can reach as much as 30% as observed in 1997, when $W_\lambda \approx -12$ Å , and $E/C \approx 3$. By contrast, the outburst phase appears more conspicuous when the mean emission strength is weak. This was the case in 1995, whereas after the additional increase of the Hα emission strength in 1996 and 1997 the outburst phases were mostly missing in Hα and still weak in the Paschen lines. The above also suggests how the appearance of line emission outbursts will evolve further if the

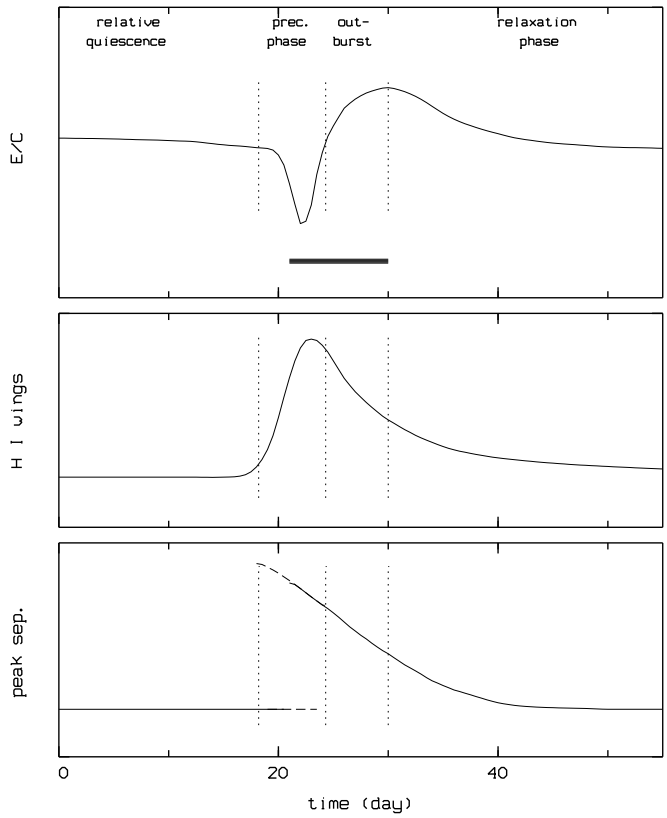

Figure 3.2: A schematic picture of a line emission outburst. The outburst phases described in Sects. 3.1 and 3.2 are marked. For outbursts at times of weak mean line emission, the upper panel rather describes the variability of the E/C ratio whereas the ordinate is more nearly equivalent width (which numerically would increase towards the bottom of the figure) when the average emission is strong. The bold line represents the time interval, in which the quasiperiodic V/R variations appear (see Sect. 3.3). The middle panel shows the emission in the wings of the higher Balmer lines, which can be used as a convenient indicator of the outburst onset, regardless of the mean emission level in the quiescent phase (for more details see Sect. 3.1). The run of the emission peak separation was derived from the Si II lines. The Fe II lines show the same variability, but the value in the quiescent phase is mostly not defined, except for the strongest lines at times of highest quiescent emission (see Fig. 3.5)

emission at quiescence from the disk continues to strengthen. It would be interesting to test this prediction observationally.

3.2 Phases of a Line Emission Outburst

3.2.1 Relative Quiescence

According to Fig. 3.1, the emission strength of μ Cen is changing most of the time. Therefore, one can only define phases of relative quiescence when the variations are minimal. Even during such relative quiescence the Balmer emission slowly decays. This definition is independent of the emission strength.

In the observations, the end of such a phase can be found in 1996 at Modified Julian Date (MJD $\equiv$ JD-2 400 000.5) $\approx$ 50 170, nearly 80 days after the last major event had occured. The following description is based on this period, but the spectra during the relative quiescence before MJD 49 785 look essentially the same. The small differences might be explained by the shorter time that had elapsed since the preceding outburst.

Balmer lines: At this stage, the emission profiles have sharply defined edges, and the central reversal is very pronounced. The V/R-ratio is only slightly variable around unity. The contribution of NLTE effects and scattering to the line wings is quite weak, so that the photospheric absorption wings are still visible. The quiescent Hα-line is shown in Fig. 3.4.

Paschen lines: The emission in the Paschen series is shallow in the spectral range observed (Paschen discontinuity to Pa_{14}). The peak height of Pa_{15}, the blue side of which is slightly blended with Ca IIλ8542, does not exceed $E/C = 1.1$. This level of the Paschen emission during quiescent phases may be crudely recurrent whereas the strength of the Balmer emission during

Table 3.1: Times and relative amplitudes of line emission outburst detected in the HEROS observations in the period 1995 – 1997. MJD refers to the beginning of the outbursts as derived from the time of increase of the strength of the Hδ emission wings and is accurate to within a day (see Sect. 3.1). The relative change of the (total) equivalent width of Hα and Pa_{15} is expressed as a percentage of the value at the beginning of the respective outburst. The typical errors are 1-4 percentage points for the Hα values and 10-20 for Pa_{15}. The range of this errors reflects mainly the gradual long-term increase of emission. The usage of $\leq$ indicates that the actual beginning of the burst was not covered by the data, but must have been shortly before

Season	MJD	Hα		Pa_{15}	
		precursor	burst	precursor	burst
1995	49 787	+13	−12	+55	−46
	49 836		−30		−60
	49 858		−19		
1996	$\leq$ 50 103		−15		−10
	50 152	+8	−9		−51
	50 181	+18	−13	+43	−69
	$\leq$ 50 219		−6		−14
1997	50 454	+13		+18	−15
	50 515	+38		+52	−19
	50 533	+5		+9	
	50 544	+5		+12	

quiescence takes on a much larger range of values. The central reversal is much less pronounced than in the Balmer series, though detectable. Apart from the Paschen lines, three other lines within the Bracket continuum were detected in the observed spectral range: Ca II$\lambda\lambda$ 8498,8542 and O Iλ8446. The first two are weak and moreover blended with Paschen lines. But the latter is stronger than one would expect judging from the O Iλ7774 blend. It is a fluorescence line of the Lyβ transition (Briot, 1981), and its strength should, therefore, scale with Hα. The quiescent Pa_{15} line profile is shown in Fig. 3.4.

Silicon: Weak Si IIλ6347 emission is present (Fig. 3.4) whereas Si II$\lambda\lambda$ 4131,5056 are missing. Of the two main phases of relative quiescence in 1995 and 1996, the later one was weaker in Si IIλ6347 emission. As can be seen in Fig. 3.5, also the peak separation was smaller.

Iron: During relative quiescence, Fe II emission is not detectable down to the noise limit which, given the large number of potential lines, corresponds to a peak height of half a percent above the continuum level.

Helium: The emission profiles of He I are highly variable in both shape and strength even at quiescence. However, the absolute level of activity and the velocities of the emission peaks are generally lower than during an outburst, and the emission peaks are narrower than in other stages.

3.2.2 Precursor Phase

An imminent outburst announces itself by a short (5-13 days) significant (see Sect. 3.1 and also Fig. 1.1) drop in the peak height of all emission lines present at the time. A second defining constituent of this phase is an increase of the extended emission wings which is best visible in higher Balmer lines (cf. Fig 3.3). In Hα these wings may compensate the change in equivalent width caused by the drop of the peak height, however not quite in all cases. The balancing is more perfect in Hβ, and from Hγ on the wings grow more strongly than the peaks decrease.

In most outburst cycles, this phase is the most distinctly recognizable feature; a proto-typical

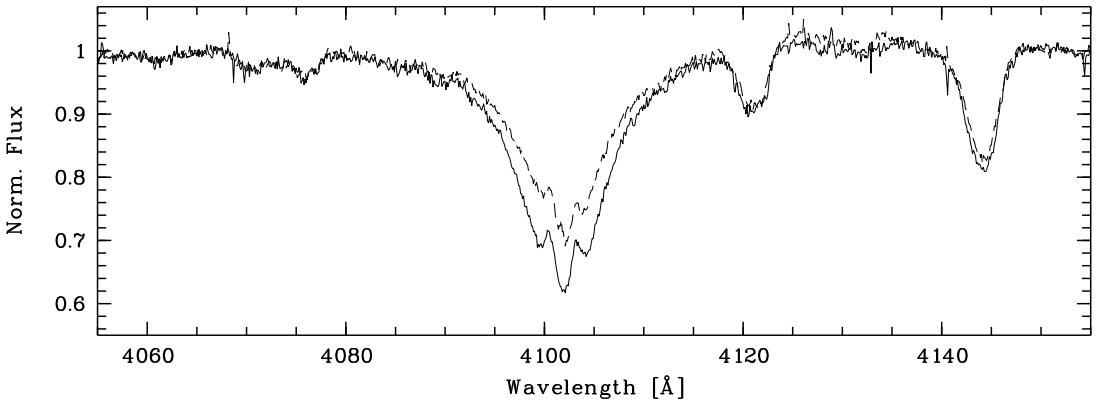

Figure 3.3: The Hδ line of μ Cen shortly before (full line) and during an outburst (dashed line). The strength of the wings is measured by means of fitting a Gaussian to the complete line profile. Although the absolute numbers of the equivalent width measured by this procedure have obviously systematic errors and should therefore not be taken at face value, the quantity is far more sensitive to changes of the broad emission superimposing the wings than to variations of the emission peaks. Since the wings were found to be the most general indicator for outbursts, this quantity can be used to monitor the activity

example is displayed in Fig. 3.1 around MJD 50 510, but the reduced Hα-peak height is also well visible in Fig. 3.4. This behaviour is not peculiar to μ Cen as is shown by the case of the Be star HD 76 534 in which Oudmaijer & Drew (1997) observed the full recovery of a previously drastically reduced Hα emission in only 3 hours.

Because no photometry was obtained parallel to the HEROS observations, the possibility cannot be directly dismissed that the precursor drop of the E/C ratio is caused predominantly by a corresponding increase of the continuum flux. In the precursor phase of the outburst on MJD 50 515, which was the deepest observed, the Hα E/C value temporarily dropped from 3.0 to 2.4. If the decrease was caused only by a change of the continuum flux, a brightening by nearly $0\overset{m}{.}2$ would be implied. This is more than virtually all optical peak-to-peak light variations reported by Cuypers et al. (1989), Balona (private communication), and the HIPPARCOS photometry (Perryman et al., 1997) for the period 1987 to 1992. Taking into account also the frequency of the outbursts and the density of the photometric data, such a large change in the continuum flux appears improbable. Another test is to check the E/C amplitudes of various lines for consistency with pure continuum variability. Unfortunately, there are too few metal lines that are of sufficient strength throughout the outburst cycle and to which the test can be applied. However, accompanying major Balmer decrement variations indicate that the results of this test, too, would be negative.

3.2.3 Outbursts

Baade et al. (1988) present arguments that previous rapid increases in line emission from μ Cen were due to the ejection of material by the star to its circumstellar disk. This justifies the notion of outbursts. Hanuschik et al. (1993) distinguish between two different kinds of outbursts which can be identified by their strength. Two major and many minor bursts are found in the data but no compelling evidence that they are genuinely different events. The difference between bursts of different strengths may be blurred further by the dependency of the appearance of bursts on the mean emission strength. In 1995, the major burst unfortunately started shortly before a gap in our observing schedule (cf. the description of the behaviour of the Fe II lines given below). Both

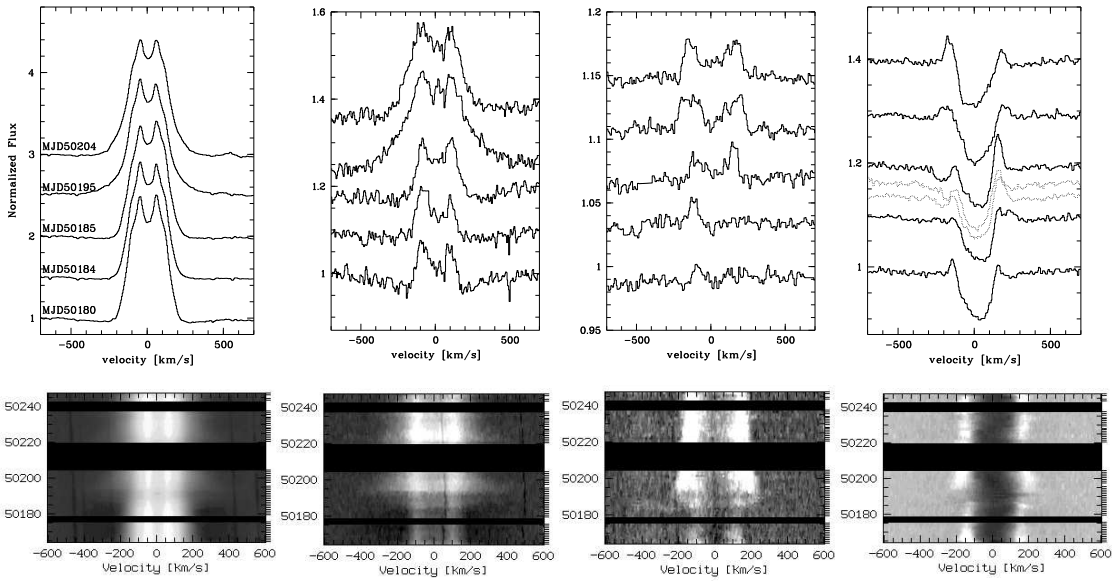

Figure 3.4: The variations of Hα (leftmost), Pa$_{15}$ (mid left), Si IIλ6347 (mid right), and He Iλ6678 (rightmost), from relative quiescence (lowermost spectrum, MJD 50 180) over the very first trace of circumstellar variability, the beginning of the precursor (second, MJD 50 184), the high velocity absorption event as described in Sect. 3.4 (third, MJD 50 185), and the appearance at the end of the burst phase ($V/R_{\mathrm{H}\alpha} > 1$, fourth, MJD 50 195) to the late relaxation phase ($V/R_{\mathrm{H}\alpha} \approx 1$, fifth, MJD 50 204). The dates of the spectra are indicated as arrows in Fig. 3.1. Two similar high-velocity absorption events (Table 3.2 and Sect. 3.4) in January 1997 are overplotted as dotted lines on He Iλ6678 (MJD 50 457 in the lower and MJD 50 461 in the upper spectrum). In the lower row it is shown how the dynamical spectra develop from relative quiescence through a major burst into the relaxation phase. The dynamical spectra also cover two smaller bursts around MJD 50 223 and MJD 50 232. The apparent long-term radial-velocity variations in the He Iλ6678 line are due to the highly uniform sampling of one spectrum per day, which results in a strong beat pattern with the photospheric periodicity is described in Chapter 4. The feature in the Pa$_{15}$ line seen in the dynamical spectrum at $\sim 50\,\mathrm{km\,s^{-1}}$ is a CCD artifact

major outbursts were sampled with one spectrum per day. At higher temporal resolution only minor bursts were observed with HEROS; the series of Boller&Chivens spectra was probably also obtained during a minor outburst (Sect. 3.3.2).

Balmer lines: In 1996, the peak height of Hα dropped after the short precursor phase within a few days by 0.3 in units of the local continuum, while the equivalent width change is roughly compensated by the increasing wings (indicated by the dotted line in Fig. 3.1, 1996 panel). The rapid V/R variability may occasionally have started already even in the precursor phase, depending on the strength of the burst. The emission wings still continued to rise and, depending on the level of the quiescent emission, may finally also in Hα overcompensate the decrease in emission strength caused by the loss in peak height.

During the 1995 HEROS observations a major burst occurred, but unfortunately very close to a gap in the observing run, when the instrument was for two weeks off the telescope. Nevertheless, the onset of the burst on MJD 49 801 can be detected both in the equivalent widths (the dotted line in Fig. 3.1, 1995 panel) and in the dynamical spectra.

Owing to the increasing optical thickness of Hα during the past few years, the distinction between major and minor bursts becomes on the basis of the variation of the Hα emission less clear than before when only a non-persistent emission disk surrounded the star. However, this classification

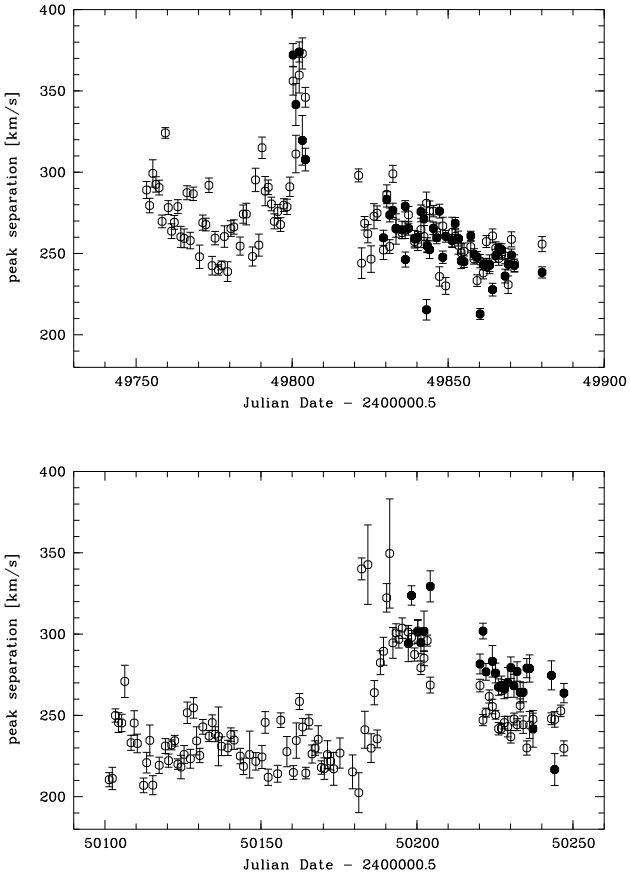

Figure 3.5: The peak separation of the Si IIλ6347 ($\circ$) and Fe II ($\bullet$) lines. For 1995 (top), the peak separations of Fe IIλ5169 and Fe IIλ5317 are averaged. For 1996 (bottom), only Fe IIλ5169 was measurable with sufficient accuracy. Note that Fe II emission becomes detectable only at the peak of an outburst (Fig. 2.1)

can still be retained if applied to other lines within the HEROS wavelength range, for instance to those of Fe II described below.

Paschen lines: The Paschen series exhibits the most drastic changes during an outburst. The emission strengthens by several Å, which is due not only to a strengthening in peak height, but also to strongly enhanced wings. The central reversal has nearly disappeared and the peak height of the line is of the order of $E/C \approx 1.2$ to 1.3. The O Iλ8446 line is not showing this strong variability. It has nearly not changed its peak height and is only slightly broader than before so that after an outburst it is weaker than the neighbouring Pa_{18} line, whereas it is stronger during quiescence. Similarly to Hα, major and minor outbursts are distinguishable by the amplitude of the increase in emission as long as the persistent emission is not too strong. This was the case in 1995 and 1996, while in 1997 the distinction was less clear.

Silicon: The Si II-emission becomes visible in $\lambda\lambda$4131,5056 and strengthens for λ6347. The peaks are at higher velocities compared to the stage of relative quiescence. In Si IIλ6347 also remnants of the emission from the previous outburst are still visible at lower velocities. This behaviour is displayed in Fig.3.4 as a dynamical spectrum and is reflected in the peak separation which seems to reach high values immediately (Fig. 3.5). It can also be seen that major outbursts are far more efficient in driving up the peak separation than are minor ones.

Iron: At the peak of major outbursts, the Fe II emission appears rather suddenly and within 10 days attains its maximum strength (cf. Fig. 2.1). It then persists throughout the outburst phase

and shows a similar behaviour as the SiII-emission. The distinction between major and minor outbursts is clearest for these iron lines: only a major burst leads to persistent emission, while the emission of a minor burst, if present at all, vanishes as the burst ceases.
Helium: In He Iλ6678 additional emission shows up at relatively high velocities. The differences between major and minor bursts are less strong in helium than they are in lines formed farther away from the star.
Finally, it should be pointed out that the pre-outburst loss in emission peak height (Sect. 3.2.2) is not always quite compensated for during the outburst and that the recovery also takes part of the relaxation phase (Sect. 3.2.4). In rare cases, a small net loss may remain well into the next outburst cycle.

3.2.4 Relaxation

In the two small bursts observed with HEROS at sufficiently high temporal resolution (see Sect. 3.3) it is found that the V/R variability is most pronounced on the ascending branch of the emission strength curve. The settling of the rapid V/R-variability is therefore adopted as the end of a burst and the beginning of the following phase to which hereafter it is referred as the relaxation phase.
Balmer lines: The wings of the emission lines attain their maximum strength at the beginning of this phase. No trace of the photospheric profile is detectable.
The decline of the wings sets in slowly while the emission peak height finally increases. This increase may continue for weeks, eventually turning over into a slow decrease when relative quiescence develops.
Although the V/R-variability has stopped, the ratio is still *not* unity. There is a general trend for the red peak to remain lower than the blue one by several percent. Only after 10 to 20 days (for major outbursts), the average V/R-ratio finally reaches unity. Line profiles that are representative of these stages are provided in Fig. 3.4.
Paschen lines: They are initially also still dominated by the broad wings (Fig. 3.4). During the course of a couple of days the wings fade slowly, the peak height decreases quite linearly, and so the shapes of the profiles asymptotically approach their quiescence appearance.
Silicon and iron: Fig. 3.5 shows the measured peak separation for Si IIλ6347 and two Fe II lines. The separation attains high values immediately after a major burst and then shrinks until the next major burst. Subsequent minor bursts only have little influence on the peak separation. An example of this behaviour is given in Fig. 2.1 in the form of a dynamical spectrum for Fe IIλ5169.
Helium: Except for a further weakening and narrowing of the emission components and ongoing V/R variability, the helium lines seem to be the first to reach the quiescent phase.

3.3 Cyclic V/R Variability

V/R is variable at virtually all times. It is perhaps the most pronounced on the ascending branch of the emission strength curve of an outburst (Sect. 3.2.3) and seen best in the strong He I lines such as those at $\lambda\lambda$5876, 6678, and 7065 Å. However, only during three, maybe four, minor bursts covered sufficiently well by the observations and one in data published by Baade (1991) it was possible to detect some temporal regularity in this behaviour.

3.3.1 HEROS Data

For the strongest and best observed small outburst (32 HEROS spectra during 5 nights) around MJD 50 232, a time series analysis using Scargle's (1982) method indicates a fixed time scale of 0.622 ± 0.005 days. The peak-to-peak amplitude is $\pm 4\%$ around unity (Fig. 3.6, lower panel).

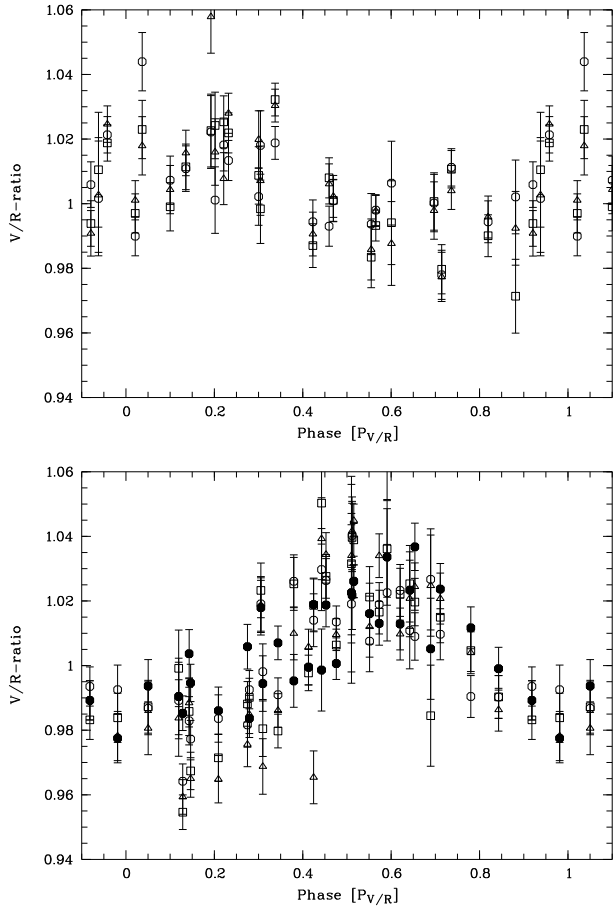

Figure 3.6: The rapid variability of the V/R-ratio of He Iλ5876 ($\Box$), He Iλ6678 ($\circ$), and He Iλ7065 ($\triangle$) during the minor bursts from MJD 50 219 to 50 225 (top) and from MJD 50 232 to 50 237 (bottom). The data have been folded with periods of 0.593 days (top) and 0.622 days (bottom), respectively. In the lower panel the V/R-ratio is also shown for Hα($\bullet$)

This variability is also visible in the emission of Hα where not only the peak height but also the position of the edges of the emission is varying with the same period. Phase diagrams for Hα and the He I lines are shown in Fig. 3.6, lower panel.
For the other well-observed (25 HEROS spectra during 6 nights) small outburst around MJD 50 223 the time scale is significantly different. During this event the same analysis technique as above reveals a period of 0.593 ± 0.009 days with a lower amplitude of $\pm 2\%$ around unity (Fig. 3.6, upper panel). No significant hydrogen V/R-variability was detected during this phase; this might be due to the lower amplitude. For a third minor outburst on MJD 50 246 the phase coverage is not good enough to allow a reliable time series analysis (9 spectra during 2 nights). However, the variability has a similar time scale and a high amplitude. Fig. 3.8 compares the power spectra corresponding to the first two events to the power spectrum of all HEROS data.

3.3.2 Boller&Chivens Data

A simple MIDAS procedure was written which automatically fits a second order polynomial to the continuum between 4820 and 4910 Å and one Gaussian each to the broad absorption and the two emission components of Hβ. Although both the full width at half maximum (FWHM) and the separation of the two emission components exceed the nominal width of a spectral resolution element by no more than 30% and their peak heights amount to only 10$\pm$5% of the local continuum, the fitting procedure seriously diverged in less than 5-10% of all spectra. The results proved

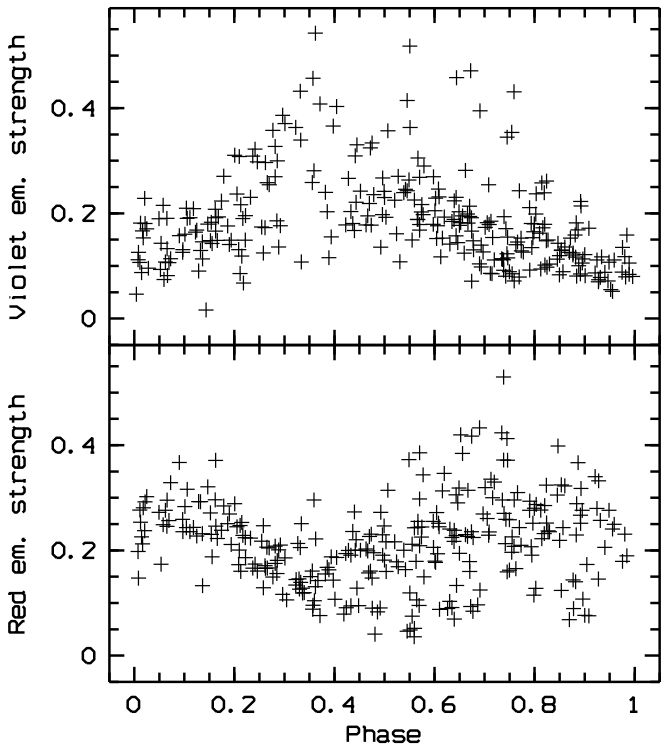

Figure 3.7: The trend-corrected cyclic variability of the Hβ emission in the Boller&Chivens spectra folded with a period of 0.583 d (Sect. 3.3.2). Shown is the product of the peak height (in units of the continuum) and the FWHM (in Å) of the violet (top) and the red (bottom) component, respectively. For details see Sect. 3.3.2

to be fairly robust against modifications of the initial guesses. Since, furthermore, the parameters derived from 'upper' and 'lower' spectra agree well, the large number of spectra and the high temporal sampling provide for a meaningful time series analysis (TSA).

The period search in the Boller&Chivens spectra was performed with the analysis-of-variance (AOV; Schwarzenberg-Czerny 1989) and Scargle's (1982) method implemented in the MIDAS TSA package (Schwarzenberg-Czerny, 1993; ESO-MIDAS, 1995). The analysis covers the frequency range from 0 to 10 c/d within which the window spectrum virtually consists of nothing but strong features at 0, 1, and 2 c/d. Albeit the two methods yielded essentially the same results, the peaks of the window spectrum turned out to be much less disturbing in the AOV statistics. Therefore, the results reported below rest mainly on the AOV method. Results on other quantities measured in the B&C data, such as the radial velocity of different absorption lines, are reported in Sect. 4.1.3.

Of the parameters fitted to the emission components, the FWHM, the peak height (in units of the continuum), and the radial velocity were subjected to a separate TSA for the absorption and the violet and red component. Only the results of the period search in the radial velocities (RVs) of the emission peaks were negative, with a crude detection limit of 10 $\mathrm{km\,s^{-1}}$ (peak to peak). The positive detections are as follows:

1. The height of the violet peak varies with a cycle time of 0.576 d.
2. The red peak height varies cyclically with $\mathcal{P} = 0.571$ d but in antiphase with respect to the violet peak.
3. The FWHM of the violet peak varies with a cycle time of 0.571 d and is in phase with the variability in height of the violet peak.
4. The variability of the red FWHM has a cycle length of 0.569 d but is in antiphase with the

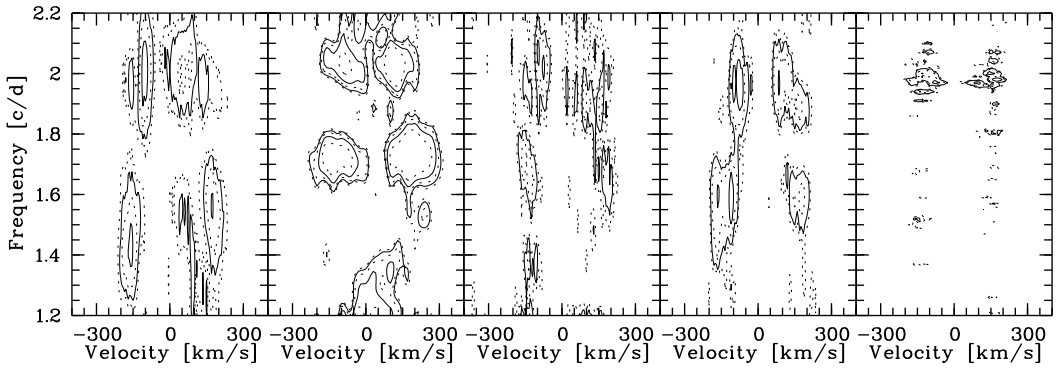

Figure 3.8: Power spectra of He Iλ6678 during the bursts described in Sect. 3.3. Contours in each panel mark areas of constant power (in arbitrary units) as a function of radial velocity (w.r.t. the star's systemic velocity) and frequency. They were derived by Fourier analysing the flux in narrow slices of the line profile. From left to right are shown (i) the burst during April 1986 found in Baade's (1991) CAT/CES data (Sect. 3.3.3), (ii) the burst detected in the 1995 B&C observations (Sect. 3.3.2; since He Iλ6678 was not covered by these data, He Iλ4471 is used instead), (iii) the burst on MJD 50 223 and (iv) the one on MJD 50 232, both observed in 1996 with HEROS (Sect. 3.3.1), and, for comparison, (v) the power spectrum of *all* HEROS spectra from 1995 to 1997. The first four panels display enhanced power in the range 1.4-1.7 c/d and at the RVs of the emission components. These features correspond to the cyclic V/R variability during outbursts Sect.3.3. The fifth panel does not contain significant power at these frequencies because the proportion of HEROS spectra taken during outbursts is very small compared to the whole dataset. Finally, the features at $f = 2$ c/d and somewhat lower radial velocities are due to the photospheric variability (cf. Chapter 4). Note that for the CAT/CES data and the burst on MJD 50 232 (panels i and iv, respectively) the blue power peak is stronger than the red one at $f = 2$ c/d

violet FWHM.

5. The velocity of the underlying broad absorption line also varies cyclically, the cycle time being 0.583 d.

For the peak heights, only a relatively minor part of the total power is accounted for by the periods stated, and none of the variations should be considered to be truly periodic. But the reality of the repetitive behaviour is indisputable in all 4 cases whereas the differences between the quasi-periods is regarded as insignificant. Fig. 3.7 shows the data folded with $\mathcal{P} = 0.583$ d, which is derived from the RVs of the broad absorption component and probably the most reliable. It clearly illustrates the pronounced cyclic V/R variability of the Hβ emission. (In the phase diagram for the B&C data MJD = 0.0 has been arbitrarily chosen as the epoch of phase zero, irrespective of the period.)

The length of the V/R cycles in the Boller&Chivens spectra is quite similar to those found at other epochs with HEROS (Sect. 3.3.1). Since furthermore the prominence of rapid cyclic V/R variability seems to be linked to the outburst activity, the Hβ observations suggest that the observing run with the Boller&Chivens spectrograph fell into an outburst of μ Cen. This is also supported by the preliminary periodic ephemeris for the outbursts which was derived from a time series analysis of stellar and circumstellar lines (Rivinius et al., 1998c, Chapter 6).

3.3.3 Previous CAT/CES Data

Only the profiles of He Iλ6678 obtained on April 1–5, 9, and 10, 1986 (Baade, 1991) were studied in more detail because only in them significant V/R variations were visible, especially during April 1-5. After a re-analysis of the 71 spectra from these five nights, a cycle length of about 0.69

Table 3.2: Velocities and equivalent widths of the temporary high velocity absorption components during 3 events described in Sect. 3.4 for different He I lines. The typical errors are $\sim 7\,\mathrm{km\,s^{-1}}$ for v_{hivel} and ~ 15 mÅ for W_λ. For the He I$\lambda\lambda$3820,4026,4471 lines the average profile of the 1996 run has been subtracted before fitting a Gaussian to the additional absorption. Therefore, larger errors are to be expected especially for v_{hivel} in these lines

Mod. Jul. Date	50 185.31		50 457.36		50 461.36	
	v_{hivel} [$\mathrm{km\,s^{-1}}$]	W_λ [mÅ]	v_{hivel} [$\mathrm{km\,s^{-1}}$]	W_λ [mÅ]	v_{hivel} [$\mathrm{km\,s^{-1}}$]	W_λ [mÅ]
He Iλ6678	–212	80	–181	70	–210	60
He Iλ5876	–218	45	–194	15	–226	15
He Iλ4471	–218	42	–173	20	not detectable	
He Iλ4026	–238	43	not detectable		not detectable	
He Iλ3820	–250	33	–174	40	not detectable	

days became apparent for the V/R variability. The corresponding power spectrum is presented in Fig. 3.8.

Like for the Boller&Chivens spectra (Sect. 3.3.2), the similarity of the time scales and the correlation between the occurrence of V/R variability and outbursts (Sect. 3.3) suggest that also the CAT/CES spectra of April 1-5, 1986 were obtained during an outburst. In fact, this is again (cf. Sect. 3.3.2) confirmed by the preliminary periodic ephemeris described and explained by Rivinius et al. (1998c) for the times of outbursts. The few contemporaneous Hα profiles and their extreme V/R variability are reminiscent of those observed by Baade et al. (1988) during the 1987 February outburst. But the phase of the initial sharp rise of the emission strength seems to have been just missed.

3.4 Transient High-Velocity Absorption Components

During the precursor phase, but also at the beginning of an outburst, transient high velocity absorption components may develop. They only appear at RVs more negative than $-v \sin i$, i.e. only on the blue side and at super-rotational values. When they are present, they can be seen in *all* stronger He I lines (Table 3.2 and Fig. 3.4). However they were not detected in hydrogen or other lines. In μ Cen, such an event was first observed by Peters (1986) in March 1985 when it was also followed by an episode of enhanced Hα emission.

In 1996, the increase of the emission wings of the major outburst began around MJD 50 185 with the appearance of the high-velocity absorptions (the dotted line in Fig. 3.1, 1996 panel). A similar but weaker high-velocity absorption event was observed in January 1997 on MJD 50 457. In Peters' observations, Hα was in emission already at least one hour prior to the helium absorption event. In 1997, another event happened on MJD 50 461, i.e. only 4 days after the one described above. Interestingly, a single spectrum taken in between, namely on MJD 50 459, showed no trace of additional absorption.

In all three cases the lifetime of the high-velocity absorption features is unfortunately only ill-constrained by the sampling of the data. In 1996 it was at most one day and in 1997 at most two days. For the same reason, nothing can be said about any possible migration or not of the high-velocity features. But from Table 3.2 it can be seen that for a given spectral line all three events occurred within a narrow range of only $\pm 20\,\mathrm{km\,s^{-1}}$. Even the most pronounced event had only a depth of about 2% of the continuum flux.

4. Stellar Absorption Line Profile Variability

4.1 Time Series Analysis of Scalar Parameters

4.1.1 FLASH/HEROS Observations

4.1.1.1 Radial Velocities

In the 392 spectra obtained between 1992 and 1997 radial velocities (RV's) were interactively measured in two groups of lines by fitting Gaussians to the line centers.

Note that the bare position of the measured Gaussian has no direct physical meaning. But in the presence of noise a fitted function has the purely technical advantage of better numerical robustness than quantities such as line profile moments. Moreover, the interactive fitting of only the line cores proved to provide a critical safeguard against temporarily occuring profile anomalies (Sect. 4.3) which would otherwise have seriously hampered the time series analysis.

The groups of lines consist of the He I$\lambda\lambda$4121,4168,4438 and the Si III$\lambda\lambda$4553,4568 lines, respectively. They were chosen since they are least influenced by line emission. It was also attempted to measure the RV in the wings of the lines. But the results proved to be much noisier than the ones measured in the line centers. This could either be caused by the selection of relatively weak lines at the S/N limit or it could be a more principal problem of undetected variable, double-peaked trace emission in the line wings.

Si III$\lambda\lambda$4553,4568 never showed intrinsic emission in the available database. Although the blue wing of Si IIIλ4553 is blended with Fe IIλ4549 emission, the line center can be measured with the same accuracy as Si IIIλ4568. Nevertheless, these silicon lines seem to be slightly less well behaved than the helium lines measured. For the helium lines, too, trace emission cannot be excluded at the 0.5% level. However, intrinsic emission, if present, would be concentrated in the line wings whereas there are no obvious inconsistencies between the selected lines (which would arise from contamination by line emission). Accordingly, the velocity variations in the line centers should be of the star itself.

On both data sets, a time series analysis was performed in the frequency range from 0 to 6 c/d. For this purpose, Scargle's (1982) method was adopted and previously found periods were iteratively removed using the procedure described by Kaufer et al. (1996). Owing to the highly uniform sampling, the window function is nearly featureless except for n c/d-features, with n being small integer numbers (Fig. 4.1). It turned out that the previously suspected period of 0.505 day (Baade, 1984a) actually consists of four periods, $\mathcal{P}_1$-$\mathcal{P}_4$, close to 0.5 day. They are so closely spaced (< 0.01 day) that they cannot be resolved in data strings resulting from single-season observing runs. The possibility of $\mathcal{P} = 0.33$ d considered by Baade (1991) as an alternative to the (then unresolved) 0.505-day period can be firmly rejected. A fifth and sixth period around 0.28 day were found in the He I RV's only. Of all these, $\mathcal{P}_1$ by far has the largest power and amplitude associated with it (Table 4.1). In Fig. 4.2 the original RV data are shown together with the residuals after recursive, sinusoidal prewhitening and folded with the respective next period to be removed.

Prewhitening for $\mathcal{P}_5$ reduces the scatter of the 392 He I RV's after previous removal of $\mathcal{P}_1$ from 13.5 to 12.2 $\mathrm{km\,s^{-1}}$. In the power spectrum (Deeming, 1975) it is, in fact, as strong as $\mathcal{P}_2$ of the He I radial velocity data after a sinefit with $\mathcal{P}_1$ has been subtracted (Fig. 4.1). As can be seen in Fig. 4.7, folding the data with $\mathcal{P}_5$ and $\mathcal{P}_6$ not only yields reasonable-looking RV curves but also

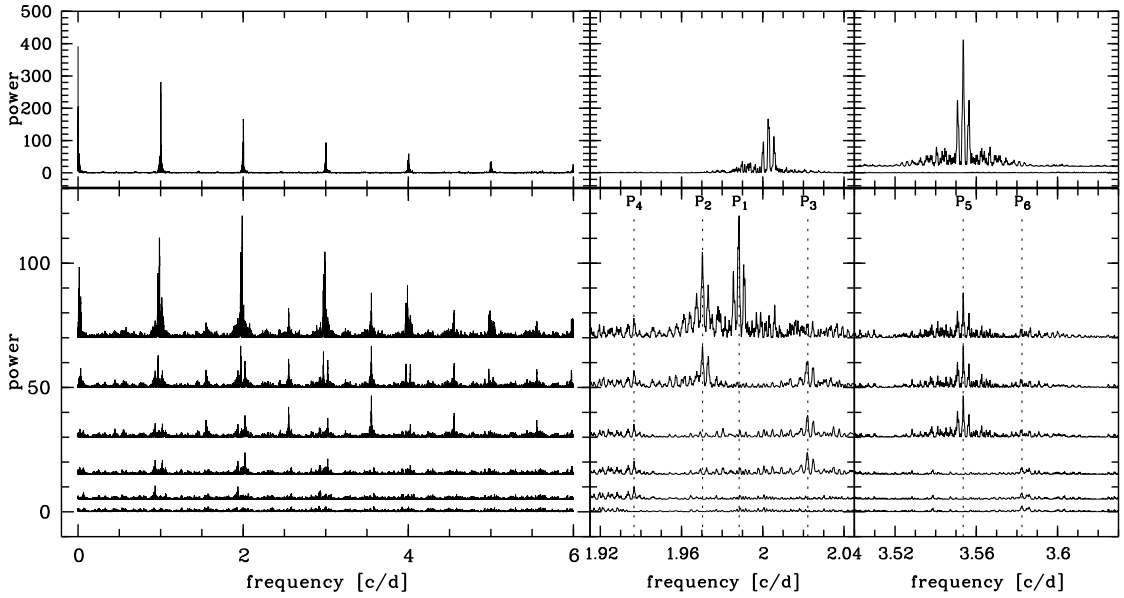

Figure 4.1: Window functions (top panels) and power spectra (bottom panels) of the HEROS radial velocities of the He I group of lines (Sect. 4.1.1). From left to right the full power spectrum between 0 and 6 c/d and the windows around the two groups of periods (Table 4.1) are shown. In the region around 3.5 c/d the window function is featureless. The window centered on $\mathcal{P}_5$ is overplotted with an offset of 20. In the lower panels, the power spectrum is plotted for the original data as well as after successive prewhitening for sinusoidal variations with periods $\mathcal{P}_1$, $\mathcal{P}_2$, $\mathcal{P}_5$, $\mathcal{P}_3$ and $\mathcal{P}_4$. In the bottom power spectrum only $\mathcal{P}_6$ is left

coherent patterns of the associated line profile variability. The amplitudes and phases, which are by-products of the prewhitening by subtracting fitted sinewaves, are also listed in Table 4.1.

4.1.1.2 Other Quantities

The radial velocities used in the previous section were measured interactively in spectral lines that were chosen with great care to be free of emission effects. These measurements were made in lines cores only, so that fitted parameters other than the position have no meaning. It was therefore also tried to characterize the overall profile variations by applying an automatic procedure to a larger number of spectral lines.

It turned out that the parameters of Gaussians fitted to the whole line profile showed significant medium-term variations. They are probably connected to the line-emission activity (Chapter 3) and possibly also to the temporary occurrence of additional absorption spikes (Sect. 4.3). This suggests that TSA's of global parameters can only be made over time scales shorter than the typical outburst cycle length of 1-2 months (Chapter 3). This is much too short to resolve the fine structure of the 0.5- and 0.28-day groups of periods.

4.1.2 CAT/CES + HEROS He Iλ6678 Radial elocities

The CAT/CES spectra obtained in the 1980's were all collected in annual runs of typically 10 nights. They themselves do not permit a proper analysis of the multiperiodicity to be performed. But a combined TSA together with the FLASH/HEROS data is desirable because this could lead to more precise values of the periods and an assessment of their phase coherence on long time scales. The latter is important for the interpretation of the nature of the variability.

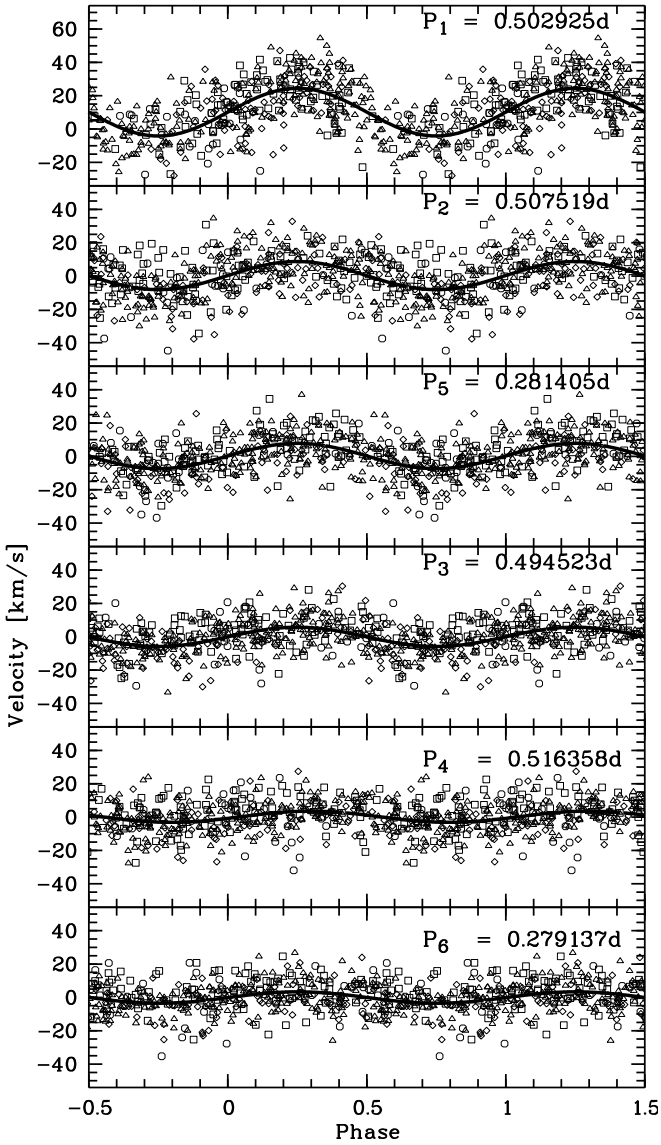

Figure 4.2: The iterative prewhitening of the averaged radial velocities of the cores of the He I $\lambda\lambda$4121,4168,4438 lines (Sect. 4.1.1). The periods, phases and amplitudes of the fitted sine curves (smooth lines) are given in Table 4.1, upper panel. The uppermost panel of the figure shows the original data folded with $\mathcal{P}_1$. The next panels contain the residuals from the respective previous fit folded with the next period to be prewhitened for. The symbols denote the years 1992 ($\circ$), 1995 ($\square$), 1996 ($\triangle$), and 1997 ($\diamond$). Note that the prewhitening is done in the order of decreasing associated power, i.e. does *not* follow the numbering scheme of the periodicities

Unfortunately, the CAT/CES spectra are not ideally suited for this purpose: (i) They only cover the single line of He Iλ6678 which is significantly contaminated by line emission. (ii) Some of the CAT/CES observing runs happened to take place close to an outburst so that the line emission is strongly variable. (iii) The narrow absorption spikes described in Sect. 4.3 are particularly prominent in this line.

These shortcomings are partly compensated for by the very high S/N and spectral resolution. Furthermore, the recovery of the FLASH/HEROS periods in the CAT/CES spectra, which have a completely different temporal sampling, would further consolidate the results of the TSA of the FLASH/HEROS data.

For such a combined analysis, also the RVs of the He Iλ6678 line were measured in the FLASH/HEROS spectra as described for the emission-free lines in Sect. 4.1.1. The CAT/CES He Iλ6678 line profiles were filtered with a Gaussian with a half-width corresponding to the one of the HEROS

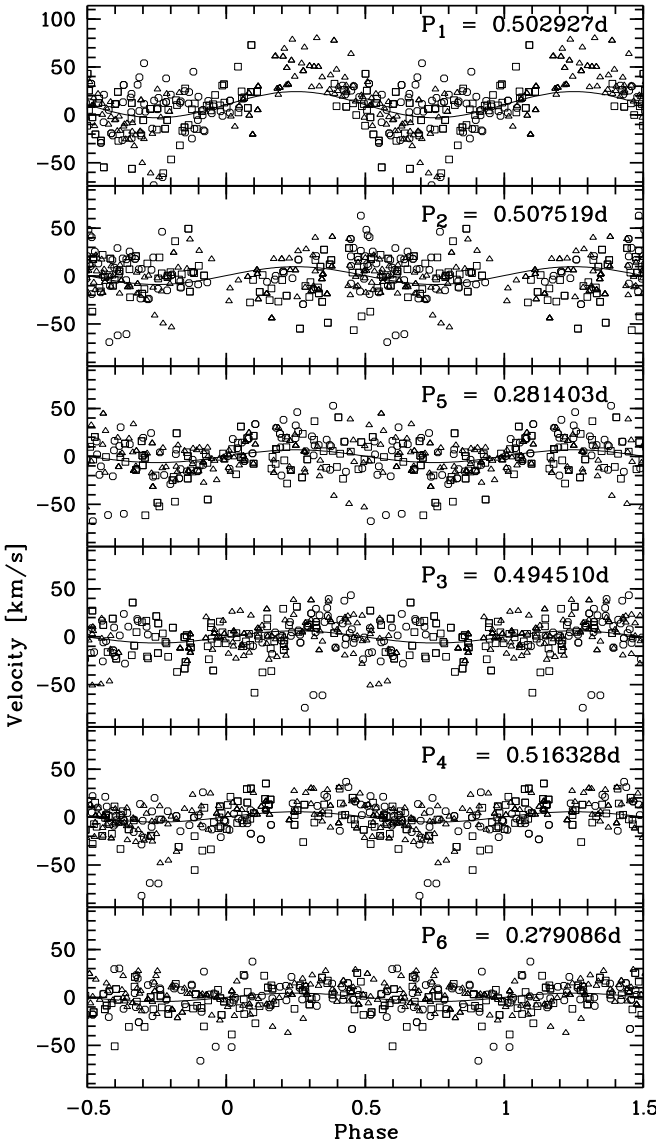

Figure 4.3: Similar to Fig. 4.2, the CAT/CES data (cf. Sect. 4.1.2) of λ6678 in 1985 ($\circ$), 1986 ($\square$), and 1987 ($\triangle$) are shown folded with the periods given in Table 4.1, bottom panel. The uppermost panel displays the original data, the following panels the residuals after prewhitening. Since the CAT/CES data proved to have significant deviations from a sinusoidal variability, the data were for each period sorted into 20 phase bins and in each bin the mean value was subtracted for prewhitening. The sinusoids overplotted were derived only from the HEROS data of λ6678. They underline the agreement of both data sets as well as the long-term phase coherence of the variability

line-spread function ($\approx 7.5\,\mathrm{km\,s^{-1}}$). The radial velocities were measured in the same way as for the FLASH/HEROS spectra.

First, a TSA only of the CAT/CES data over the range from 0 to 15 c/d was performed, for each observing run as well as all 1985-1987 data together. Significant power appears again at periods of 0.5 and 0.28 day. No evidence was found for other periods (or groups of periods) with significant power. The structure of the power spectrum at 0.5 day cannot be used to establish the periods found in the FLASH/HEROS data. But it clearly cannot be accounted for by a single period and is fully compatible with the TSA results of the FLASH/HEROS data.

A comparison of the FLASH/HEROS and the CAT/CES He Iλ6678 radial velocities indicates a somewhat higher amplitude for the CAT/CES data. This is probably a consequence of the imperfect degradation of the resolving power to that of FLASH/HEROS. The large difference in S/N, namely > 500 for CAT/CES vs. 100-200 for HEROS would have a similar effect. More impor-

Table 4.1: Parameters for the sine fits (Sects. 4.1.1 and 4.1.2 and Figs. 4.2 and 4.3) of the RV-variability in the line cores of He I$\lambda\lambda$4121,4168,4438 (top), of Si III$\lambda\lambda$4553,4568 (middle), and He Iλ6678 (bottom). The He Iλ6678 data also include 291 CAT/CES spectra taken from 1985 to 1987. The apparent lack of $\mathcal{P}_2$ in this data set is a consequence of the limited time base of the data sets in 1985 to 1987. Although the amplitude associated with $\mathcal{P}_5$ and $\mathcal{P}_6$ is strong enough to be detected in the He I lines, it is not seen at the 3-$\mathrm{km\,s^{-1}}$ level in the Si III lines. Note that the periods in the upper and middle panel have been derived using Scargle's method, while those in the lower panel were determined with Stellingwerf's phase dispersion minimization method. The reasons for using different techniques are discussed in Sect. 4.1.2

He I$\lambda\lambda$4121,4168,4438 (FLASH/HEROS 1992-1997):			
	Period $\mathcal{P}$ [days]	Phase ϕ at MJD 50 000	Amplitude A [$\mathrm{km\,s^{-1}}$]
$\mathcal{P}_1$	$0\overset{\mathrm{d}}{.}502925 \pm 0\overset{\mathrm{d}}{.}000006$	$0\overset{\mathrm{p}}{.}897 \pm 0\overset{\mathrm{p}}{.}010$	14.3 ± 1.0
$\mathcal{P}_2$	$0\overset{\mathrm{d}}{.}507519 \pm 0\overset{\mathrm{d}}{.}000009$	$0\overset{\mathrm{p}}{.}150 \pm 0\overset{\mathrm{p}}{.}016$	8.4 ± 0.9
$\mathcal{P}_3$	$0\overset{\mathrm{d}}{.}494523 \pm 0\overset{\mathrm{d}}{.}000011$	$0\overset{\mathrm{p}}{.}646 \pm 0\overset{\mathrm{p}}{.}019$	5.8 ± 0.7
$\mathcal{P}_4$	$0\overset{\mathrm{d}}{.}516358 \pm 0\overset{\mathrm{d}}{.}000015$	$0\overset{\mathrm{p}}{.}922 \pm 0\overset{\mathrm{p}}{.}022$	4.8 ± 0.7
$\mathcal{P}_5$	$0\overset{\mathrm{d}}{.}281405 \pm 0\overset{\mathrm{d}}{.}000005$	$0\overset{\mathrm{p}}{.}850 \pm 0\overset{\mathrm{p}}{.}017$	7.6 ± 0.7
$\mathcal{P}_6$	$0\overset{\mathrm{d}}{.}279137 \pm 0\overset{\mathrm{d}}{.}000008$	$0\overset{\mathrm{p}}{.}425 \pm 0\overset{\mathrm{p}}{.}032$	3.3 ± 0.7
Si III$\lambda\lambda$4553,4568 (FLASH/HEROS 1992-1997):			
	Period $\mathcal{P}$ [days]	Phase ϕ at MJD 50 000	Amplitude A [$\mathrm{km\,s^{-1}}$]
$\mathcal{P}_1$	$0\overset{\mathrm{d}}{.}502917 \pm 0\overset{\mathrm{d}}{.}000007$	$0\overset{\mathrm{p}}{.}872 \pm 0\overset{\mathrm{p}}{.}013$	14.8 ± 1.2
$\mathcal{P}_2$	$0\overset{\mathrm{d}}{.}507519 \pm 0\overset{\mathrm{d}}{.}000010$	$0\overset{\mathrm{p}}{.}177 \pm 0\overset{\mathrm{p}}{.}018$	9.7 ± 1.1
$\mathcal{P}_3$	$0\overset{\mathrm{d}}{.}494523 \pm 0\overset{\mathrm{d}}{.}000009$	$0\overset{\mathrm{p}}{.}612 \pm 0\overset{\mathrm{p}}{.}018$	9.0 ± 1.0
$\mathcal{P}_4$	$0\overset{\mathrm{d}}{.}516262 \pm 0\overset{\mathrm{d}}{.}000024$	$0\overset{\mathrm{p}}{.}884 \pm 0\overset{\mathrm{p}}{.}041$	3.8 ± 1.0
$\mathcal{P}_5$	not significant		
$\mathcal{P}_6$	not significant		
He Iλ6678 (CAT/CES 1985-1987 and FLASH/HEROS 1992-1997):			
	Period $\mathcal{P}$ [days]	Phase ϕ at MJD 50 000	Amplitude A [$\mathrm{km\,s^{-1}}$]
$\mathcal{P}_1$	$0\overset{\mathrm{d}}{.}502927 \pm 0\overset{\mathrm{d}}{.}000003$	$0\overset{\mathrm{p}}{.}950 \pm 0\overset{\mathrm{p}}{.}011$	17.0 ± 1.2
$\mathcal{P}_2$	not applicable		
$\mathcal{P}_3$	$0\overset{\mathrm{d}}{.}494510 \pm 0\overset{\mathrm{d}}{.}000004$	$0\overset{\mathrm{p}}{.}610 \pm 0\overset{\mathrm{p}}{.}022$	8.0 ± 1.1
$\mathcal{P}_4$	$0\overset{\mathrm{d}}{.}516328 \pm 0\overset{\mathrm{d}}{.}000005$	$0\overset{\mathrm{p}}{.}898 \pm 0\overset{\mathrm{p}}{.}016$	10.1 ± 1.1
$\mathcal{P}_5$	$0\overset{\mathrm{d}}{.}281403 \pm 0\overset{\mathrm{d}}{.}000002$	$0\overset{\mathrm{p}}{.}841 \pm 0\overset{\mathrm{p}}{.}019$	8.5 ± 1.0
$\mathcal{P}_6$	$0\overset{\mathrm{d}}{.}279086 \pm 0\overset{\mathrm{d}}{.}000003$	$0\overset{\mathrm{p}}{.}136 \pm 0\overset{\mathrm{p}}{.}043$	3.6 ± 1.0

tantly, the comparison finds no hint of a difference between the two data sets in the zero point. This conclusion is necessarily somewhat uncertain due to the obviously limited phase coverage of all 0.5-day periods by the 10-day CAT/CES observing runs. But a correction for any such systematic difference was not applied.

The final combined data set consists of 392 FLASH/HEROS and 291 CAT/CES radial velocities of He Iλ6678. The latter only comprise the main data strings from the observing runs in 1985, 1986, and 1987. Given the very high level of activity of the star in this line, inclusion of a few isolated profiles would do more harm than good.

The TSA was done as described for the emission-free lines in Section 4.1.1, i.e. with Scargle's method. In addition, Stellingwerf's (1978) phase dispersion minimization (PDM) technique was used. Since the merged data are not as homogenous as the FLASH/HEROS data alone, Scargle's method, which is based on the assumption of sinusoidal variability, is less effective than the PDM method which is independent of the signal shape. I.e. the close aliases produced by the five years

Table 4.2: Overview of the periods derived from the time series analysis of the Boller&Chivens spectra as a function of spectral line group and (absorption) line profile parameter. Note that the 0.28 day period value is the *adopted* number; for a discussion see Sects. 4.1.3.1-4.1.3.3, and Sect. 3.3.2 respectively. The short time base of only 8 nights excluded detection of the 0.505-d group of periods (Sect. 4.1.1)

	V/R	RV	Depth	FWHM
Hβ	0.58	0.58	0.28	0.28
Hγ(-Hϵ)	–	0.58	0.58	0.28
H10-H12	–	0.58	0.62	0.28
He I	–	0.58	–	–

gap between 1987 and 1992 are of comparable height if computed by Scargle's method due to the significant non-sinusodial shape of the CAT/CES RV curve (see Fig. 4.3). Besides this problem, the Scargle statistics always gives sharp peaks that coincide within the errors with the results of the PDM method. It is however not possible for the Scargle method alone to distinguish these peaks from their close aliases.
The periods listed in Table 4.1 (bottom panel) are based on the PDM method. They do not only agree with those derived from the FLASH/HEROS spectra but actually improve on them. Conversely, the phases and amplitudes for the combined data set had to be derived using Scargle's method (Table 4.1, bottom panel). Owing to the amplitude inhomogeneity, they are less certain than are those of the FLASH/HEROS data subset.
A histogram of the $\mathcal{P}_2$ phases of the CAT/CES data shows that the observations are rather unevenly distributed (see also Fig. 4.3, second panel). For the other periods some phase-clustering is still noticeable but much less pronounced. For this reason, it is only possible to conclude that the CAT/CES results are not in conflict with the hypothesis of $\mathcal{P}_2$ being present. Its value can, therefore, not be improved by combining the two data sets.
The remarkable agreement of the periods derived for the three groups of spectral lines and the two data sets from two different instruments as evidenced by Table 4.1 is indicative of their numerical and physical stability and their phase coherence on a time scale of a decade. Nevertheless, Sect. 7.3 carefully analyses (and rejects) numerous possible sources of systematic errors.

4.1.3 Boller&Chivens Observations

As described in Sect. 3.3.2, we used the analysis-of-variance (AOV; Schwarzenberg-Czerny 1989) and Scargle's (1982) method implemented in the MIDAS TSA package (ESO-MIDAS, 1995; Schwarzenberg-Czerny, 1993) to analyze the Boller&Chivens data in the range from 0 to 10 c/d. As for the emission lines, results achieved with both methods for the photospheric lines do not significantly deviate from each other. However the main peaks in the window function at 1 and 2 c/d are less strong in the AOV statistics so that the following mainly rests on this method. In most of the parameters fitted, there are quite noticeable night-to-night variations, the elimination of which made the features in the AOV statistics reported below become more significant. But it was carefully verified that this trend removal did not introduce these features.
'Upper' and 'lower' spectra (see Sect. 3.3.2) Sect. 2.2 for a description of the observations and their reduction) were at least initially always kept separate. However, robust regression analyses showed the information content of the sets of 'upper' and 'lower' spectra to be very much the same. Apart from the modulation-to-noise ratio, which for some observables differed quite noticeably, significant differences were neither found between the time dependence of 'upper' and 'lower'

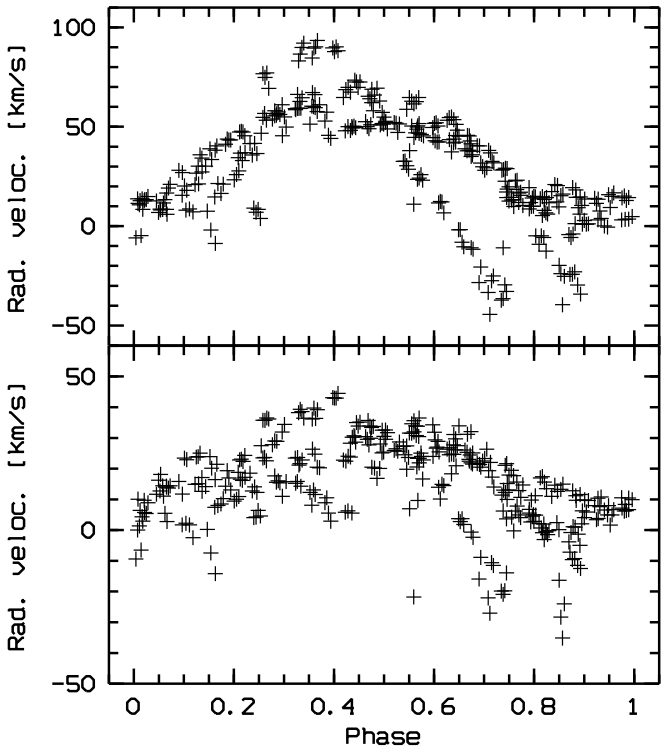

Figure 4.4: The Boller&Chivens radial velocity data folded with $\mathcal{P} = 0.583$ d. Upper panel: Balmer lines Hγ-H12; lower panel: Helium lines (in both cases mean of 'upper' and 'lower' spectra'). For details see Sect. 4.1.3.1

spectra.
The short time baseline of only 8 nights a priori excluded detection of the 0.505 d period found in the HEROS spectra (Sect. 4.1.1). But it can be suspected to contribute noticeably to the apparent noise associated with some other variabilities. Moreover, the short time baseline does not permit the question to be addressed whether the variations are truly periodic, i.e., not merely a transient phenomenon. In fact, the latter appears relatively likely.
An overview of the results is provided in Table 4.2.

4.1.3.1 Radial Velocities

A non-interactive MIDAS procedure was used to measure positions, full widths at half maximum (FWHM), and line depths by simultaneously fitting a second-order polynomial (to approximate the continuum) and a Gaussian over a range of $\pm 650\,\mathrm{km\,s^{-1}}$ around the nominal positions of 26 spectral lines. Separate mean values were formed for Hγ-H12 as well as for the He I lines at 3820, 3927, 4009, 4026, 4121, 4144, 4388, 4471, and 4922 Å. For either data set a linear regression analysis was performed between the measurements made in the 'lower' and the 'upper' spectra. From these regression analyses, a typical error of $\pm\,14\,\mathrm{km\,s^{-1}}$ was derived.
Furthermore, there is a systematic difference between 'upper' and 'lower' spectra which decreases linearly from $30\,\mathrm{km\,s^{-1}}$ at 3500 Å to $13\,\mathrm{km\,s^{-1}}$ at 4500 Å and from there on remains constant. The explanation for this difference is that, as RV measurements were not among the original aims of the observations, the arc spectrum was only extracted at the center of the slit but used to calibrate both the 'lower' and 'upper' spectra. The arc spectra were also taken relatively infrequently. Since the difference between 'lower' and 'upper' spectrum is systematic and because of the very high temporal sampling, the overall significance of a time series analysis should at the frequencies of interest (0.5-2 c/d) be unabated.

The most prominent feature in the AOV (and Scargle) statistics appeared at a position corresponding to 0.585 ± 0.003 d which correction for a small trend changed only insignificantly to 0.583 day. For the Balmer lines this feature is 2.5 times as strong as the n c/d peaks whereas in the case of the helium lines they are of comparable strength. The peak-to-valley amplitudes are $\sim$50 and $15\,\mathrm{km\,s^{-1}}$ for the Balmer and the helium lines, respectively. Fig. 4.4 displays examples of the resulting RV curves.
It is obvious from Fig. 4.4 that even though the formal significance of the 0.583-day time scale is high, the deviations from a simple sinusoidal variation are equally important. On the other hand, after prewhitening for a sinusoidal variation with the 0.583-day period, no significant peaks remained in the AOV and Scargle statistics that were not obviously related to the window spectrum. Because even after explicit separate fitting of the two emission components described in Sect. 3.3.2 the broad stellar absorption of Hβ shows the same RV curve as do the other Balmer lines, it is not likely that in the higher Balmer lines underlying undetected V/R variability masquerades as RV variability. However, it is not excluded that in Hβ there are variable broad emission wings which the decomposition process described in Sect. 3.3.2 does not include. An indication of this possibility may be that the violet emission peak is highest when the absorption core is most redshifted and vice versa.
Given the special nature and purpose of the Boller&Chivens spectra, one must be concerned that the RV variations, even though quasi-periodic, are only an artifact. In fact, this could be imagined in several ways. However, we have not found a possibility to trace back any of them to the antiphased variability of the peak height and width of the very closely spaced V and R components of the Hβ emission (Sect. 3.3.2). The virtual identity of the quasi-periods should, therefore, prove the reality of the RV variations.
Folding the stellar RV's with both 0.281 and 0.622 day (cf. Sects. 4.1.1, 4.1.3.2, and 4.1.3.3) did not yield meaningful phase diagrams.

4.1.3.2 Line Depths

Line depths in units of the adjacent continuum were derived by ratioing the fitted height of the Gaussian (Sect. 4.1.3.1) with the value of the simultaneously fitted second-order polynomial approximating the run of the neighbouring continuum. Four data sets were studied: (i) the mean of the Balmer lines H10-H12, (ii) Hγ, (iii) Hβ, and (iv) the mean of the He I lines at 3820, 4026, 4388, and 4471 Å. Periodic variability of the helium line depths was not found even after a sophisticated correction for the night-to-night variations.
In the Scargle statistics for H10-H12, the strongest feature is at a period of 0.62 day, and the one for Hγ appears at 0.59 day. The modulation-to-noise ratio of the phase diagrams is low with a peak-to-peak amplitude of only $\leq$2% of the continuum flux. Furthermore, even though the difference between 0.62 and 0.583 day is not large, the latter quasi-period, which is also the one of the RV's (Sect. 4.1.3.1), including Hγ, does not nearly adequately describe the variability of the depths of H10-H12. Still more discrepant is the case of the fitted depth of the broad Hβ absorption (Sect. 3.3.2). In the AOV statistics of the trend corrected data only the 0.395/0.653/0.283-d group of periods is clearly visible which are discussed in Sect. 4.1.3.3. Phase diagrams for all 3 groups of Balmer lines are shown in Fig. 4.5.

4.1.3.3 Full Widths at Half Maximum (FWHM's)

Using the same procedure as before (Sects. 4.1.3.1 and 4.1.3.2; a distinction between upper and lower spectra proved to be unnecessary), the TSA of the mean FWHM of Hβ (Sect. 3.3.2), Hγ-Hϵ,

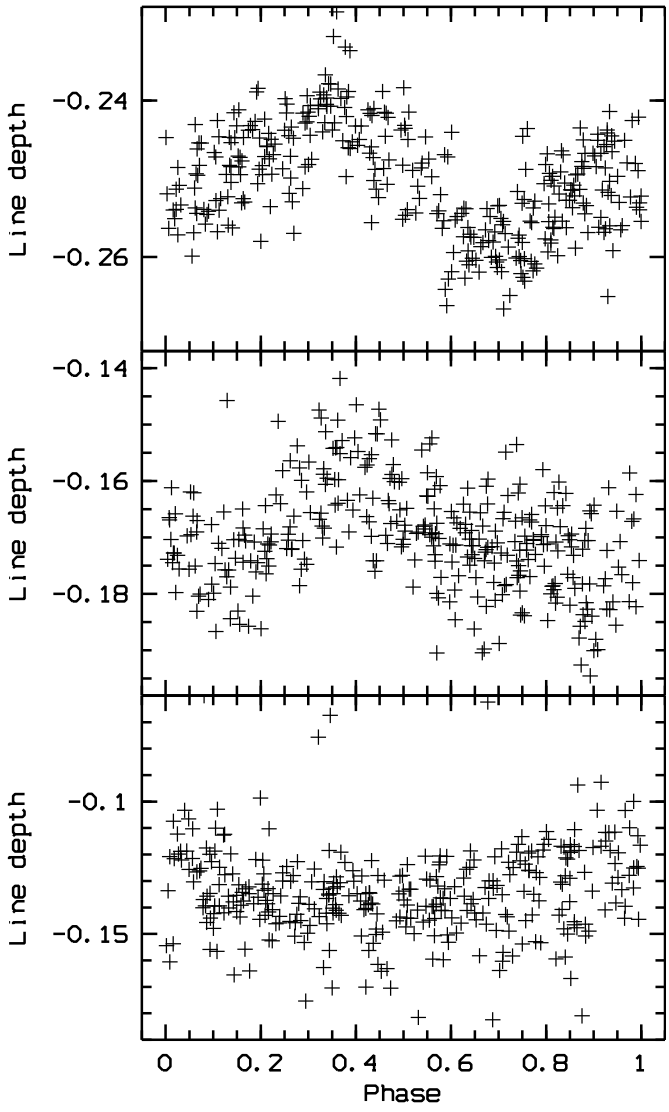

Figure 4.5: Variation of the line depths measured relative to the ambient continuum in the Boller&Chivens spectra of H8-H10 with $\mathcal{P} = 0.62$ d (top), of Hγ with $\mathcal{P} = 0.583$ d (middle), and of Hβ with $\mathcal{P} = 0.281$ d (bottom; all after correction for night-to-night variations). In all three cases, MJD = 0 has been arbitrarily chosen as epoch of phase zero. For details see Sect. 4.1.3.2

and H8-H10 found pronounced peaks in the AOV spectra near (in order of decreasing strength) 0.395, 0.653, and 0.283 d, respectively, which are all 1 c/d aliases of one another. By contrast, no trace of a variation with 0.58 d could be detected, even after removal of substantial night-to-night variations. The peak-to-valley amplitudes are slightly less than 5, 10 and 15%, respectively, for the three sets of Balmer lines.

Phase plots with these three periods do not permit their significance to be distinguished. The practical identity of the period of 0.283 d (only the third-strongest feature in the AOV spectra of the FWHM values) with $\mathcal{P}_5 = 0.281$ d in the HEROS RV's is striking. $\mathcal{P}_5$ is associated with the RV's of He I lines but apparently not of Si III lines (Sect. 4.1.1). It is, therefore, disturbing that in the mean of the FWHM's of the helium lines at 3820, 4026, 4388, and 4471 Å significant periodic variation was not found even after careful removal of the night-to-night variability. Fig. 4.6 nevertheless shows the H8-H10 data plotted versus phase of a 0.281-day period.

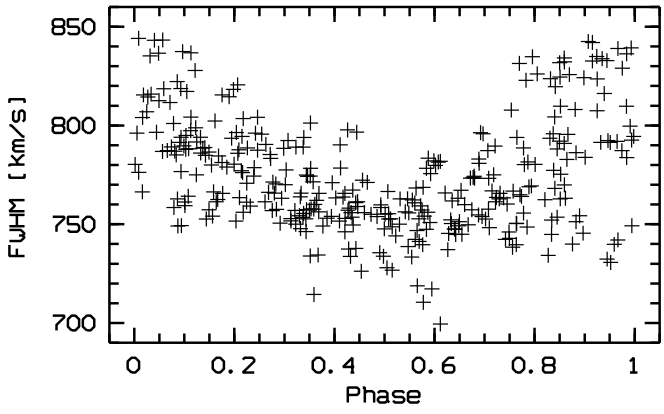

Figure 4.6: Variation of the FWHM measured in the Boller&Chivens spectra of H8-H10 corrected for night-to-night variations and folded with $\mathcal{P} = 0.281\,\mathrm{d}$. For details see Sect. 4.1.3.3

4.2 Full-Profile Time Series Analysis of the 1995-1997 HEROS Spectra

Radial velocity, line depth, and FWHM are similar to photometric data global, stellar disk-integrated quantities that strongly underutilize the Doppler and phase information contained in the line profiles by mixing it all into just one number. In addition to these parameters, we have therefore for several spectral lines also analyzed the temporal flux variations as a function of the position within the line profile. A full description of the procedure is given in Kaufer et al. (1996); it is based on the MIDAS TSA package ((ESO-MIDAS, 1995; Schwarzenberg-Czerny, 1993)). For any non-chaotic global stellar variability, a global relation can be expected between the phases of the flux variations in all bins. The detection of such a phase relation increases the confidence level of the associated period considerably.

Albeit the analysis of the line-profile variations is given here, their physical interpretation are postponed to Chapter 5. Here the method is applied to a homogeneous subset of the database, also to provide independent evidence of the multiperiodicity derived from the scalar quantities. Such a subset is formed by the HEROS data observed from 1995 to 1997. A schematic summary of the results of all 21 lines analyzed is given in Table 4.3.

Based on the periods and phases derived from the time series analysis of the RV data (Table 4.1), phase-dynamical spectra of the pulsation cycle patterns of all six periods in He Iλ4121 (free of detectable line emission) and C IIλ4267 (only slightly contaminated) are shown in Figs. 4.7 and 4.8. Both lines have a central depth of about 10% below the local continuum. The typical peak-to-peak amplitude of the patterns is of the order of 1% for the stronger modulations.

Note the similarity of the cycle patterns for $\mathcal{P}_1$, $\mathcal{P}_2$, $\mathcal{P}_3$, and $\mathcal{P}_4$ (Fig. 4.7) whereas the ones associated with $\mathcal{P}_5$ and $\mathcal{P}_6$ (Fig. 4.8) are distinctly different from the former ones but very similar to one another. Also in in all other lines without strong emission the patterns basically look the same within each group of periods (i.e. 0.28 and 0.5 d, respectively).

Below the dynamical spectra, Figs. 4.7 and 4.8 also include the results of the full-profile time series analysis. They fully confirm the periods found in the radial velocities (Table 4.1). However, the uncertainties are higher because the noise in the $5\,\mathrm{km\,s^{-1}}$-wide profile slices is obviously much larger than in a line-integrated quantity such as the radial velocity. This analysis method also returns, for each velocity bin, the phase and the power of each detected period. These quantities provide strong diagnostics of the nature of the variability (Gies & Kullavanijaya, 1988; Telting & Schrijvers, 1997); their exploitation will be presented in Chapter 5.

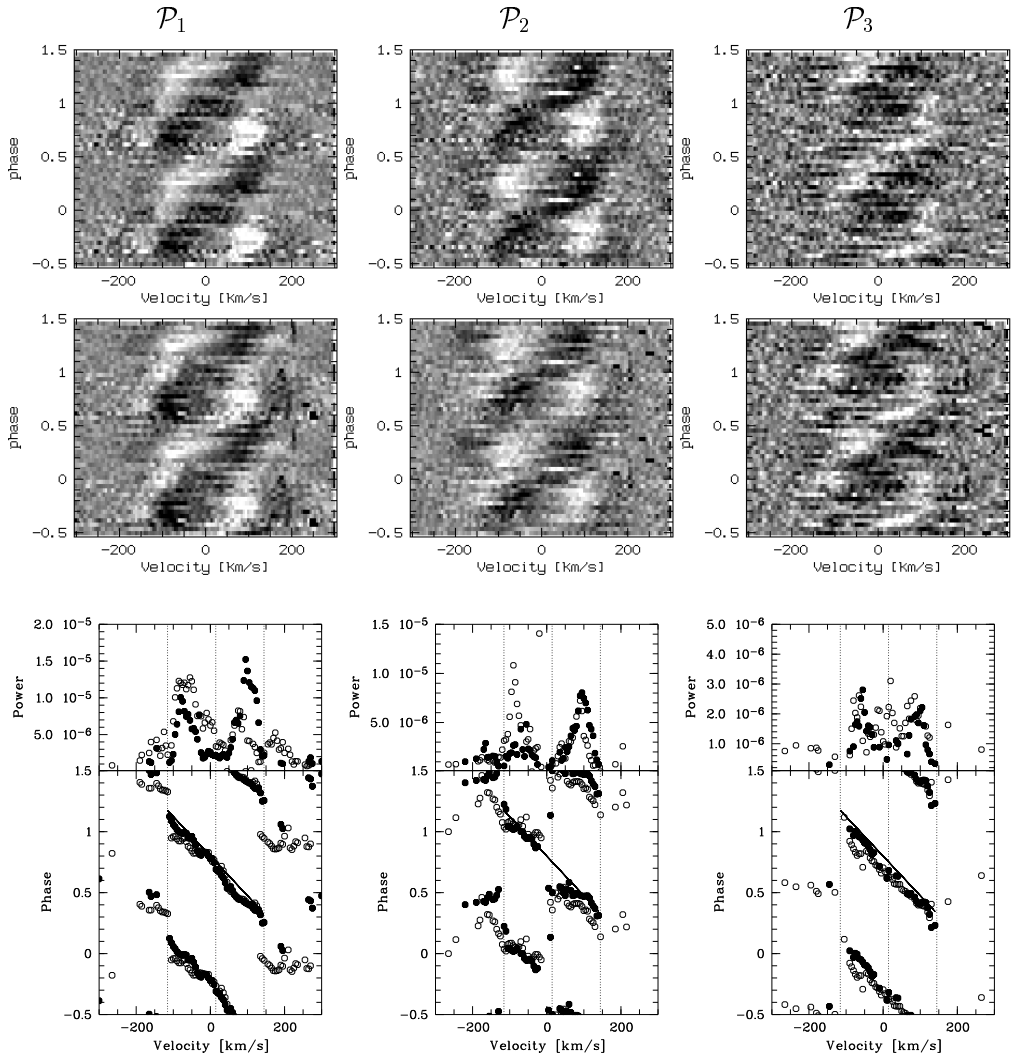

Figure 4.7: Spectral variability patterns of μ Cen (cf. Sect. 4.2). The grey-scale pictures are dynamical spectra of the pulsation cycles for the He Iλ4121 (top row) and C IIλ4267 (middle row) lines; they are presented as residuals from the respective mean profile in order to enhance the visibility of the variability pattern. Note that for each period all phases are shown twice. A total of 381 spectra from 1992 to 1997 were sorted into 25 phase bins. All spectra falling into the same phase bin were averaged to minimize the influence of other variabilities and noise (i.e. no prewhitening was applied). From left to right, periods $\mathcal{P}_1$, $\mathcal{P}_2$, and $\mathcal{P}_3$ as derived from the RV's of helium lines (Table 4.1) were used to phase the spectra. The similarity of the variations is striking. The lower row shows the results of the time series analysis of the line fluxes in bins of $5\,\mathrm{km\,s^{-1}}$ width as described in Sect. 4.2. In the upper and lower row of the lowermost sub-panels the power and the phase of the variability are shown, respectively, in both cases separately for each velocity bin. Filled symbols are used for values derived from He Iλ4121 ($\bullet$), open symbols for C IIλ4267 ($\circ$). The dotted lines mark the systemic velocity of $v_{\mathrm{sys}} = 14.5\,\mathrm{km\,s^{-1}}$, which was derived from the mean RV of the Si III$\lambda\lambda$4553,4568 lines, and the range of $v_{\mathrm{sys}} \pm v \sin i$. The power outside this range in C IIλ4267 visible in $\mathcal{P}_1$ is due to trace emission variablity in this line. In lines with stronger emission like He I$\lambda\lambda$6678,5876 this contribution is stronger. The solid lines in the bottom panels are the linear regression of the phase with velocity computed for $\mathcal{P}_1$ only (in order to underline again the similarity between the properties of these four variabilities)

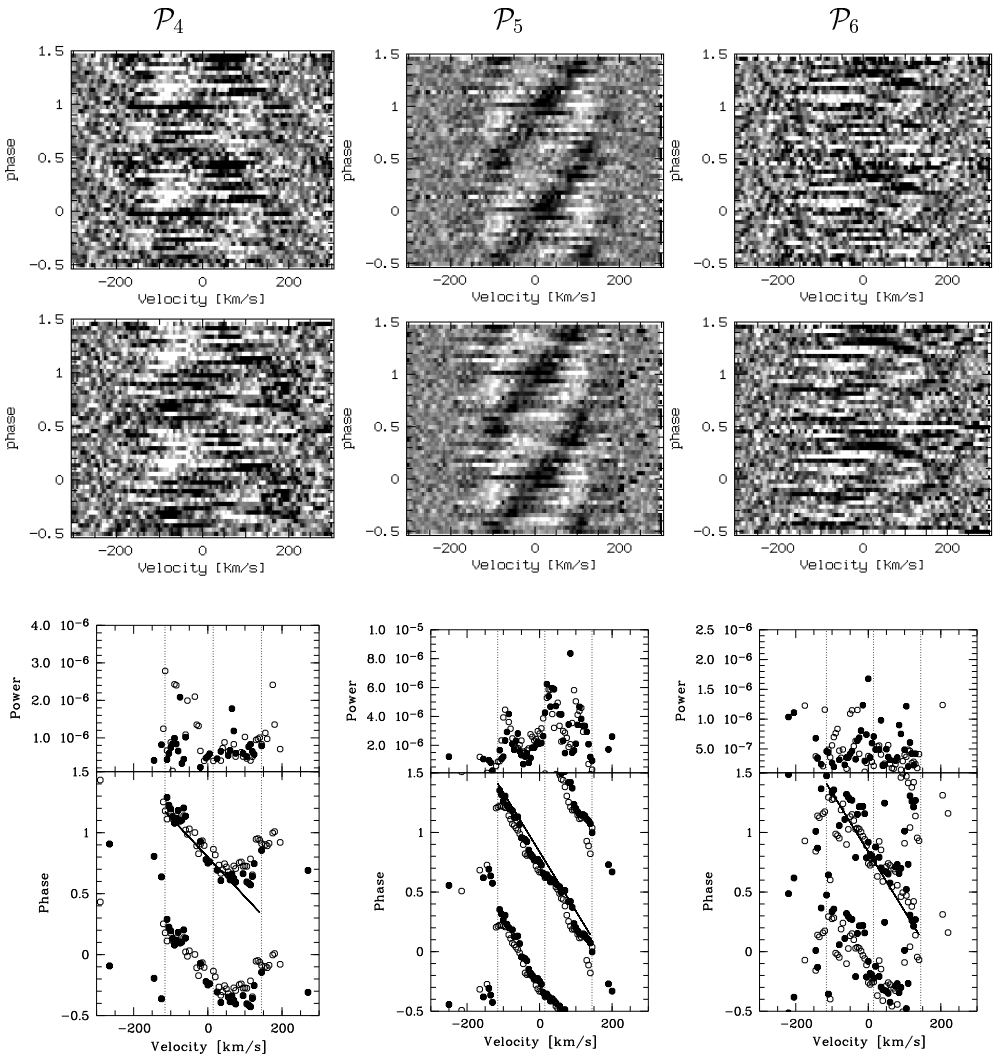

Figure 4.8: Same as Fig. 4.7, but for $\mathcal{P}_4$ and the $\mathcal{P}_5/\mathcal{P}_6$ group of periods. Note the difference in slope (rate of phase progression) between the $\mathcal{P}_1$ group of periods displayed in Fig 4.7 and represented by $\mathcal{P}_4$ and the $\mathcal{P}_5/\mathcal{P}_6$ group of periods

Table 4.3: The spectral lines studied with the full-profile time series analysis technique (Sect. 4.2). The symbols show in a self-explanatory way how significant the detections of periods $\mathcal{P}_1$-$\mathcal{P}_6$ (Table 4.1) are

Line	$\mathcal{P}_1$	$\mathcal{P}_2$	$\mathcal{P}_3$	$\mathcal{P}_4$	$\mathcal{P}_5$	$\mathcal{P}_6$
He I λ3820	√	√	√	(√)	√	–
N II λ4317	(√)	(√)	–	–	(√)	–
He I λ4009	√	√	√	√	√	(√)
He I λ4026	√	√	√	√	√	(√)
He I λ4121	√	√	√	√	√	(√)
He I λ4144	√	√	√	(√)	√	(√)
C II λ4267	√	√	√	(√)	√	√
O II λ4317	(√)	(√)	–	–	(√)	–
He I λ4388	√	√	√	√	√	√
He I λ4471	√	√	√	√	√	√
Mg II λ4481	√	√	(√)	–	√	(√)
Si III λ4553	√	(√)	(√)	(√)	(√)	(√)
Si III λ4568	√	(√)	(√)	–	–	–
He I λ4713	√	√	√	√	√	√
He I λ4922	√	√	√	√	√	√
He I λ5016	√	√	√	√	√	–
He I λ5048	√	(√)	√	√	√	–
He I λ5876	√√	√	√	√	√√	√
Si II λ6347	√	(√)	(√)	–	√	–
He I λ6678	√√	√	√	√	√√	√
He I λ7065	√	√	√	(√)	√	(√)

4.2.1 The $\mathcal{P}_1$ Group of Periods

4.2.1.1 Blue Power Excess

A striking property of this variability is the strong asymmetry in a part of the observed spectral lines. This asymmetry is not a consequence of forbidden components in the triplet He I lines, but present in both singlet and triplet lines. Rather it scales with the strength of the line. Figure 4.9 shows some weak lines in the upper left edge, some stronger lines in the upper row from left to right and He I $\lambda\lambda$4026, 4471 as maximal asymmetry in the lower left. In a rough sense this sequence probes the formation depth of the lines, the weakest ones being formed at deepest locations. However lines of He I that are formed even higher again show perfectly symmetric profiles. These are He I $\lambda\lambda$5876, 6678, 7065 and are shown in the lower row, middle and right. A behaviour with similar properties was found by Tubbesing for 28 Cyg (1998). In this star he found a correlation between the mean radial velocity of a line and its strength, that points to the same direction, i.e. the stronger, the more the line was shifted bluewards. Again the He I $\lambda\lambda$5876, 6678, 7065 lines did not follow this trend. Tubbesing showed that these He I lines can be understood as transitional between stellar and circumstellar variability, represented by the He I lines without emission and the Balmer lines, respectively. Further support for this finding is given by Štefl et al. (Štefl et al., 1998a) and in Sect. 4.2.1.2.

The asymmetry of the pulsational power is not well understood. Suggested solutions include abiabaticity, but also the dissipation of pulsational energy (wave leakage) into the circumstellar environment (Townsend, 1997b).

4.2.1.2 Periodic Variability beyond $v \sin i$

To some extent an influence of the photospheric variability on the close circumstellar environment can be shown directly. In He I lines exhibiting clear emission contribution, secondary peaks of variation power appear well outside $v \sin i$. The variability causing this power is detected at the very same frequency as the photospheric variability. I.e. a fixed phase relation to the photospheric features is maintained. Already earlier a searchlight analogy was proposed by Penrod, (reported e.g. by Baade, 1987) in which a hot *nrp* wave crest (or a spot) would excite the material in the disk above this region stronger than in the rest of the disk. This was rejected by Smith (1989) on the base of his extensive λ Eri dataset. However, we found this phase-locked emission in some of our program stars to be undoubtly present only for real strong emission and therefore quite massive disks. λ Eri was not observed in such a stage.
In turn, the presence of a hot crest was reported already by Peters (1991) based on IUE data. She derived a timescale of 10.8 ± 2 hours for UV flux variations, which she interpreted as temperature variability in the order of 500 K. Peters also concluded that the rapid V/R behaviour of Be stars is more complex than a simple phase locked variability in the stars observed by her. Albeit this certainly also holds for μ Cen, the "searchlight" might still be part of the observed variability. In stars for which none or only minor irregular variability is observed, as e.g. ω CMa or 28 Cyg, the searchlight type of behaviour is clearly dominant (Tubbesing, 1998, and Sect. 7.2of this work).

4.2.2 The $\mathcal{P}_5$ Group of Periods

The phase progression throughout the profile amounts to about 2.3π, while the power distribution across the profile is a triple structure with the main peak at the systemic velocity. The only property that cannot be modelled by state-of-the-art nonradial pulsation models (Sect. 5.4) is the presence of slight power beyond $v \sin i$, again in the He I lines emerging from the upper photosphere/inner disk regions.

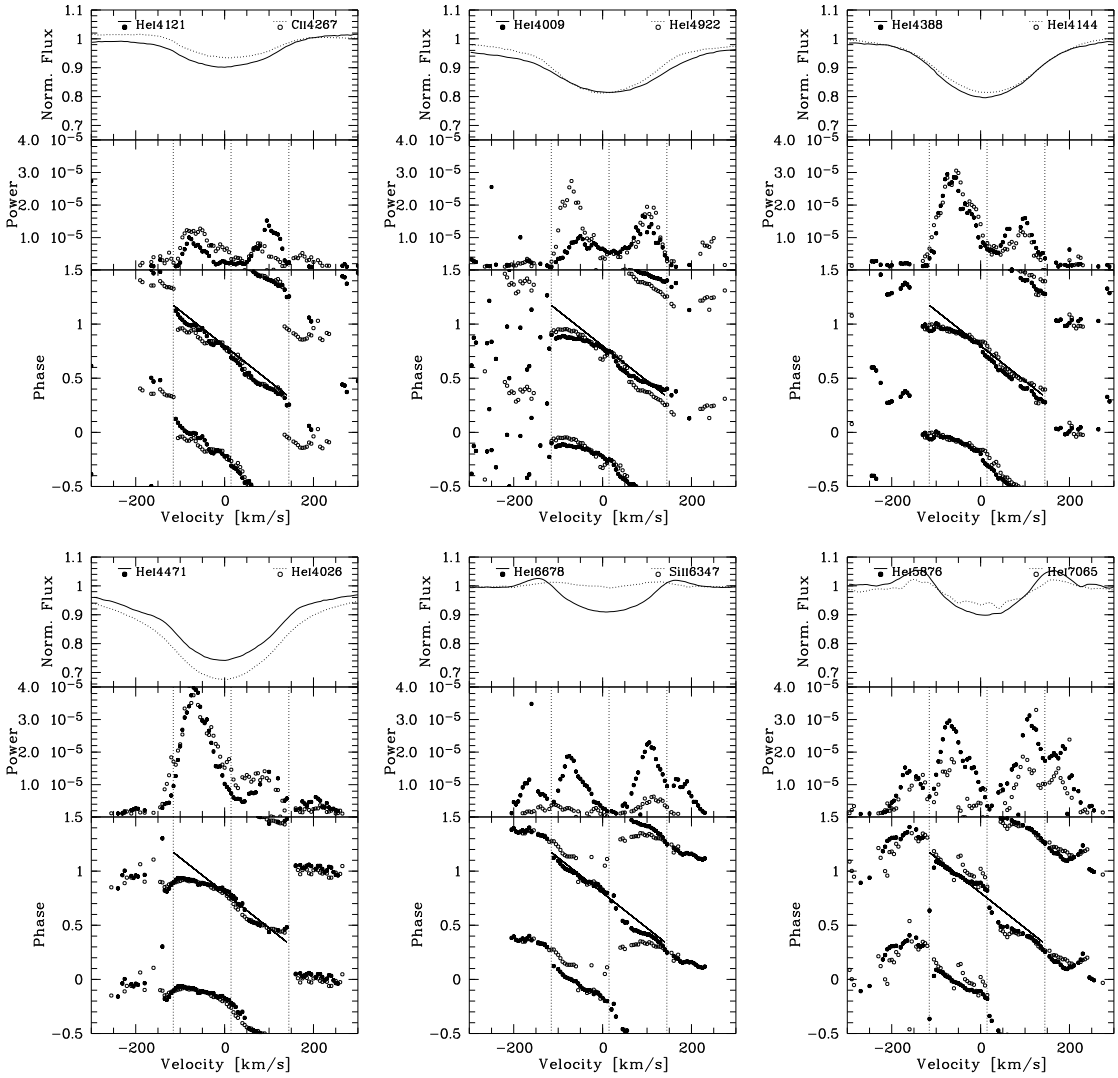

Figure 4.9: Spectral variability patterns of $\mathcal{P}_1$ for twelve spectral lines observed from 1992 to 1997 with HEROS. Shown are the mean profiles in the respective upper panels, the power distribution in the middle panels and the phase propagation across the line profile in the lower panels. The power excess on the blue side for some lines is discussed in Sect. 4.2.1.1, the additional power outside $v \sin i$ for lines showing emission in Sect. 4.2.1.2

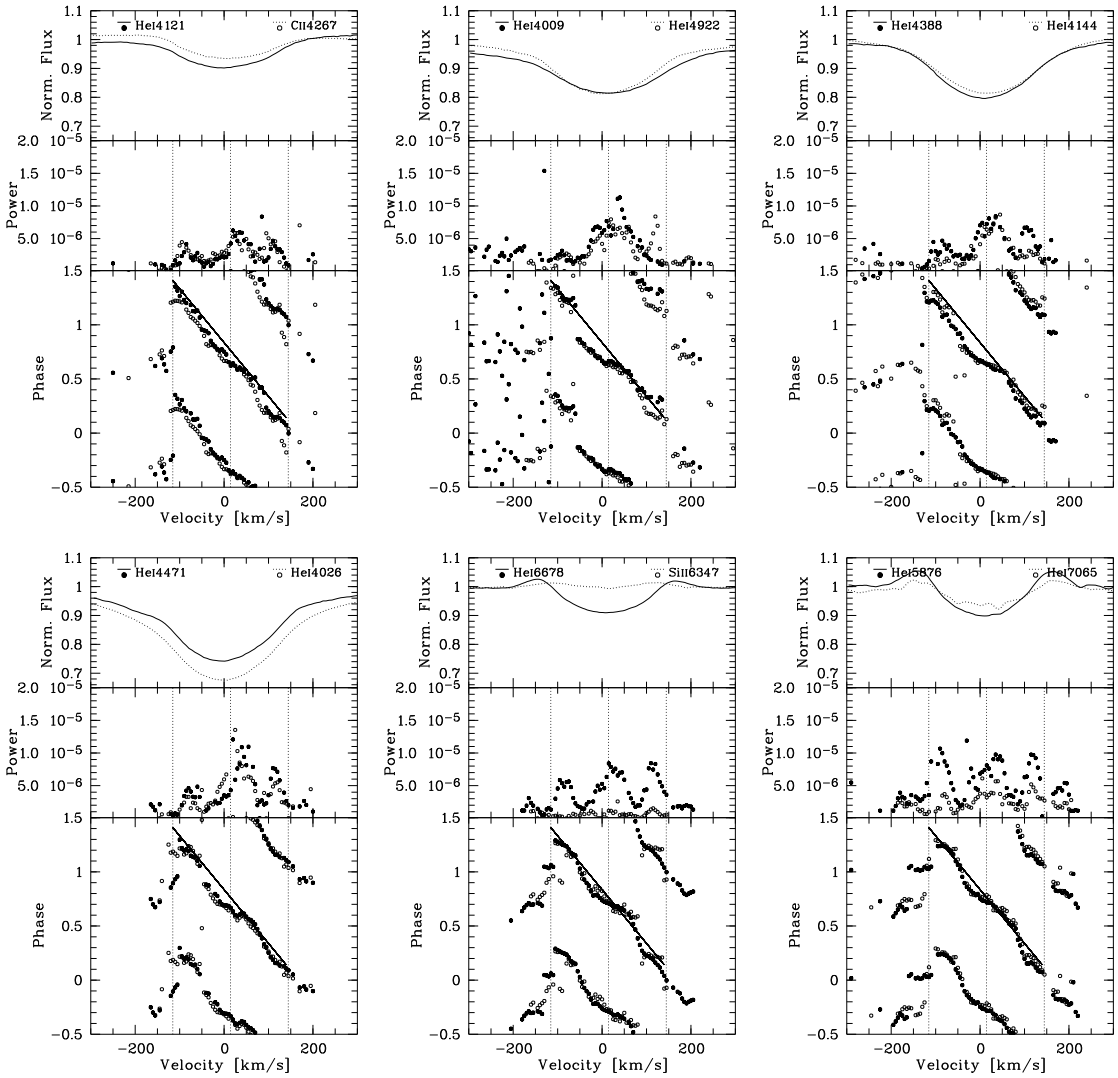

Figure 4.10: Similar to Fig.4.9, but for $\mathcal{P}_5$

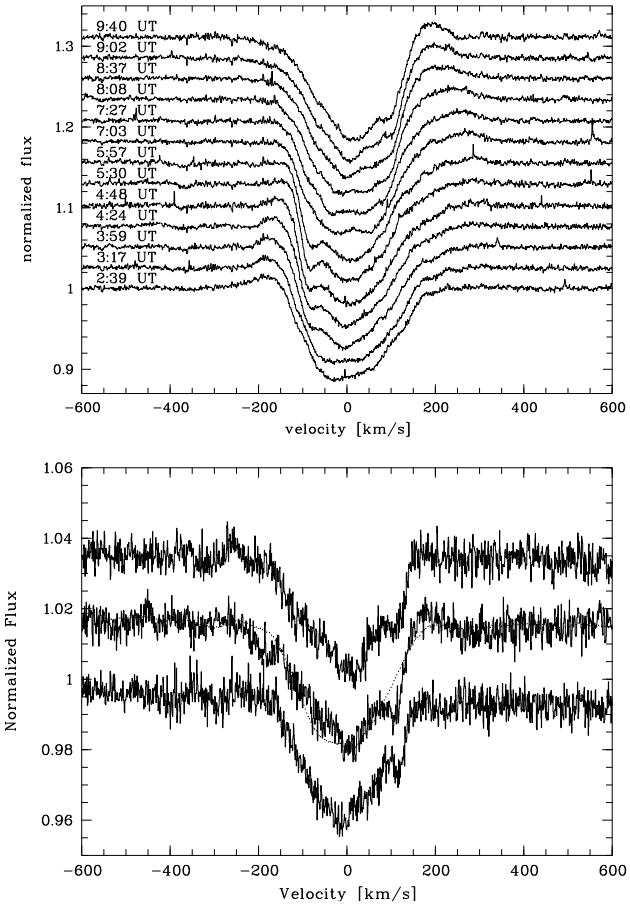

Figure 4.11: Upper panel: A proto-typical example of a sharp blue absorption spike (cf. Sect. 4.3) and its development observed on April 4, 1986 by Baade (1991). Note the signs of an appearing red spike about 5.7 hours after the blue spike was first visible. Lower panel: Three examples of sharp red absorption spikes in the Si IIIλ4553 line observed with the CAT/CES on June 26, 1995 (lower spectrum) and June 27, 1995 (upper spectra). The temporal separation of the spectra was 22.5 and 0.7 hours, respectively. From the 1995 spectra contaminating neighbouring Fe II emission lines have been subtracted. The mean line profile at that time is indicated by the dotted line

4.3 Sharp Absorption Spikes

In addition to the features migrating across most of the full width of the profiles (Figs. 4.7 and 4.8), conspicuous narrow absorption spikes appear from time to time close to the line wings (Figs. 4.11 and 4.13). Although such features may be observed in any night, their occurence is strongly enhanced during precursor and early phases of a line emission outburst (see Sect. 3.2 for the definition of the phases of an outburst cycle). Since the extra absorption features in question appear even in lines which seem to be the least contaminated by the presence of the circumstellar disk (e.g., Si III$\lambda\lambda$4553,4568) they are unlikely to be circumstellar in origin.
The FWHM of these spike-like features only amounts to 40 km s^{-1}, i.e. about 15% of $2 \times v \sin i$. Their life cycle lasts 2-3 hours during which their equivalent width (EW) rises and falls following roughly one half of a sine curve. The maximum equivalent width is about 6–8% of the main line's mean value. Since the contribution of irregular EW-variability is equally strong, it cannot be judged if a spike is true additional absorption or if the flux is just redistributed. During their evolution, the features shift in radial velocity by no more than 15 km s^{-1}. Even in different years, they appear at the same position to within $<$20 km s^{-1}. An example of the development of these parameters during the lifetime of such a feature is shown in Fig. 4.12.
Narrow absorption spikes can occur in both the blue and the red wing but are never seen in both wings simultaneously. Although the data do not cover one full cycle of this variability, the spectra

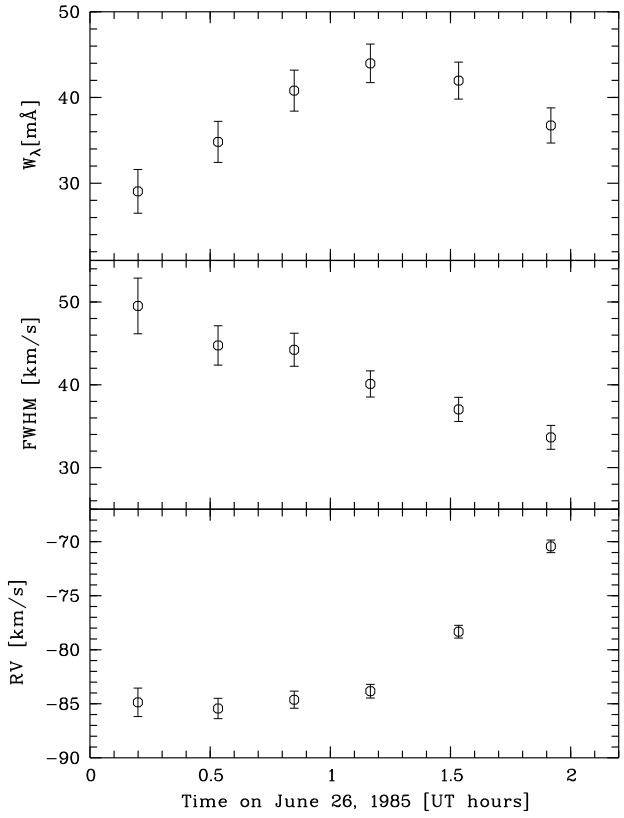

Figure 4.12: The parameters of a blue spike (cf. Sect. 4.3) observed on June 26, 1985 with the CAT/CES in He I λ6678. A spectrum taken only 5 minutes before 0 hrs (UT) does not display any indication of a growing spike, while after the last data plotted no further spectrum was taken for one hour. The panels show, from top to bottom, equivalent width, full width at half maximum and radial velocity of the spike in the residual spectra after subtraction of the mean of all CAT/CES spectra

shown in Figs. 4.11 and 4.13 suggest that the blue and red spikes are part of one and the same pattern, separated by about 0.5 in phase (the cycle length is discussed below). This is well supported by their occurence at about the same distance from the line center, namely 90-100 km s^{-1} or three-quarters of $v \sin i$.

A remarkable related variability is the simultaneous appearance and disappearance of very extended (up to 250 km s^{-1} from the line center) absorption in the respective other wing which takes on the shape of a straight, linear ramp. However the HEROS data, other than CAT/CES data, have too low a resolution and too strong noise to study more than the bare occurence of spikes. Not even this is possible of course for the B&C data.

During outbursts, when spikes are observed more regularly, a cyclic behaviour becomes apparent. Spikes in successive nights can well be phased with a cycle time of 0.5 day, which in such short time strings is indistinguishable from the photospheric 0.5-day group of periods. The enhanced power at 2 c/d in the blue wing of He I line profiles observed during outbursts in 1986 April and on MJD 50 232 (Fig. 3.8) is due to the waxing and waning of these spikes at roughly constant RV during outbursts. That only in the blue such enhanced power is visible is probably an artifact of the insufficient phase coverage.

Spikes and ramps not only have a recurrence time as the main photospheric variability, they also appear always at the same phases of the line profile variability. Blue spikes always coincide with

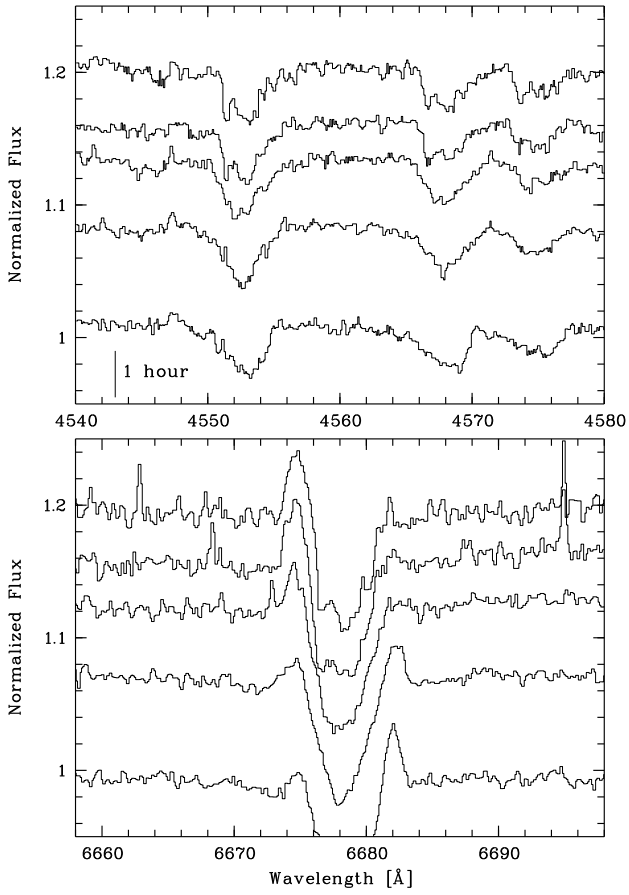

Figure 4.13: The development of a blue absorption spike (cf. Sect. 4.3) in HEROS spectra taken on May 25, 1996 (MJD 50 232), the beginning of a minor burst. Time increases from bottom to top with the spacing between spectra being proportional to the time elapsed between them; a vertical bar in the upper panel provides the scale. The upper panel shows the photospheric Si III triplet around 4560 Å, while the lower panel displays He Iλ6678, where also the V/R variability (cf. Sect. 3.3.2) is visible. Note again (cf. Fig. 4.11) the presence of a nearly linear wing ("ramp") on the side opposite to the extra absorption. A similar wing on the blue side is visible in the first (lowermost) spectrum of this night

phases of maximum blue shift of the line core, whereas spikes on the red side of the line appear around the phase of maximum redshift of the core. Whether the phasing of the spikes is governed by only one period of the 0.5 day group or by any combination of periods, is however not possibly to say. The spikes do not occur over time spans long enough to allow the recurrence time to be identified with one of the photospheric periods.

The above description of the absorption spikes and accompanying ramp-like wings in μ Cen is practically identical to that given by Smith (1985) for Spica (= α Vir). This well-known, bright β Cephei star had according to photometric reports (e.g. Lomb 1978, Sterken et al. 1986) by the time of Smith's observations already stopped its photometric β Cephei type activity. However, in 3 observing runs in 1983 February, 1984 February, and 1984 May, Smith found line-profile variability, including spikes, always to be present in Spica. Only the amplitude of the spikes varied quite considerably. A handful of spectra taken of Spica by Baade (unpublished) in 1984 February and 1985 January also show traces of the spikes discovered by Smith. Other unpublished spectra obtained in 1993 with FLASH (cf. Chapter 2) still show prominent spikes from time to time. The presence of such variability in a non-emission line star like Spica re-inforces the conclusion drawn for μ Cen that the variability is probably not circumstellar in origin. Finally, the line profile variability observed in the Mg II λ4481 line of 28 CMa (Baade, 1984b) may also fall into the same category.

It was shown already in Sect. 3.4 that in the very early phases of an outburst the line profile variability pattern can deviate significantly from its mean appearance. While the main periodicity persists, additional power appears at slightly lower frequencies (Fig. 3.8). This shows well that the power spectrum of μ Cen is variable. Such a behaviour was found in other Be stars, too, (Štefl et al., 1998b) and might well be related to the finding of Kambe (1993b), who observed different power distributions across the profiles of λ Eri at different stages of this star's activity.

5. Nonradial Pulsation Modelling

The variability analysis of a scalar quantity derived from the entire profile has the advantage that the information content is focused in a single number and the effects of noise are reduced. However, especially for asymmetry variations physical information is lost. To exploit this information two techniques have been developped in recent years, the moment method (Aerts et al., 1992; Aerts & Waelkens, 1993), and the full-profile 2D method (Gies & Kullavanijaya, 1988; Telting & Schrijvers, 1997). However, it is not entirely clear how the presence of circumstellar emission in the line wings influences the moment method. Štefl et al. (1998a) have shown for the star ω CMa that the moment method alone would give misleading results for a line like He Iλ6678. Only with prior knowlegde, derived from HEROS data (cf. Table 2.3), about the present periods and the fact that part of the variability resides mainly in the emission, the moment method could be used to fit a biperiodic solution. Since μ Cen shows clear emission components in the stronger He I lines and trace emission cannot be excluded for even the weakest lines, I restrict myself to the full-profile 2D method.

5.1 The Nonradial Pulsation Model

The observed distribution of the periods leave little room for other interpretations than nonradial pulsation (*nrp*). However, a mode identification by means of accurate physical modelling is still to be derived.

Townsend's (1997a; 1997b) spectroscopic modelling codes BRUCE and KYLIE are used to investigate the variability observed in μ Cen. BRUCE calculates the pulsational disturbances of a rotating stellar surface. The technique used to calculate the rotational modifications is based on the similarity transformation technique introduced by Eckart (1960) as given by Lee&Saio (1987a). This technique is especially suitable for slow pulsators, and thus for g-modes. The input for BRUCE are the stellar parameters, and the angular pulsational indices and amplitude of each mode.

BRUCE starts with a rotationally modified but pulsationally undisturbed star, that is represented by a grid of about 50 000 points, of which the half is visible. The rotational modifications include von Zeipel's (1924) gravity darkening theorem, using the standard value of $\beta = 0.25$ being appropriate for early type stars (Townsend, 1997b).

While for a non-rotating star the disturbances caused by a pulsational mode can be described completely by one single set of angular indices l and m, the coupling between modes becomes more and more important the faster the star rotates (Nevertheless a mode can still be identified unambigously by these numbers). Lee&Saio (1987a) have shown that the equations can be written in vector form, so that the coupling is completely described by a matrix of infinite dimension. However, according to Townsend (1997b), a matrix dimension of 100 is sufficient in practice to ensure a stable result. These rotationally modified modes are then used, under Cowling approximation and adiabatic conditions, to calculate the pertubations to be applied to the grid that represents the undisturbed star:

1. The pulsational velocity field that superimposes the rotation
2. The temperature pertubations
3. The variations of the visible surface

Table 5.1: Adopted stellar parameter ranges. Note that the combinations of v and i are restricted to $v \sin i = 130\,\mathrm{km\,s^{-1}}$. The finally chosen parameters are emphasized

Parameter		Range
Radius, $R_{\star,\mathrm{polar}}$	$[\mathrm{R}_\odot]$	4.8 . . .**5.8** . . . 6.2, step 0.2
Temperature, $T_{\mathrm{eff},\mathrm{polar}}$	[kK]	20, 21, **22**, 23
Mass, $M_\star$	$[\mathrm{M}_\odot]$	7, **8**, 9, 10
Rotation, v	$[\mathrm{km\,s^{-1}}]$	170, **200**, 260
Inclination, i	[degree]	50, **40**, 30

4. The deviation of the local surface normal vector from the radial direction

The information of these perturbations for each visible grid point is written to an unformatted output file to be used by the subsequent calculation of observable quantities.
KYLIE then reads this file and integrates over the grid calculated by BRUCE to derive observables. To do so, KYLIE needs an input grid containing information about the undisturbed instrinsic observables of a stellar surface element. These intrinsic observables depend on temperature, gravity, wavelength and inclination angle.
KYLIE can be used not only to calculate phase-dependant spectral line profiles but also to estimate the photometric variability due to a given mode. In the first case the input grid would have to contain intrinsic line profiles of a given spectral line, while for the second case the flux emerging from a standard surface element under different conditions is needed.

5.2 Grid of Stellar Models

5.2.1 Stellar Parameters

To represent the undisturbed configuration of the rotating star, the stellar parameters polar radius $R_{\star,\mathrm{polar}}$, polar temperature $T_{\mathrm{eff},\mathrm{polar}}$, mass $M_\star$, the rotational velocity v, and the inclination i are required. Since the latter two are not independant for a given star but conncted via the observed $v \sin i$, only certain combinations are acceptable. A complete set of parameters is given by $R_{\star,\mathrm{polar}}, T_{\mathrm{eff},\mathrm{polar}}, M_\star$ and (v, i).
Physical parameters for μ Cen have been derived using Walraven photometry by de Geus et al. (1989). They derived $T_{\mathrm{eff}} = 21\,000$ K, $\log g = 3.94$, $\log L_\star/\mathrm{L}_\odot = 3.6$, and a distance of 145 pc. However, the HIPPARCOS distance is a little greater, 162 pc, indicating that radius and luminosity could be higher. Brown & Verschueren (1997) derived $v \sin i = 130\,\mathrm{km\,s^{-1}}$ from high resolution echelle spectroscopy. The emission line profile type (Hanuschik et al., 1996) points to a low to intermediate inclination of about 30 to 45 degree. From these observations the edge values of the parameter grid shown in Table 5.1 were derived, for which pulsational models were calculated.
For the calculation of the flux variability to estimate the photometric amplitudes an absolute calibrated flux grid described in Sect. 5.2.2.1 was used.
To compute the spectroscopically observable stellar variability from the perturbations of the stellar surface calculated by BRUCE, KYLIE needs the intrinsic profile for each surface element. They were interpolated from the models introduced in Sect. 5.2.2.2

5.2.2 Stellar Atmospheres

Gummersbach et al. (1998) have calculated a grid of ATLAS 9 atmospheric models for different metallicities. The grid was meanwhile extended by Korn & Wolf (1998), now reaching from

Table 5.2: Adopted and derived parameters for the pulsationally undisturbed star

Adopted	
Parameter	Value
Polar radius, $R_{\star,\mathrm{polar}}$	$5.8\,\mathrm{R}_\odot$
Polar temperature, $T_{\mathrm{eff},\mathrm{polar}}$	22 000 K
Mass, $M_\star$	$8\,\mathrm{M}_\odot$
Rotation, v	$200\,\mathrm{km\,s^{-1}}$
Inclination, i	40°
Derived	
Parameter	Value
Equatorial radius, $R_{\star,\mathrm{equ}}$	$6.278\,\mathrm{R}_\odot$
Equatorial temperature, $T_{\mathrm{eff},\mathrm{equ}}$	20 216 K
Polar gravity, $\log g_{\mathrm{polar}}$	3.814
Equatorial gravity, $\log g_{\mathrm{equ}}$	3.667
Stellar luminosity, $\log L_\star/\mathrm{L}_\odot$	3.797
Rotational period, $\mathcal{P}_{\mathrm{rot}}$	1.59 days
Critical period, $\mathcal{P}_{\mathrm{crit}}$	0.76 days
Critical velocity, v_{crit}	$418\,\mathrm{km\,s^{-1}}$

$T_{\mathrm{eff}} = 9000\,\mathrm{K}$ to 50 000 K in steps of 1000 K, and from the lowest numerically converging $\log g$ to an upper limit of $\log g = 5.0$, stepwidth 0.1 dex. Of these a subset of solar metallicity models in the range of $18\,000\,\mathrm{K} \leq T_{\mathrm{eff}} \leq 23\,000\,\mathrm{K}$ and $3.5 \leq \log g \leq 4.3$ were selected . The parameter chosen finally and the derived quantities for the undisturbed stellar surface are given in Table 5.2.

5.2.2.1 Fluxes

The stellar fluxes computed from this grid were used as input data for KYLIE to model the photometric variability. This grid is however not able to cover the variations due to point 4 in the above list. The proper way out would have been to calculate angle dependant intensity spectra instead of flux spectra.

To overcome this difficulty, the correct treatment of limb darkening is crucial. In this work parametrized linear limb darkening coefficients for the standard photometric bands (*UBV* and *uvby*) by Díaz-Cordovés et al. (1995) are used, obtained by least square fits to the computed values for ATLAS 9 atmospheres.

5.2.2.2 Intrinsic Line Profiles

Besides the absolute flux, ATLAS 9 also gives the atmospheric structure needed as input to model the intrinsic line profiles. For the selected models above, an LTE line profile grid has been calculated using the BHT-code (Baschek et al., 1966). The calculated profiles indlude Hα, Hβ, Hγ, Hδ, and the He I$\lambda\lambda$ 4009, 4026, 4144, 4168, 4388, 4437, 4713, 4713, 4922, 5016, 5048, 5876, and 6678 lines. The microturbulence was chosen to be $10\,\mathrm{km\,s^{-1}}$, a typical value derived for early B stars analysed with this method (Kaufer et al., 1994, e.g.).

Townsend (1997a, his Sect. 7.5.6) has compared the intensity spectra based method with integration techniques using limb darkened intrinsic flux spectra and limb darkened Gaussians for *lpv* modelling.While the deviations from the complete method are only minor for limb darkened computed intrinsic profiles, the results based on Gaussians as intrinsic profiles might differ strongly.

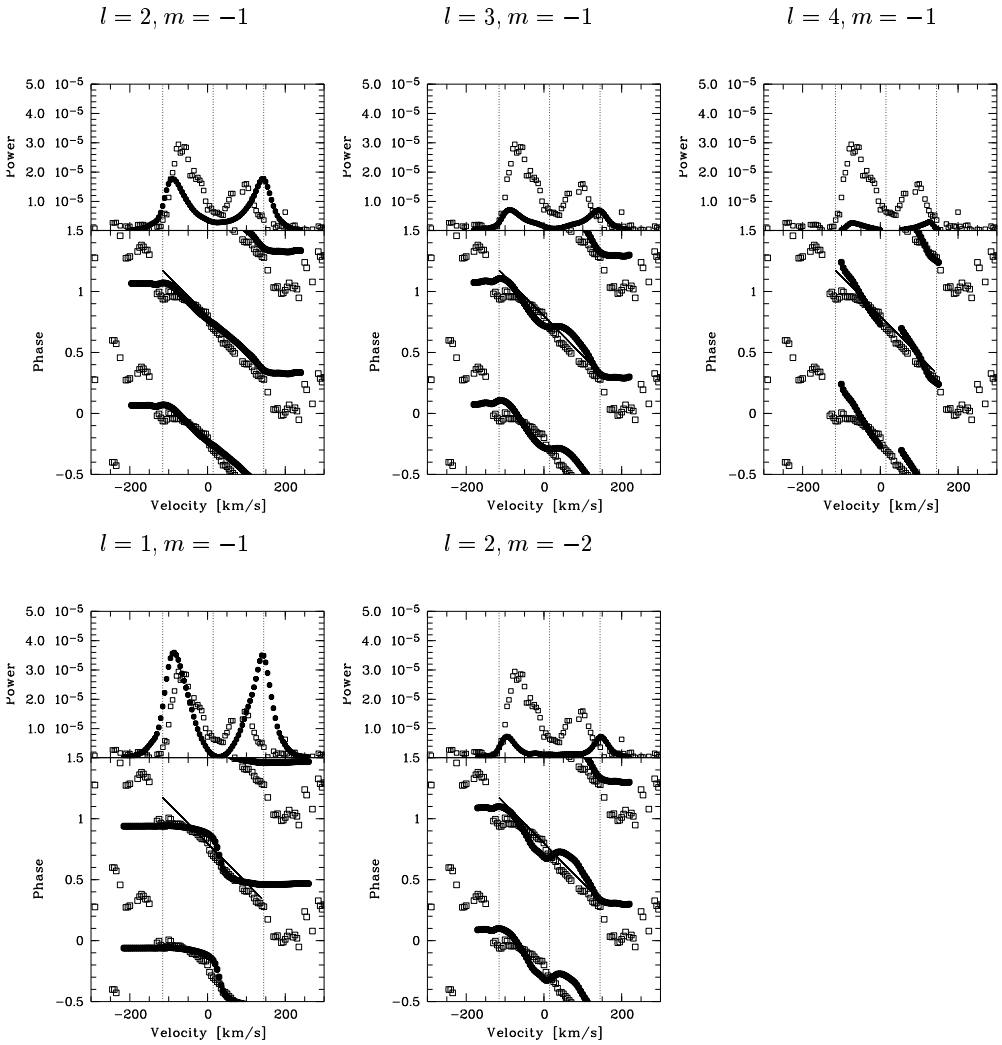

Figure 5.1: A set of calculated pulsational modes for $\mathcal{P}_1$ at fixed stellar parameters ($5.8\,\mathrm{R}_\odot$, $22\,000\,\mathrm{K}, 8\mathrm{M}_\odot, 200\,\mathrm{km\,s^{-1}}, 40°$) and pulsational amplitude ($A = 13\,\mathrm{km\,s^{-1}}$). The model data is displayed as bullets (•), while the He Iλ4388 line data is plotted for comparison with circles (∘). Only (2,-1), (2,-2), and (3,-1) reproduce the power and phase distribution, while the other modes do not fit the phase variation across the profile very well. However, for (2,-2) and (3,-1) the reproduction is not only less good, but to be strong enough, unphysical flow velocities on the stellar surface would have to be assumed. Asymmetries in the variability wrt. the line center are a consequence of the use of intrinsic stellar profiles, that is not entirely symmetric itself for He Iλ4388 due to a weak blend on the violet side

Since the limb darkening can vary strongly across a spectral line, any smooth parametrization might be entirely wrong (Townsend, 1997a, his Fig. 7.9). Deviations from the intensity spectra based method to the limb darkened intrinsic profile method can be fully attributed to an incorrect limb darkening law used. As mentioned above however, these deviations are usually small, even if the continuum value for limb darkening is applied across the line profile. So rather than using the approach suitable for the continuum variability (Sect. 5.2.2.1) the linear limb darkening parameter is adopted to be constant here with a value of 0.4.

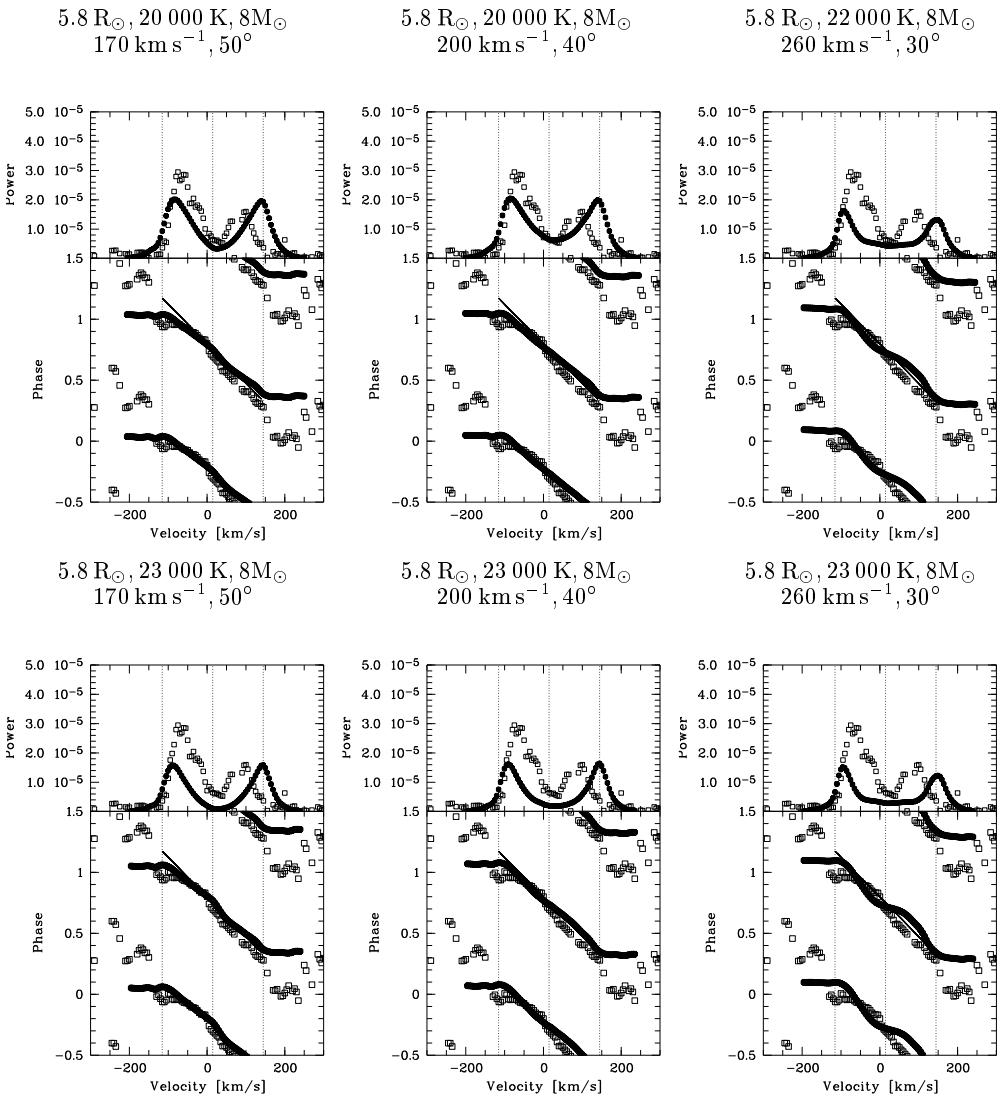

Figure 5.2: A sequence of models for $\mathcal{P}_1$, (2,-1) to illustrate the influence of the stellar parameters R and (v,i). In the upper right the model for $T_{\rm eff,polar} = 22\,000$ K is shown, because the fast rotating models with lower temperature had equatorial temprature extrema outside the lower boundary of the atmosphere grid

5.3 Modelling μ Cen

In Chapt. 4 it was shown that each period group has a common variability pattern. The analysis is therefore concentrated on the strongest variability in either group, i.e. $\mathcal{P}_1$ and $\mathcal{P}_5$. Already from a naked-eye inspection of the phased spectra (Fig. 4.7) it also becomes clear that the angular indices cannot be too high.

5.3.1 Spectroscopic Modelling of $\mathcal{P}_1$

The variations that are connected to $\mathcal{P}_1$ are concentrated in the line wings. The associated power of the variability reaches a minumum at or close to the adopted stellar radial velocity $v_{\rm sys}$. In the case of pulsation, this behaviour is indicative for large horizontal velocities.

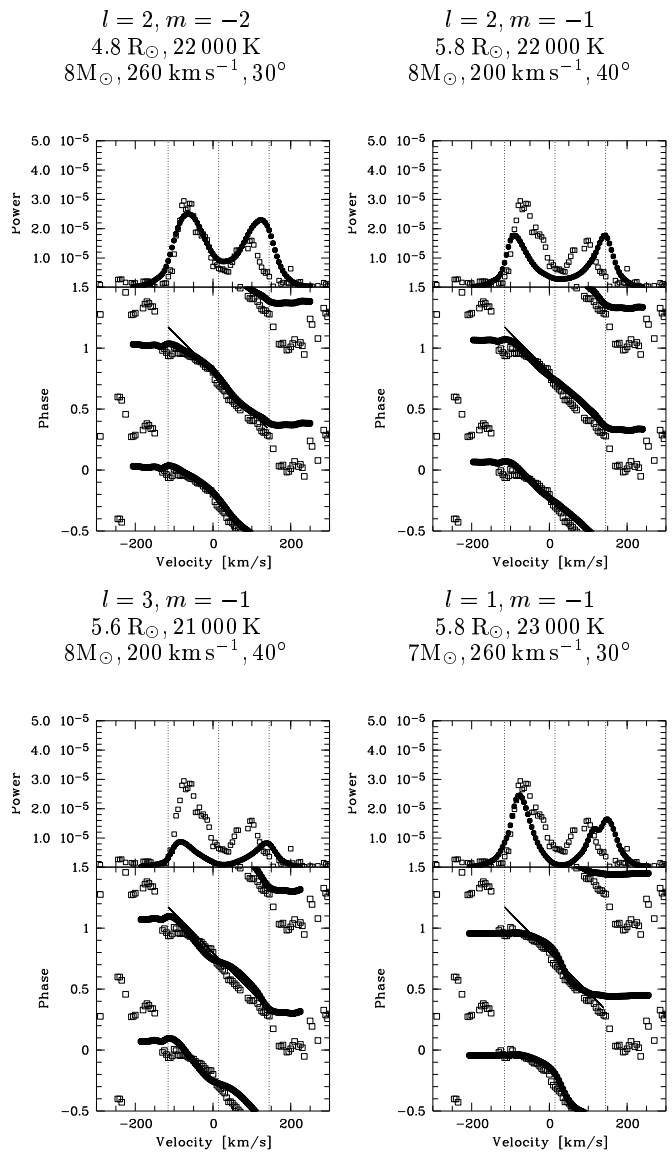

Figure 5.3: Best spectroscopic fit models for the (2,-2), (2,-1), (3,-1), and (1,-1) modes for $\mathcal{P}_1$. Asymmetries in the modelled variability wrt. the line center are a consequence of the use of intrinsic stellar profiles, that is not entirely symmetric itself for He Iλ4388 due to a weak blend on the violet side

This points to long-period pulsation, compared to the radial fundamental mode, in gravitationally controlled g-modes in which the flows are mostly horizontal. The phase distribution across the line profile is nearly a straight line that spans a phase difference from $-v \sin i$ to $+v \sin i$ of about $1.6\,\pi$.

As snapshot calculations of pulsational modes revealed, no retrograde sectorial or tesseral ($m > 0$), as well as no zonal modes ($m = 0$) were able to reproduce the observed spectral variability. Also all prograde modes with $m > 2$ could be excluded, for they would have resulted in extremly high temperature pertubations in the order of several thousands of Kelvin.

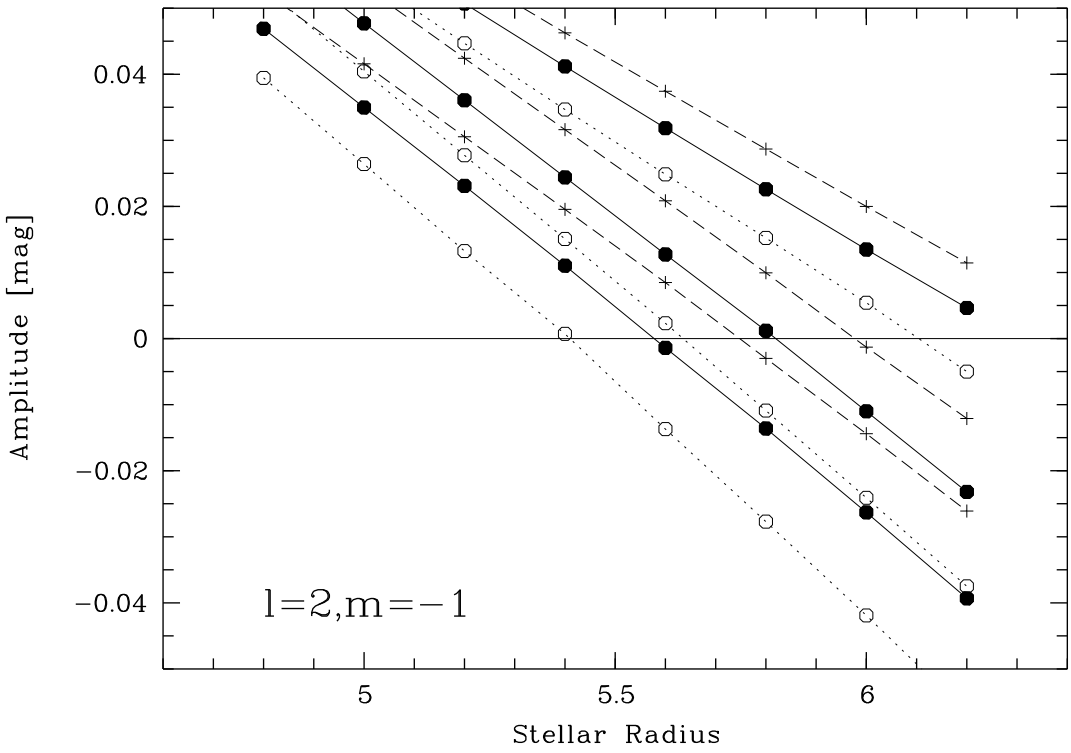

Figure 5.4: Photometric model amplitudes of the Strömgren *b* band for the $\mathcal{P}_1$ (2,-1) mode as function of the stellar radius. Displayed are only models with $T_{\mathrm{eff,polar}} = 22\,000\,\mathrm{K}$. Each symboltype denotes a common stellar mass of the models: $7\,\mathrm{M}_\odot$(∘), $8\,\mathrm{M}_\odot$(•), and $9\,\mathrm{M}_\odot$(+), while the lines connect points of common (*v,i*), the uppermost having the most rapid rotation for each mass. "Negative" amplitudes are used to denote the phase-jump of $180°$

Of the remaining possibilities the only $m = -2$ mode with, at first order, acceptable pertubation amplitudes was (2,-2), noted as (*l,m*).
So five modes have been selected to be calculated in detail, i.e. covering the entire stellar parameter grid of 288 combinations presented in Table 5.1. The amplitude was chosen in a way that the maximal vectorial velocity pertubation on the star was $13\,\mathrm{km\,s^{-1}}$ in all cases. These modes are: (1,-1), (2,-1), (2,-2), (3,-1), and (4,-1). The spectral line chosen to be modelled was the He Iλ4388 line, which represents best the cross section of the variability displayed in Figs. 4.9 and 4.10.
For a given mode, with respect to the spectroscopic variability, the results depend on the chosen stellar parameter set as follows (cf. Fig. 5.2):
Polar radius: The influence on the spectroscopic signature is neglectible
Polar temperature: The cooler the star is adopted, the more power is detectable close to the center of the line
Stellar mass: The influence on the spectroscopic signature is neglectible
Rotation/inclination The faster the star rotates, the more the power is "smeared" towards the center
Four modes exist with different sets of stellar parameters that satisfy the spectroscopic input conditions, i.e. fit the observed phase and power distributions for $\mathcal{P}_1$ (Fig. 5.3).

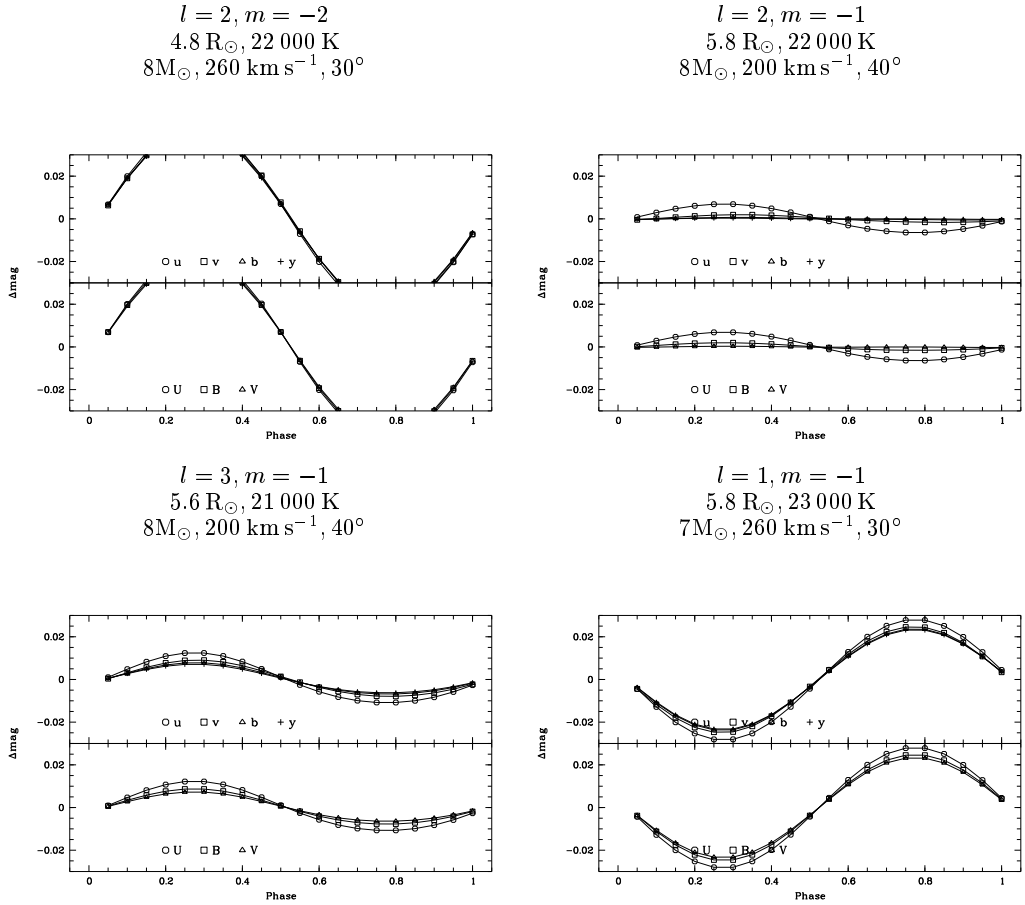

Figure 5.5: Photometric variability of the best spectroscopic fit models for the (2,-2), (2,-1), (3,-1), and (1,-1) modes. Only the (2,-1) mode can reproduce the non-detection of photometric variability with the Period $\mathcal{P}_1$

5.3.2 Photometric Modelling of $\mathcal{P}_1$

The dependance of the photometric behaviour of a given mode on the stellar parameters however looks entirely different than for the spectroscopic results (cf. Fig. 5.4):

Polar radius: The variation strength changes strongly and may even cross zero and invert (i.e. exhibit a phase jump of $180°$)

Polar temperature: The influence is neglectible

Stellar mass: The variation strength changes slightly

Rotation/inclination The variations may change strongly, depending on the respective mode

Especially the first point in this list is of special relevance for μ Cen. The theoretical possibility of such a behaviour, the cancellation of the photometric perturbations, was investigated already by Townsend (1997a; 1997b). A common argument against *nrp* in Be stars is that the periods derived from spectroscopy are photometrically not or only weakly detectable. As Townsend has shown, the cancellation of the photometric variations is mainly depending of the interplay of pulsational vs. rotational vs. critical period. Thus if in μ Cen this cancellation is applicable (cf. Figs. 5.5 and 5.4), it might also explain other Be stars.

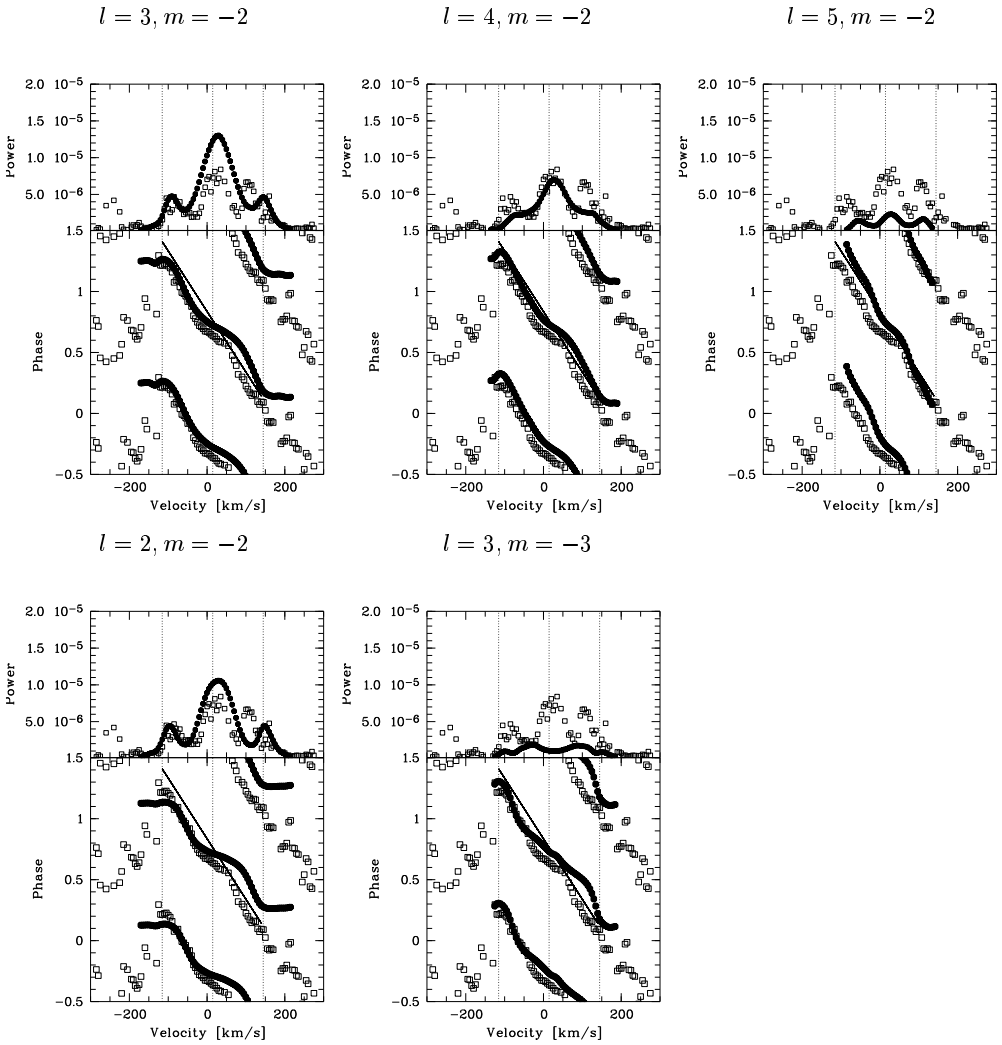

Figure 5.6: A set of calculated pulsational modes for $\mathcal{P}_5$ at fixed stellar parameters ($5.8\,\mathrm{R}_\odot$, $22\,000\,\mathrm{K}, 8\mathrm{M}_\odot, 200\,\mathrm{km\,s^{-1}}, 40°$) and pulsational amplitude ($A = 8\,\mathrm{km\,s^{-1}}$). The model data is displayed as bullets (•), while the He Iλ4388 line data is plotted for comparison with circles (∘). Only (3,-2) and (4,-2) reproduce the power and phase distriution, while the other modes do not fit the phase or power variation across the profile very well.

5.3.3 Spectroscopic Modelling of $\mathcal{P}_5$

Similar as for $\mathcal{P}_1$, most values of (*l*,*m*) could be excluded on the base of snap-shot calculations, rendering the calculation of an intensive grid necessary only for again five modes: (2,-2), (3,-3), (3,-2), (4,-2), and (5,-2) which are shown in Fig. 5.6. While both (2,-2) and (3,-2) reproduce the triple peakedness of the power very well, (4,-2) and (3,-2) reproduce the phase variability best. Thus (3,-2) is the pulsational mode of choice for $\mathcal{P}_5$. Generally the appearance of this shorter period is less sensitive on the choice of the stellar parameters than it is for $\mathcal{P}_1$.

5.3.4 Photometric Modelling of $\mathcal{P}_5$

Both (4,-2) and (3,-2) have modelled amplitudes that would be small enough to remain undetected in photometric studies, i.e. a few mmags, taking into account the high level of incoherent variability (Sect. 7.4). (2,-2) however can safely be excluded by its high expected amplitude.

5.4 Other spectral lines

It was possible to model the behaviour of the He Iλ 4388 line in quite some detail. As Figs. 4.9 and 4.10 show however, there are differences from line to line. The questions how representative the line chosen was and if can one and the same pertubation pattern account for these differences remains. Partly this was discussed already non-parametrically in Sect. 4.2.1. Still yet unexplained differences mainly about the power ratio of the line center to the wing exist.
Due to the advantage of the use of intrinsic stellar profiles, the individual dependance of the line on $T_{\rm eff}$ and $\log g$ can be taken into account. Albeit all modelled lines are of He I, differences clearly exist. Since the surface effects in the list of pertubations are evaluated equally for all lines, the modelled differences have to arise from the $T_{\rm eff}$-$\log g$ dependance.
Figures 5.7 and 5.8 show the modelled variability compared to the observed properties for a set of six spectral lines each. If one neglects the blue power excess and the power beyond $v \sin i$ in some lines, the variability is modelled well with the parameters derived from the modelling of the He Iλ 4388 line. For $\mathcal{P}_1$ this is expressed mainly in the reduced power in the line center in some line, especially He Iλ 4121. For $\mathcal{P}_5$ the observed lines did behave more diverse. These differences are modelled especially well:

1. The supressed power in the center of He Iλ 4121
2. The enhanced power in the center of the He I$\lambda\lambda$ 4026, 4144 lines
3. The nearly equally strong power in the wings of He Iλ 5875

As to my knowlegde, this is the first study in which different spectral lines, observed simultaneously, are modelled by *nrp* in such a (successful) way.

Table 5.3: Pulsational model parameters of all observed modes. k is the fraction of horizontal/vertical amplitude, while $|v|_{\rm max}$ is the actual maximal velocity on the stellar surface due to the respective mode

Period	l	m	$\mathcal{P}_{\rm obs}$ [day]	$\mathcal{P}_{\rm corot}$ [day]	k	$\lvert v\rvert_{\rm max}$ $\rm km\,s^{-1}$
$\mathcal{P}_1$	2	-1	$0\overset{\rm d}{.}5029$	$0\overset{\rm d}{.}7358$	1.65	13
$\mathcal{P}_2$	2	-1	$0\overset{\rm d}{.}5075$	$0\overset{\rm d}{.}7458$	1.70	10
$\mathcal{P}_3$	2	-1	$0\overset{\rm d}{.}4945$	$0\overset{\rm d}{.}7180$	1.57	7
$\mathcal{P}_4$	2	-1	$0\overset{\rm d}{.}5164$	$0\overset{\rm d}{.}7650$	1.79	4
$\mathcal{P}_5$	3	-2	$0\overset{\rm d}{.}2814$	$0\overset{\rm d}{.}4358$	0.58	7
$\mathcal{P}_6$	3	-2	$0\overset{\rm d}{.}2791$	$0\overset{\rm d}{.}4303$	0.56	3

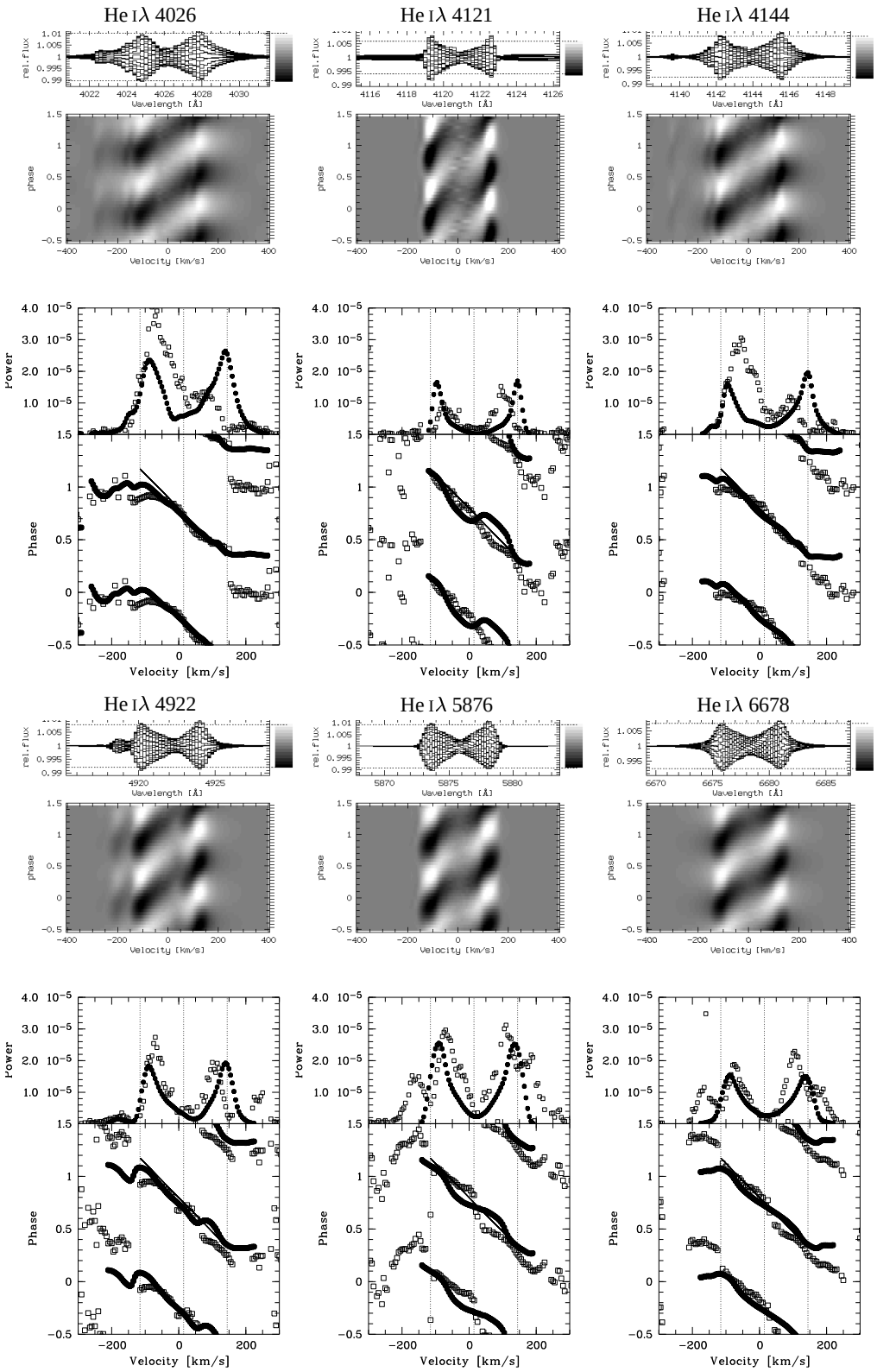

Figure 5.7: The variability of other He I lines modelled by the (2,-1) mode of $\mathcal{P}_1$ (•) compared with the respective data (○). The parameters used are noted in Tables 5.2 and 5.3

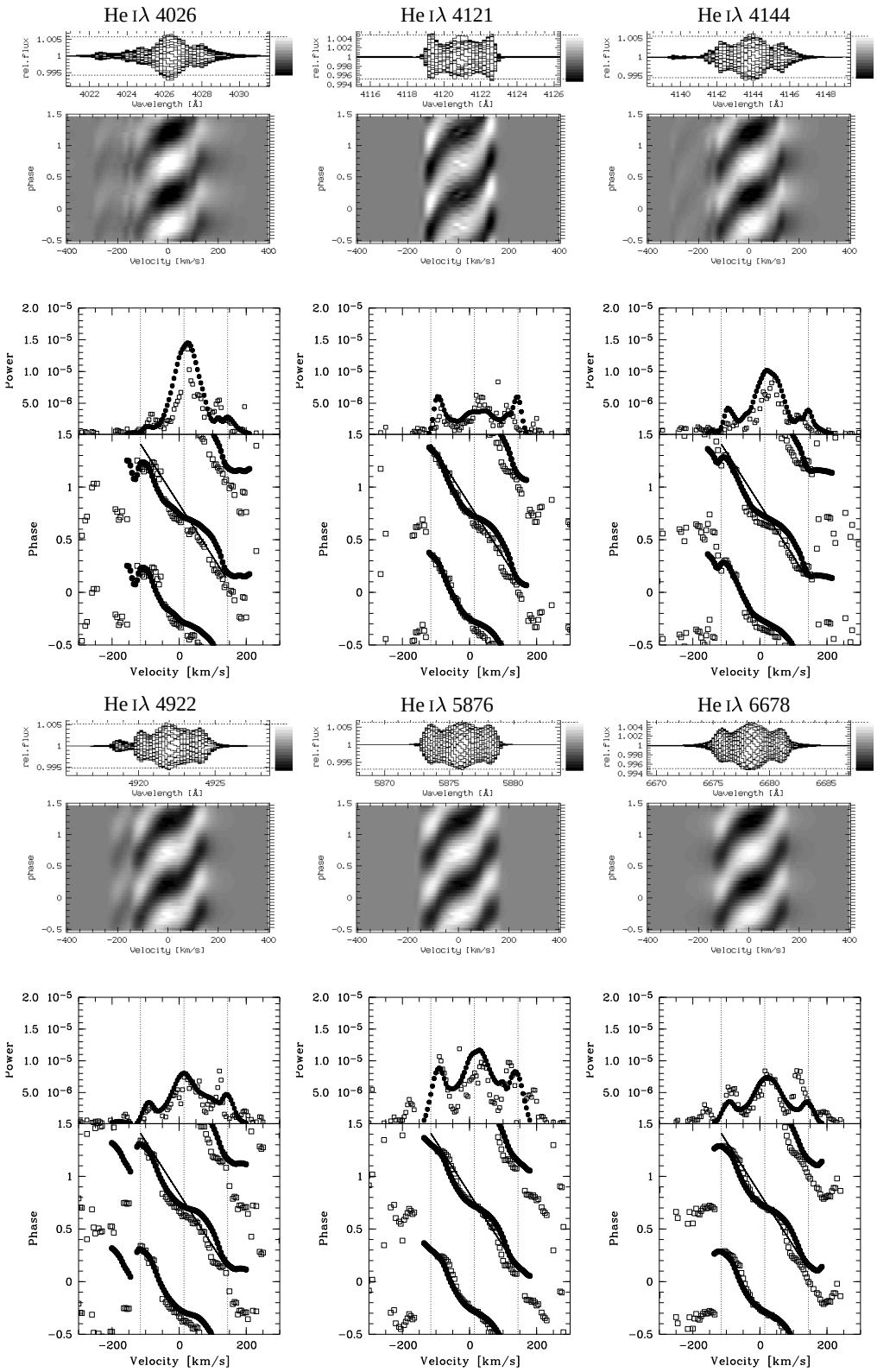

Figure 5.8: The variability of other He I lines modelled by the (3,-2) mode for $\mathcal{P}_5$ (•) compared with the respective data (○). The parameters used are noted in Tables 5.2 and 5.3. Note especially that both the absolute power as well as the power ratios of the core and wings agree well

6. Serendipity: The Timing of Outbursts

While the latter chapters the data was introduced, classified and the immediate findings were discussed, this chapter tells the story of the most important result of this work, that was derived by assembling the previous findings into a unified scheme:
Working on the datasets available in November 1996, I got the first multiperiodic solutions for the photospheric variability. As a test I summed up all then known four sinewaves to see how good the reconstruction of the data would be. Doing so, I calculated also the overall beating-modified amplitude as a function of time. It became apparent that there are strong maxima with secondary maxima due to the tri-periodicity of the $\mathcal{P}_1$ group. It reminded me to the dataset taken by Hanuschik et al. (1993), who have observed a sequence of major – minor – major – minor – major outbursts. A first estimate of the time elapsed between two major outbursts quite well agreed with the beat-period.
I then compared the calculated overall amplitude to the emission specifically for the 1996 season, when the outbursts were easily recognizable (cf. Fig. 6.1, lower left). Obviously something was in the air. Reconstructing the amplitudes for 1995 gave less obvious, but by no means inconsistent results (cf. Fig. 6.1, upper right). Encouraged, I calculated back the (then) ten years to Hanuschik's data. The dates did not fit very well. The temporal structure did, however (cf. Fig. 6.1, upper left). Even the minor outbursts observed by Hanuschik had a correspondence in the overall amplitude. The pattern seemed shifted, what can well be attributed for by the accuracy limit of the derived periods.
In an experimental model the amount of ejected mass was calculated by:

1. allowing the amplitudes of all three modes to grow
2. defining an outburst threshold for the vectorial amplitude sum
3. damping the amplitudes and ejecting mass so long as the threshold was exceeded

At this stage I was quite confident that I had found something, but yet did not dare to tell anybody but my advisors and collaborators. For the next run in early 1997 however I precalculated the expected beat amplitude and mass ejections. Unfortunately the run should start quite exactly with an outbursts and end with one, with little happening in between. We have been lucky. The onset of the outburst in the beginning was clearly observed, and maybe even the first hints of rising activity in the end (cf. Fig. 6.1, lower right, first datastring). This convinced not only myself, but also my colleagues, and following a suggestion of Dietrich Baade when I visited him at ESO we prepared a Be Star Newsletter (BSN) contribution for the following issue, in which we would submit an activity prediction for Summer 1997 (Rivinius et al., 1997d). It was received by the BSN editors on 1997 February 20 (MJD = 50 500).
Our final run at ther ESO 50cm telescope was scheduled for this season, again unfavourably framed between two expected larger outbursts and only two smaller ones during the run. Since the ESO 50cm was already planned to finish operations and being mothballed immediately after our last observing night, it seemed to be the last chance to verify such a prediction with a timebase of two months. Again, we've been lucky enough to observe the outburst at the beginning and the minor ones, but this time the one at the end was missed (cf. Fig. 6.1, lower right, second datastring). Conny Aerts, Michelle Thaller, and Martin Kürster kindly agreed to take a few follow up spectra

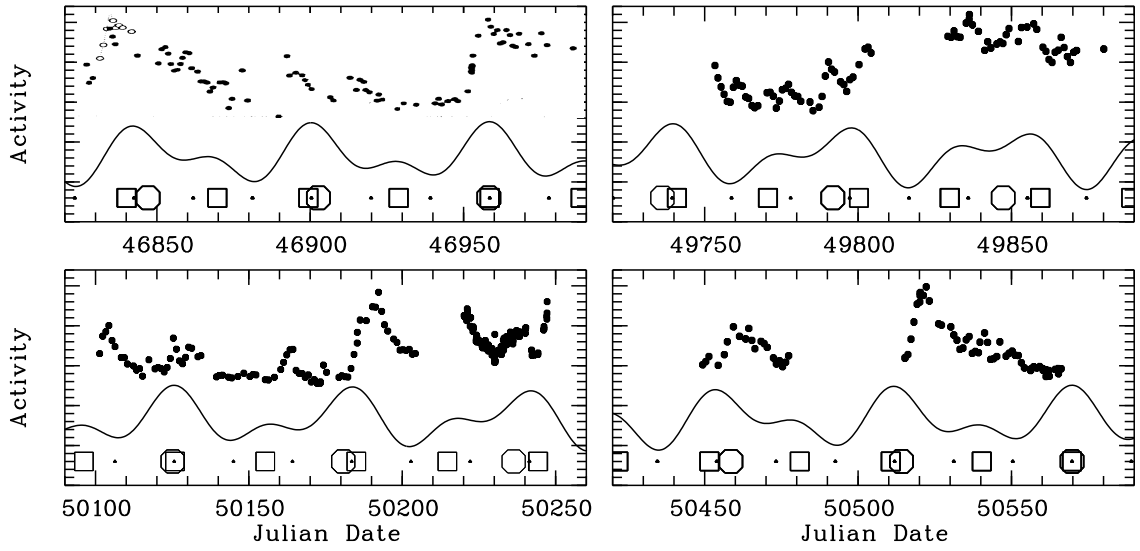

Figure 6.1: The observed emission activity (upper dots), the overall reconstructed amplitude of the $\mathcal{P}_1$ group (solid lines) and the times of zero phase difference for $\Delta\phi_{1-2}(\circ)$, $\Delta\phi_{1-3}(\square)$, $\Delta\phi_{2-3}$(dots) (bottom part of the panels). The sizes of the symbols denote the relative importance. It can be well seen that $\mathcal{P}_2+\mathcal{P}_3$ causes only minor additional effects, if at all. The observed activity was derived from Hα for Hanuschik's data (upper left), while for 1995 (upper right), 1996 (lower left), and 1997 (lower right) the Hδ data (see Fig. 3.3) is shown. The uncertainty of the periods may cause shifts in the order of ten days, but the temporal pattern of the outbursts can still be recognized

with CAT/CES and from the United States, but with the restricted wavelength coverage of the instruments used it unfortunately was not possible to extract a clear activity monitoring quantity from the wavelength range taken.

It became apparent that the above model reconstructed well the fast rise of emission and the relative sizes of outbursts, but the stronger an outburst was, the earlier it was calculated compared with observations. The smaller an outburst was, the better it was reconstructed. Since this systematic error was stable for all calculated seasons, i.e. also for 1986, it was not related to the accuracy of the periods. As, entirely phenemenological, solution it was found that the outburst *date* is actually constrained not by the overall amplitude sum, but by the difference of the phases, while the *strength* of an outburst can be explained with the overall amplitude.

There are at least two conditions for an outburst to be statisfied: First the phase difference of two given modes must be close to zero, and second the amplitude sum of these two modes has to exceed a threshold.

With the additional detection of $\mathcal{P}_4$, but the outbursts still being well reproduced by the Periods $\mathcal{P}_1$ to $\mathcal{P}_3$, the lucky circumstances of this finding became even more clear:

At one hand, the outbursts are abundant enough to observe a sufficient number of events. At the other hand, only two out of six possible combinations lead to strong outbursts, not even counting the non-contribution of $\mathcal{P}_5$ and $\mathcal{P}_6$ that will be discussed later (Sect.8.2.2). If the mechanism would be more efficient, it is well imaginable that a kind of quasi-permanent mass-ejection would happen, so that no timing scheme could have been derived. This also ensures that no further modes of the $\mathcal{P}_1$ group are excited with significant amplitude.

7. Discussion

7.1 Summary of the Results for μ Cen

The circumstellar variability largely consists of discrete events which can be characterised as outbursts during which matter is ejected by the star and possibly even (partly) transferred to the disk. The relative contributions of outbursts and stellar wind to the total mass of the disk are currently unconstrained. In any event, μ Cen is building up a new persistent disk which was not detected between 1977 and 1989.

An outburst cycle appears to be composed of a sequence of relative quiescence, a short pre-outburst phase (precursor), the outburst, and an extended relaxation phase. However, outbursts may differ substantially not only in amplitude and duration, but also in the relative prominence of the above noted constituents. This depends on the absolute strength of the disk emission already present, i.e., on the mass and optical thickness of the disk. Especially the burst and the relaxation phases can be missing completely in outbursts during which the disk emission is strong. By contrast, the precursor phase is the stronger the higher the disk emission is.

Even at low emission levels a new outburst may appear before the relaxation to the pre-outburst level is completed. Also, relaxation may proceed more slowly with increasing disk mass, so that relative quiescence as defined in this paper may eventually never be reached any more once a strong disk has been built up.

The relative quiescence is a phase of merely minor variability in the hydrogen lines, the smallest separation between double emission peaks of all phases, and the absence of Fe II emission lines. As a precursor to an outburst, a sudden decrease in emission peak height occurs. At the same time, broad emission wings appear. The outburst is defined by a rapid increase of the emission strength, rapid cyclic V/R-variability, high velocity absorptions, and a rapid increase of the emission peak separation. In major outbursts, also Fe II emission lines appear. The relaxation phase can be described briefly as the development from outburst into quiescence phase.

For the first time in a Be star the time scale of the rapid cyclical V/R-variability was found to be quite different from the period of the stellar line-profile variability (cf. Sect. 3.3). However, this V/R variability seems to be linked to the outbursts. In fact, the differences of $\pm 5\%$ of the former between different outbursts and the mean value of about 0.6 day are consistent with an ejected cloud of gas which orbits the star a few times at a small radius until it is dispersed or merges with the disk or falls back to the star or some combination of these processes.

Especially at times of enhanced V/R variability, short-lived discrete absorption components of the stronger He I lines may appear which are blueshifted by about 1.5 times the stellar $v \sin i$. They are, therefore, unlikely to arise from the photosphere. The opposite is true of other sharp absorption features which appear at both positive and negative velocities but are restricted to about $\pm 0.7\, v \sin i$. Because of their probable photospheric origin and association with the photospheric line-profile variability, they are described only in Chaper 4.

Some of the generalizations that have been attempted in this study of the outbursts of μ Cen *may* also apply to other Be stars. However, with no second case known in nearly as much detail, this is arbitrarily uncertain. Especially the geometry of the disk and its orientation with respect to the observer may lead to some modifications.

7.2 Comparison with other Be Stars

Outbursts do not seem to have been observed at the same level of detail in other classical Be stars. But those (less complete) observations that are available suggest a number of similarities which are worthwhile recalling:

1. Rapid de- and/or increases in equivalent width of emission lines have been seen in stars like FY CMa (Peters, 1988), λ Eri (Smith, 1989), ω Ori (Guinan & Hayes, 1984; Hayes & Guinan, 1984), or HD 76 534 (Oudmaijer & Drew, 1997).
2. Enhanced wings of the Hα emission during an outburst have also been detected in ω Ori (Baade, 1986). Also the anticorrelation between Hα and Fe IIλ5317 that has been observed in a few profiles of HR2825 and HR5223 by Hanuschik et al. 1996 (their Figs. 34d and 56d) would fit into the description of an outburst phase. While the Hα peak height is reduced in these spectra, Fe IIλ5317 and the Hα wings are enhanced. Also the peculiar shape of Brγ in 59 Cyg observed by Waters & Marlborough (1994) is remarkably similar to the Pa_{15} profile of μ Cen during an outburst. But the example of γ Cas (McDavid & Gies, 1988) may be indicative of this not being a uniform behaviour.
3. Rapid cyclic, or possibly even periodic, V/R variations have been reported for various other Be stars, e.g. ω CMa (1.37 days in Hβ, Baade 1982), λ Eri (0.701 days, Bolton 1982; 0.714 days, Smith 1989) and EW Lac (0.7 days, Pavlovski & Schneider 1989).
4. A clear example for a precursor event in our own database is seen in κ CMa (cf. Fig.7.1). Also the photometric activity of this star found by Balona (1990), a sudden increase in brightness together with the onset of rapid variability ceasing within the next few days, is compatible with the scenario sketched in Sect. 8.4.
5. ω CMa and 28 Cyg in the HEROS dataset both show mono-perodic *lpv* photospheric and corresponding searchlight type behaviour. This is clearly seen only for real strong emission and no or only little irregular variability (Rivinius et al., 1998f, Fig. 7.2). Only the time series analysis did reveal this kind of variability also in μ Cen.
6. η Cen exhibits the most similar disk variability to μ Cen (Rivinius et al., 1998f). The peak separation variability typical for the relaxation, the outburst bevaviour, weak precursor events, and even indications for rapid V/R variability are observed.
7. HD 183 133 has been identified photometrically as SPB star and therefore as g-mode pulsator (Waelkens et al., 1998), but has a high $v \sin i$ of 370 $\mathrm{km\,s^{-1}}$. It consequently has not only been reported to exhibit Hα-emission temporarily, but even periodic outbursts were found with a spacing of 48 days (Lawson et al., 1994). This regularity was attributed to an unknown companion then, but a re-investigation of this case seems promising.
8. The photometric observations by Hipparcos are suited for period analysis of Be stars only in cases with not too strong medium term trends because of their unfavourable sampling. However they have also been examined with respect to outbursts (Hubert & Floquet, 1998). Three types of outbursts are found, i) short lived brightenings, ii) long-lived brightenings and iii) short lived fadings. The short lived patterns i) and iii) are proposed to be caused by the same mechanism seen under different angles, i.e. the brightenings would be outbursts observed in face-on disk, while the fadings would be outbursts observed in edge-on disks. So e.g. μ Cen and ω CMa are listed as type i) stars, while ϵ Cap is noted as type iii) star.

It would, therefore, appear not only a necessary but perhaps even reasonably promising undertaking to search other Be stars for a similar behaviour so that it becomes clearer to what extent μ Cen is a representative case (cf. Sect. 8.5).

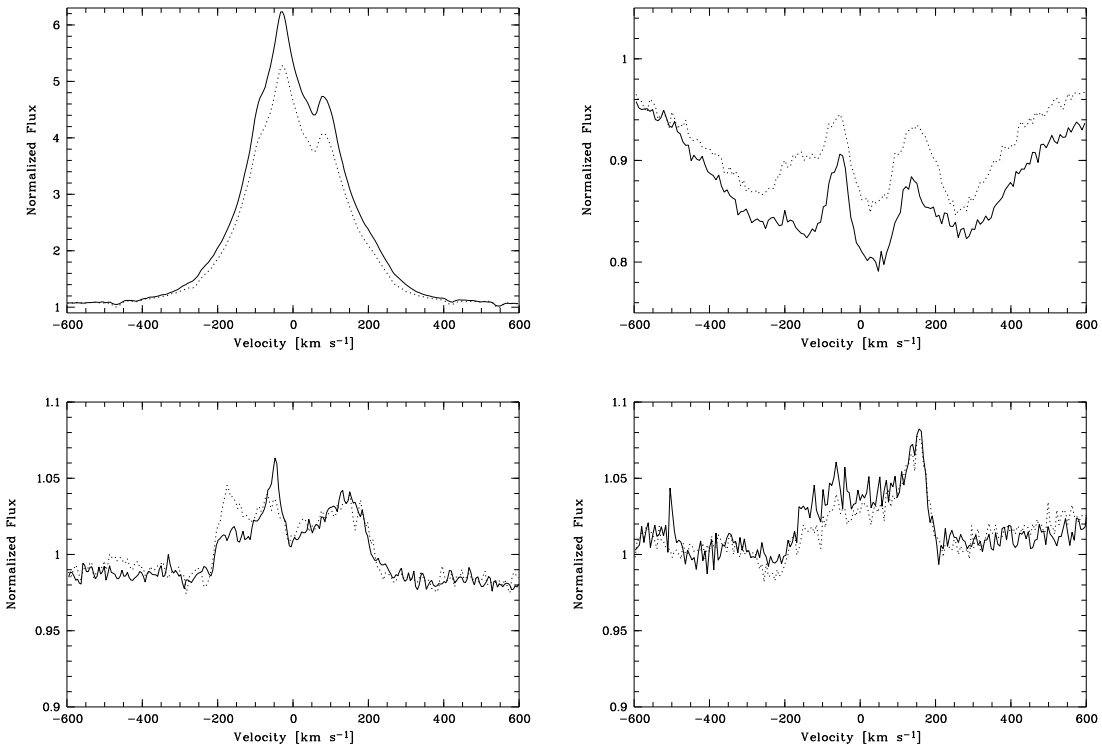

Figure 7.1: Following a phase of non-variability, the Hα-emission of κ CMa was reduced significantly within four days (upper left), while the other Balmer lines did show the typical broad wing increase connected to an outburst (Hδ, upper right, cf. Fig. 3.3). A localized, high velocity emission component was detected in lines of mostly close circumstellar origin, as in Si IIλ 6347 (lower left), while lines formed in the outer disk regions as Fe II (lower right) are, as in μ Cen, not (yet) affected.

7.3 The Genuineness of the Periods

Low-order line-profile variability such as the one of μ Cen seems to be almost a secondary defining characteristic of Be stars (Baade, 1987b; Gies, 1994); in broad-lined B stars without emission lines or β Cephei-type photometric variability (sometimes called Bn stars) it is much less frequently found (Baade, 1987b). High-order line-profile variability is another commonality of most Be and Bn stars (Vogt & Penrod, 1983; Baade, 1987b; Gies, 1994; Kambe et al., 1993a; Štefl et al., 1995, e.g.). Low- and high-order line profile variabilities usually have different, presumably incommensurate periods (or time scales, cf. Gies 1994). However, persistent multiperiodicity has so far been found only in ζ Oph (Kambe et al., 1993a; Kambe et al., 1997) with periods being in the order of hours.

This study presents one of the most complex and perhaps also most complete documentations compiled so far of the spectroscopic variability of any Be star. It is tempting to argue that, if the first Be star, which is observed in this detail and, moreover, very nearby, reveals such a wealth of information, many, if not most, other Be stars will do the same if observed in the same way. However, it must be kept in mind that μ Cen was selected because of its known record of considerable activity of various types. Furthermore, before prematurely elevating the behaviour of μ Cen to a proto-type (a designation that ignores that proto-types are never like the serial models), the

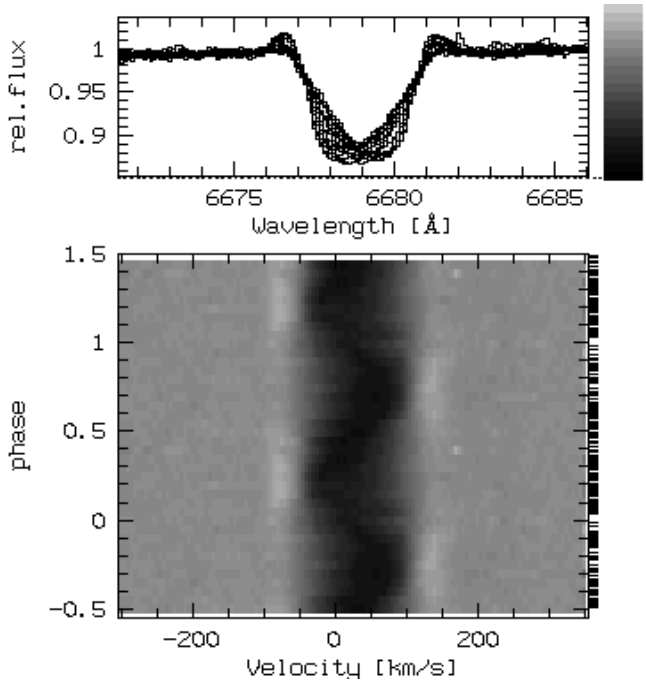

Figure 7.2: The searchlight-type variability of ω CMa in 1997. Displayed is the He Iλ 6678 line folded with the photospheric period. The photospheric core of the line varies with the well known photospheric period. Additionally at about -100 and +150 $\mathrm{km\,s^{-1}}$emission peaks appear at the phases of maximal asymmetry of the profile. That this variation is caused by variations of the underlying wings is excluded by a) the variation amplitude in flux is higher than any expected wing, b) the dependance of the variation power on the absolute emission strength, and c) that a local minimum exists in the Fourier power across the profile at $\pm v \sin i$ (cf. Fig. 4.7)

correctness of our analysis of this behaviour needs critical assessment:
In fact, fundamental problems with the TSA of μ Cen derive from (i) the proximity of the first group of periods to an integer fraction of a day, (ii) the single longitude at which all observations were made, and (iii) the, at this moment, unparalleled complexity of the power spectrum. Another curious point is the regularity of the spacing of the frequencies, namely $f_1 - f_2 \approx 0.5 * (f_2 - f_4) \approx 0.5 * (f_3 - f_1) \approx 0.0175$ c/d. (With presently only two frequencies, no such pattern can be found in the second group. The difference $f_5 - f_6 \approx 0.029$ c/d is not in any direct way related to the frequency differences within the first group.) However, the database balances these circumstances, and actually helps to ascertain the credibility of the findings among them, through (a) the large number of observations, (b) their extension over some 3000 cycles (8000 merging all He Iλ6678 data from 1985 to 1997), (c) their inclusion of many spectral lines, (d) their ability to resolve well the line profile variability in velocity, (e) their origin from different instruments, and (f) their multiple coverage of all phases of mass loss events.
This potential of the database has been exploited in numerous tests, including the checking and eventual elimination of alternative hypotheses, in order to stress-test the reality of the multiperiodic behaviour described in Sects. 4.1 and 4.2:

1. The n-c/d peaks in the power spectrum (Fig. 4.1) are not all due to the sampling.
   The 2-c/d peak is with large statistical significance the highest one. Only with periods in this 2-c/d group can the dense CAT/CES series of profiles obtained over a few nights (see also (Fig. 7.3) as well as the sparser FLASH/HEROS series extending over many months (cf. Fig. 4.7) be combined into meaningful dynamical phase spectra.
2. The multiperiodicity does not arise from general aliasing.
   The periods describe not only the variability of the radial velocity, a scalar quantity, but also the one of the *phase* across the entire line profiles. It is extremely unlikely that by using the alias of a genuine period one can sort the line profiles such that the phase variation still

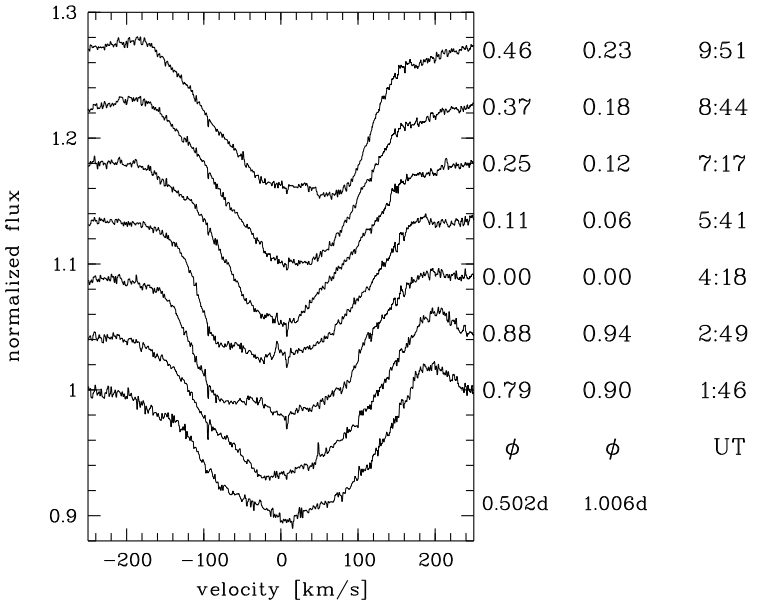

Figure 7.3: Profiles of He Iλ6678 obtained over the course of a single night (April 3, 1986) by Baade (1991) using CAT/CES. Only part of the data is shown in order not to overload the figure. The spectrum taken at 4:18 UT shows maximum blue asymmetry. The phases ϕ of the other spectra were calculated with respect to this spectrum and periods of $\mathcal{P} = .502$ and $\mathcal{P} = 1.006$ d. It can be easily seen that the profile variability over the symmetric phase at 7:17 UT to the red asymmetry at 9:51 UT is not consistent with the phase difference corresponding to $\mathcal{P} = 1.006$ d. Comparable series of profiles occurred also in other CAT/CES runs and in the HEROS spectra taken during the intensive run in May/June 1996 (albeit at higher noise and lower resolution than in the CAT/CES spectra). Note that the V/R ratio of the emission components varies on a similar but slightly longer time scale

looks smooth and monotonic as it clearly does in Figs. 4.7 and 4.8.

3. All candidate periods are robust against random selection of the data points analysed.
   When minor or major subsets of the RV measurements are excluded from the TSA, the significance of peaks in the power spectra is reduced, and the window spectrum changes. But this is all in agreement with the expectations.
4. The positions of all relevant features in the power spectrum and, therefore, the values of the periods, are very well defined.
   Due to the length of the time baseline all peaks are well isolated (Fig. 4.1).
5. The variations maintain phase coherence for more than a decade.
   Backward-extrapolation of the phase of the strongest variations, with $\mathcal{P}_1$ and $\mathcal{P}_5$, computed from the long FLASH/HEROS observing runs matches the much earlier CAT/CES spectra excellently. For the weaker variations, the phase is more uncertain for the CAT/CES data, but still in agreement with the FLASH/HEROS results. Only for $\mathcal{P}_2$ could this not be assessed (Sect. 4.1.2).
6. The frequency splitting is not an artifact of the combination of one or more periods with a slow trend.
   To within the errors the periods do not depend on whether or not prior to the TSA a fitted linear trend is subtracted from the data.
7. The same was ascertained by means of synthetic data with the same sampling in time as the

real observations. No combination of a single sinewave with period $\mathcal{P}_1$, noise, and a linear trend introduced apparent multi-periodicity. The input period was always returned as the only significant one.

8. The frequency splitting is not only apparent due to the superposition of one or more short periods and one or more longer ones corresponding to the observed pattern in the frequency differences. In particular, the regularity of the frequency differences with the 2-c/d group cannot be explained in this way.
   Prewhitening in different orders not only for the claimed periods but also for the beat periods yielded in no case results that were nearly as satisfactory as shown in Figs. 4.1 and 4.2.
9. The beat periods of the 0.5-c/d group do have a physical relevance of their own.
   They govern the occurrence of line emission outbursts (Rivinius et al., 1997d; Rivinius et al., 1998c, Chapter 6). The times of outbursts are determined in a completely different way and are moreover based on circumstellar emission lines only. Since it has been verified that the multiplicity of the 0.5-c/d periods is real, this provides entirely independent evidence of the correctness of the photospheric 0.5-day periods.
10. Effects of instrumental, calibration or measurement errors on the values of the periods or their existence must be small.
    The He I and Si III lines fall onto a number of different echelle orders, and He I λ6678 was even observed with entirely different instruments delivering different spectral formats. Nevertheless, in all cases, the periods $\mathcal{P}_1 - \mathcal{P}_4$ agree to within the uncertainties in both phase and value (Table 4.1).

In summary, the characterization by Tables 4.1 and 4.3 of the stellar spectroscopic variability of μ Cen has survived numerous critical tests and is supported by a considerable diversity of solid observational facts.

7.4 Photometry

The spectroscopic periods can be compared with the photometric double-wave period of 2.10 day observed in 1987-1988 by Cuypers et al. (1989) and the photometric single-wave period of 1.06 day reported by Dachs & Lemmer (1991) for 1986-1989. Obviously, these two periods are the same depending on whether or not even cycles are more similar to each other than to odd cycles. Only the data of Cuypers et al. are published. Our re-analysis suggests a period near 1.05 day but cannot distinguish between it and its 1 c/d alias near 23 days, while formally the longer period even has a slightly higher significance.

Finally, the Hipparcos and Tycho photometry (Perryman et al., 1997) is dominated by strong incoherent variability on longer timescales which is conceivably related to processes such as those described in Paper I. However, the sampling of these data is not dense enough to define times of events that could be compared with those of any observed line-emission outbursts (see Paper I). For the same reason it is also not possible to subtract this long-term variability from the light curve, and in the data as published none of the 6 short periods could be recovered.

The photometric data are incompatible with a 0.5-day period whereas there is no need to assume that the spectroscopic data are better represented with a 1.05-day double wave. In any event, the co-existence of a double-wave spectroscopic variability with a single-wave light curve of the same period finds no easy match in current models for the variability of Be stars. But so does the switching between single- and double-wave light curves at constant period observed in other Be stars (Balona et al., 1991). Such a mechanism, if active also in μ Cen and working in the right sense, could at least for the moment reconcile photometric and spectroscopic behaviour.

μ Cen definitively exhibits a quite complex behaviour even for a Be star. From the spectroscopic point of view there is:

1. short term periodic variability of the photosphere (Sect. 4.1.1, pulsation)
2. short term irregular variability of the photosphere (Sect. 4.3, e.g. spikes)
3. short term transient periodic variability of the close disk (Sect. 3.3, V/R variability)
4. short term irregular variability of the close disk (Sect. 3.2.1, e.g. Helium lines)
5. short term burst type variability of the entire disk (Sects. 3.2.2, 3.2.3, precursor and outbursts)
6. medium term burst type variability of the entire disk (Sect. 3.2.4, relaxation)
7. long term variability of the entire disk (Sects. 1.1.1, 8.3, e.g. B $\Leftrightarrow$ Be episodes)

While the HEROS data contains over two dozen spectral lines that probe entirely different regions of the star and disk, photometry observes the above listed variations integrated into a single number. Therefore photometry can develop its full power only in conjunction with simultanoeus spectroscopic observations to assist in the disentangling of the different variations.

7.5 Modelling Results

The combined constraints of the periodic part of the photospheric variability derived from spectroscopy and photometry can be satisfied by *nrp* modelling. The results for $\mathcal{P}_1$ unambigously favour an $l = 2, m = -1$ tesseral mode. Since $\mathcal{P}_2$, $\mathcal{P}_3$, and $\mathcal{P}_4$ do have the same constraints, this result also applies to them. The corotating period of the $\mathcal{P}_1$ group is about 0.73 day. The strongest mode, $\mathcal{P}_1$, has a maximal physical velocity of about $13\,\mathrm{km\,s^{-1}}$ on the stellar surface. $\mathcal{P}_2$ and $\mathcal{P}_3$ have a slightly lower amplitude, while it is much lower for $\mathcal{P}_4$ (cf. Table 5.3). Similarly, $\mathcal{P}_5$ and $\mathcal{P}_6$ both can be understood as pulsation in a higher mode, i.e. (3,-2), for which the corotating period would be about 0.43 day.

7.6 The Predictability of Outburst Events

In Chapter 6 it was shown how the dates of observed outburst can be reconstructed using the results of the TSA on photospheric quantities. Since the relevant parameters, once derived, do not change with the availability of new data except for an improved period accuracy, this technique can be used to predict future outbursts events. Actually such a prediction was submitted to the Be Star Newsletter prior to the observations in March/April 1997 during which this prediction was confirmed (Rivinius et al., 1997d; Rivinius et al., 1998e).

Formally a "postdicition" of previously unknown datasets is equal to a confirmed prediction, and so I have searched the data that is sampled well enough to derive outburst dates in the past ten years. Since I knew the only major non-HEROS datasource for intensive monitoring (Hanuschik et al., 1993) in advance (cf. Chapter 6), only few events remained however:

1. Peters (1995; 1998) observations of an outburst in April 1994 perfectly coincide with an computed one.
2. An outburst event must have happened in early February 1989, when the Hα profile changed from clear absorption and light activity on Feb. 4th/5th, (Peters, 1989), to nearly filled up absorption at Feb. 19th (Ghosh et al., 1991) back to nearly pure absorption on March 4th (Hanuschik et al., 1996). The outburst reconstruction gives around Feb. 11th as date, with any follow-up burst not before mid-March. Because this event was nearly ten years from now, the 6 day difference from the alleged onset on Feb. 5th to the computed date on Feb 11th could be explained by the uncertainty of the derived periods and the fact that the activity was still lightly increasing before the actual outburst started.

3. Only minor emission was present on Mar. 17th (Ghosh et al., 1991), which rose to $E/C = 1.2$ in April 2nd (Peters, 1990) and decreased at least until April 18th. The only strong computed outburst took place a few days prior to the first observation, on March 11th, for which the same accuracy arguments apply as above.

As a rule the closer any reported outburst is to the HEROS dataset, the better its behaviour is reconstructed due to the uncertainties of the TSA. Numerous other outbursts reported in the literature are derived mainly from the fact that the star had emission when it had none a few weeks before and thus an exact determination of the outburst dates was not possible. So in all of these cases at least one of the computed events is present in the gap between two observations that could account for the rise of emission.

8. Conclusions, Outlook and some Speculations

The comprehensive spectral database offers the possibility to study the time dependent phenomena in the Be star μ Cen not only as isolated events but also to assemble them into a vivid picture of an active Be star.

8.1 Photospheric Variability

In this study, detailed time series analyses of the stellar line profile variability were performed using conventional RV's as well as the flux in narrow velocity bins of fixed width and sampling the entire line profile. Both results agree to within the errors. Thanks to the long time baseline, the previously suspected 0.505-day period (Baade, 1984a) could be resolved into 4 distinct, closely spaced periods. In the Fourier domain, the spacing between the two outermost of the 4 frequencies and the respective next inner one is about 0.034 c/d, whereas the one between the two innermost ones is half that large.

The line-profile variability patterns associated with these four periods are very nearly the same for all lines investigated and can be best described as a roughly sinusoidal low-order modulation propagating across the line profiles over the full range of $\pm v \sin i$. Two additional periods close to 0.28 day and with a different pattern of the line-profile variability were also detected. Not all 6 periods were detected in all of the 21 spectral lines investigated. In stronger lines such as He I$\lambda\lambda$6678 or 5876, significant power seems to extend beyond the range of $\pm v \sin i$ which is probably due to emission from the circumstellar disk. Since the frequencies of this variability are indistinguishable from the photospheric ones, some influence of the photospheric variability on the circumstellar zone may be suspected.

Careful and fairly diverse tests could not seriously compromise the reality of the reported multi-periodicity.

Because (i) the basic period search could be performed on a single, homogeneous data set, (ii) all six periods maintained phase coherence over the course of years, and (iii) the associated variability patterns could serve nearly as textbook examples of their kind, the above findings should rank among the most significant detections of photospheric multiperiodic low-order variability in any Be star.

Especially during the precursor phase announcing imminent line emission outbursts and partly through the early stages of the outburst itself, the stellar line profile variability may change. Additional narrow absorption spikes appear at about $\pm 0.7\, v \sin i$, but always do so only in one wing at any given time. These features appear in a cyclical way, where the cycle length is indistinguishable from the 0.5-day group of periods. An accompanying second phenomenon is the occurrence of very extended, ramp-like wings which are always on the side of the profile opposite of the respective narrow absorption spike.

During a line-emission outburst the RV of some lines may temporarily be dominated by other, cyclic variations. In the one data set suitable for a TSA, a cycle length of 0.58 day was found in Balmer and He I lines. The same cycle length was also detected in the V/R ratio of the Hβ emission.

8.2 Nonradial Pulsations...

8.2.1 ...in the Photosphere

As mentioned in Chapter 5, the pulsations of μ Cen are likely to be g-modes judged already from the properties of a single one of the observed modes. From the theoretical point of view it is not clear yet if and to what extent such modes are stabilized by rapid rotation (Soufi et al., 1998; Lee & Saio, 1997; Lee & Saio, 1990; Lee & Saio, 1987b).

Pulsational g-modes are generally accepted to be present in more slowly rotators, the so called slowly pulsating B-stars (SPB). Waelkens (1991) proposed these stars to be a distinct group of variables, but only few members were found. Nevertheless a theoretical framwork for this class was given by Dziembowski et al. (1993) and recalculated and extended to other metallicities by Pamyatnykh (1998). They derived as a specific feature of g-mode pulsating B stars that they should have more but one mode excited of equal angular indices l and m, differing only in radial order n, n being a high natural number. Such modes should differ only in a slightly shifted period. The difference between such two periods is given by $\approx \mathcal{P}/\Delta n$. Recently, photometrical Hipparcos observations that do not suffer from a 1 c/d alias problem have increased the number of known SPB's by 72 stars (Waelkens et al., 1998). These stars nearly perfectly fill up the instability strip predicted by Pamyatnykh.

A major problem in extending the SPB phenomenon to rapid rotators is the low or missing periodic photometric activity of Be and Bn stars, which in turn is a defining criterion for an SPB. It is however worth to recall here that the differences between the four periods of the longer group are 1.8% – 0.9% – 1.8%, and may thus be explained if they are caused by g-mode pulsation of radial orders $n \approx 50 \ldots 100$. In such a case a mode selection mechanism would have to act to leave at least two modes unexcited; which otherwise would be located in the gaps of the double difference. Also interesting would be an investigaton if the apparent cut-off of SPB's towards faster rotators could be explained by the phometric cancellation mechanism (cf. Sect. 5.3).

8.2.2 ...Influencing the Disk

An influence of the pulsational waves on the close circumstellar environment was found for the stronger modes in the lines formed presumably in the photosphere-disk transition region, as He I$\lambda\lambda$5876, 6678, 7065. As HEROS observations confirmed also for other stars, this is a quite general behaviour for Be stars (Tubbesing, 1998, e.g.; and Fig. 7.2).

The observed asymmetry in the distribution of pulsational power across the line profile depending on line strength might indicate wave leakage. However the involved velocities are not even nearly sufficient to explain the loss of a significant amount of matter to the circumstellar environment. A strongly non-linear process has to act to accelerate the material on the observed short timescales.

As was shown in Chapter 6, the beating of the modes $\mathcal{P}_1$ to $\mathcal{P}_3$ governs the outburst dates. It remains to be shown if the process responsible for the ejection of matter can be explained by the pulsation alone or if the beating just acts as trigger. The observations might point to a solution, if one assumes that the observed absorption spikes at times of outbursts (Sect. 4.3) are indicative for the above postulated non-linearity. Smith (1985) has proposed this type of variability in Spica to be connected to Rossby waves. Rossby waves (r-modes) may attain very high horizontal velocities before turbulence puts an upper limit, since the velocity field is a closed vortex pattern. However these modes, driven by the Coriolis Force, are always directed against the sense of rotation in the equatorial plane.

Another idea was given by Osaki (1986), who proposed outward angular momentum transport by *nrp* waves. The photospheric material in the wave does move with a *particle velocity* below

the local speed of sound. The speed of the pertubation on the stellar surface however, the *phase velocity* of the wave, might not only be supersonic, but even be supercritical to the rotational velocity. If the waves in this picture would "break", the "spray" can be accelerated to the phase velocity of the wave, and thus to supercritical velocities causing mass ejection. In Osaki's original model this "spraying" is a smooth process, induced by *nrp* growth and stopped by the damping of the *nrp* due to energy leakage into the circumstellar environment.
In μ Cen this assumption of growth and damping is not necessary. The positive interference of the modes could bring the physical amplitude of the associated wave quite suddenly into the necessary high regime. The outbursts start and stop as imposed by the phase difference of the contributing modes. Also the apparent threshold that leads to observable bursts only for $\mathcal{P}_1 + \mathcal{P}_2$ or $\mathcal{P}_1 + \mathcal{P}_3$, but only to very minor ones for $\mathcal{P}_2 + \mathcal{P}_3$ and no direct contribution by $\mathcal{P}_4$ at all, may find an explanation in this model. Only the amplitude sums of the first two combinations get into the order of the speed of sound on the stellar surface ($20 \ldots 25\,\mathrm{km\,s^{-1}}$), if the physical amplitudes derived from the modelling in Table 5.3 are assumed. Thus the particle velocity might locally, in the wave, but not globally, be high enough to induce strong turbulences and maybe even shocks.
The above would also explain the missing contribution of $\mathcal{P}_5$ and $\mathcal{P}_6$, because as they belong to different pertubation pattern, the superposition of these two different pattern would not increase the vectorial velocity on the stellar surface coherently. As well does the superposition of $\mathcal{P}_5 + \mathcal{P}_6$ not exceed the postulated threshold.

8.3 B ⇔ Be Episodes

The emission characteristics of Be stars is not of truly stable nature. Albeit most Be stars are observed for decades with stable strong emission, this emission eventually may decay. In this case the star becomes undistinguishable from a normal rapidly rotating B star. A few years of no or only flickering activity later the envelope may build up again. For μ Cen two non-emission episodes are known, the first lasting for about a decade around 1918 and the second from 1977 until about 1989.
For the calculation of the outburst dates we have taken into account only the three strongest periods of the $\mathcal{P}_1$ group. However, the fourth period does not only introduce one more timescale in the order of the beat periods, but also a long term cylicity in the amplitude pattern. The derived accuracy of the period determination is not sufficient to calculate back a whole century. However, within the derived accuracy and assuming long term stability of the observed periods and amplitudes, there exist parameter sets, for which the strength of the beating events go through a minimum around 1920 and another one in the eighties, being maximal in the fifties. In view of the model sketched in the previous section, a lower maximal velocity at the time of zero phase difference could well inhibit the equatorial mass loss mechanism, if the lower maximal velocity would not exceed the critical velocity for the wave to "spray".
The property of both μ Cen non-emission phases lasting about the same time would be a natural consequence of this hypothesis. That no flickering emission was observed in the twenties is, with respect to the techniques used, no prove of its absence. The assumption of the long term stability of the period properties is at least satisfied back to 1986 (Sect. 7.6). I believe however, that this riddle will be solved prior to 2040, when μ Cen may loose its recently built-up disk for the next time.

8.4 Star-to-Disk Mass Transfer

A short, purely descriptive picture of the kinematics of an outburst is inserted here. I derive from it qualitative, observable phenomena and compare them with the actual variations. Smith et al. (1991) and Hanuschik et al. (1993) developed rather similar conjectures, which partly have old historical roots, and also go through some numerical exercises. In addition to the ephemeral mass loss, there may also be a continuous wind (see Lamers & Pauldrach 1991 and Bjorkman & Cassinelli 1993 for winds of Be stars in general and Peters 1979 for UV observations of μ Cen) which, too, is omitted from this description. This high-velocity mass loss is often assumed to be more pronounced at higher stellar latitudes.

The initial growth mainly of the wings of the emission lines probably indicates the presence of rapidly rotating or other high-velocity gas close to the star, i.e. an ejection of matter from the star. This has been observed in other stars, too (Guinan & Hayes, 1984; Hayes & Guinan, 1984; Baade, 1986), and the apparent coarse correlation in μ Cen between wing widths and excitation level would further corroborate this notion. By analogy to other Be stars, one would expect an accompanying increase in linear polarization that is also due to this matter close to the star but which would additionally show that the gas is concentrated towards a plane (Hayes & Guinan, 1984; Guinan & Hayes, 1984; Baade, 1986). Since in the stars observed only the amount of polarization increased but the polarization angle remained constant, that plane would be the plane of the circumstellar disk (Hayes, 1980; Hayes & Guinan, 1984; Clarke, 1990).

If, therefore, the origin of the outbursts is in the central star, also the steep decrease in line emission strength during the precursor phase should originate from the star. The drop in emission strength would thus not be caused by a sudden, temporary loss of circumstellar matter but rather be due to a quickly reduced rate of recombinations in that matter. For the central star to trigger this reduction, one possibility would be a partial loss of the stellar ionizing far-ultraviolet flux. The same was also surmised by Oudmaijer & Drew (1997), although mainly on the basis of a very short time scale of the recovery of the line emission. Another possibility is that some locally highly increased matter density (ejecta, see below) affects the recombination conditions by shielding of the stellar radiation.

An interesting analogy between LBV's and γ Cas was revealed by Marlborough (1997). He suggested that in extreme events as the major γ Cas outbursts "a super, μ Cen-like process," may eject a layer that would behave as "false photosphere simulating a cooler, less dense atmosphere". In the HEROS-data, already properties of the "normal" μ Cen process do support the notation of a pseudophotosphere during an outburst. These are the broad wings of the Balmer lines, that seem to be superimposed by additional emission during an outburst (cf.Fig. 3.3). The wavelength range of HEROS allowed a simultaneous study of these wings in all higher Balmer lines. It was found that they do not scale with the upper level of the respective line, i.e. are of comparable strength for all lines in which the central disk emission does not influence the outer wings.

Similar, but stable, features are known for late A to early B type super- and hypergiants (Kaufer et al., 1996; Rivinius et al., 1997c, e.g.). Clear emission wings are visible in such stars, even if the respective Balmer line has no narrow emission contribution from the stellar wind. This was proposed to be produced by NLTE effects by Hubeny & Leitherer (1989), and recent calculations by the Munich group (Kudritzki, private comm.) have not only confirmed this in principle, but shown that such wings can be suffiently strong to explain the observed cases. So the broad wings observed during the initial phases of an outburst of μ Cen might indicate a dense layer that starts to get away from the central star, while in this layer temporarily temperature and density conditions

as in supergiants prevail. Photometric evidence for such a layer arises from the Hipparcos observations by Hubert & Floquet (1998), who conclude the presence of "discrete high density emitting plasma" during outbursts in a sample of stars.
Whether the gas ejection is concentrated at particular stellar longitudes and whether an outburst consists of only one continuous (or instantaneous) outflow or several separate ejections, can at best be speculated about. The variability of the high-velocity absorptions (Sect. 3.4) could be an indication of a spatially and/or temporally inhomogeneous outflow (as might be the discrete absorption components of UV resonance lines – Grady et al. 1987a). But they could also result from instabilities in the outflow (cf. e.g., Peters 1988).
A stronger hint at spatial inhomogeneities is provided by the sudden onset of the V/R variability and the subsequent slow decline of its amplitude. It might be attributed to a cloud of gas orbiting the star. It would be most compact right after the ejection by the star. But as its azimuthal distribution (and orbit?) is circularized and/or more matter is ejected, the amplitude of the V/R variability would decrease. For a non-critically rotating star, the Keplerian orbital period of such a cloud of gas might even be shorter than the stellar rotation period. This is not impossible for plausible stellar parameters of μ Cen but requires that this gas be quite close to the stellar surface. If magnetic fields play a role in confining the cloud of gas, the 0.6-day quasi-period (Sect. 3.3.2) could also be due to the rotation of the central star. However, the $\pm 5\%$ outburst-to-outburst variation of the V/R time scales (Sect. 3.3 and Fig. 3.8) would rather favour the orbital-motion interpretation.
On the other hand, the apparent relative constancy of the 0.6-day cycle length over 8 consecutive nights (Sect. 3.3.2) would be more readily reconcilable with the magnetic model. But the weight of this argument is reduced because during the same time the nightly mean separation between the two Hβ emission peaks fluctuated by $\pm 3\%$ but did not systematically decrease. Accordingly, the radius of the Hβ-emitting zone would have remained constant (but matter could still have drifted through it).
Finally, (part of) the ejected matter merges with the disk which in this picture would be more or less detached from the star. This is in accordance with the observed decrease in separation between the peaks of emission lines. In the absence of a new outburst, this would correspond to the phase of relative quiescence. Since the emission peak separation of Si IIλ6347 during this phase was lower in 1996 than in 1995, Keplerian rotation as well as angular momentum conservation would imply a higher radius of the line forming region in 1996. Although a relative quiescence phase could not be defined in 1997, the peak separation was about the same as observed in the 1996 quiescent phase. However, now even Fe II emission was present more persistently, with a peak height of about 4–5 % above the continuum.
If the region of formation of the latter lines is purely rotationally supported, the rate of change of their peak separation, 1-1.5 $\mathrm{km\,s^{-1}\,d^{-1}}$ (Fig. 3.5), implies an expansion velocity of less than $5\,\mathrm{km\,s^{-1}}$ for basically all sets of reasonable parameters (e.g. $R_\star = 5.8 \mathrm{R}_\odot$, $v_{\mathrm{crit}} = 418\,\mathrm{km\,s^{-1}}$, cf. Table 5.2), $\sin i = 0.64$), using

$$\Delta v_{\mathrm{peak}} = 2 v_{\mathrm{crit}} \sin i \left(\frac{R_{\mathrm{peak}}}{R_\star} \right)^{-\frac{1}{2}}$$

for Keplerian orbits, following Huang (1972) but modified for the case of a non-critically rotating star. The cumulative growth during a typical relaxation phase of 50 days would then amount to $\approx 6 \cdot 10^6$ km and the radius of the region from where the emission peaks arise would accordingly increase from the initial $2.3\,\mathrm{R}_\star$ (for $\Delta v_{\mathrm{peak}} = 350\,\mathrm{km\,s^{-1}}$) by 1.5-2 $\mathrm{R}_\star$ to 4-5 $\mathrm{R}_\star$.

Note that this alone does not permit to distinguish between the two extreme possibilities of all ejected matter falling back to the star or merging with the disk. However, Fig. 2.1 indicates that the projected equatorial velocity observed in the Fe II lines at the very beginning of the outbursts can be as high as 220 km s^{-1}, which is about 170 % of $v \sin i$. For inclination angles, i, between 30 and 45 degrees, the upper limit of the actual velocity of the Fe II ions is between 440 and 340 km s^{-1}, respectively. This range is sufficiently close to the stellar break-up velocity that gas at the high end of the velocity distribution may conceivably have enough angular momentum to stay in orbit.
If, alternatively, one adopts the case of conservation of angular momentum,

$$\Delta v_{\rm peak} = 2 v_{\rm rot} \sin i \left(\frac{R_{\rm peak}}{R_\star} \right)^{-1}$$

the absolute numbers change, of course, but not their order of magnitude.
This simple picture of the kinematics of an outburst does not seem to be dominated by the presence or not of a dynamically stable disk. One might conclude this on the basis of the very similar (but poorly sampled) strong V/R variability observed by Baade et al. (1988) during the 1987 February outburst of μ Cen when there was close to no persistent Hα emission. Observations by Baade (1991) in early April, 1986, when the Hα emission disappeared within less than 10 days, permit a similar conjecture.
This description of an outburst leaves open the in some sense opposite question of the effect of the outbursts on the disk. In particular, it does not state to what extent outbursts contribute to the replenishment of the disk which under the influence of stellar radiation pressure and internal instabilities would otherwise dissipate. It would certainly be premature at this moment to attribute *all* variations of emission lines of Be stars to outbursts of the type described here because also the high-velocity component of the mass loss from Be stars, i.e. their wind, undergoes drastic variations which do not seem to be closely correlated with Hα outbursts (Grady et al., 1987b; Sonneborn et al., 1988).
The sudden drop in line emission from the disk which precedes any other early symptom of an outburst is presently the strongest indication that the outburst does not leave the disk unaffected. The simple model considered here would suggest (see above) that this effect is not the loss of mass from the disk but a loss of ionising radiation reaching the disk. Apart from a (not otherwise postulated) real temporary reduction in stellar UV flux, the model could also accommodate the notion of shielding of the disk by the ejected cloud(s) of gas.

8.5 Connected and Future Projects

The results on the HEROS data of the Be star μ Cen has stimulated a number of, partially already finished, secondary projects.

1. Sascha Tubbesing (1998, diploma thesis) observed the Be star 28 Cyg with HEROS at the Waltz telescope at the Landessternwarte. Although he found no emission line outbursts, both fast *lpv* and V/R variability was detected with a common period of $\mathcal{P} = 0.6468$ day. Variations are interpreted as non-radial pulsations of the star with a mode of $l = 2$. A correlation between the average equivalent widths of single lines and their average blueshifts was detected. For lines which are not influenced by the emission of the circumstellar disk, stronger lines exhibit a greater blueshift.
2. A further diploma thesis has been started by Monika Maintz to model the *lpv* of several Be stars using Townsend's (1997b) BRUCE and KYLIE pulsational model and integrating code.

She will model the spectroscopic as well was the photometric variability to ascertain if or if not the photometric cancellation of the *nrp* in μ Cen can be assumed as general phenomenon in Be stars.

3. A search for multiperiodicity in northern and equatorial Be stars has been started at the Landessternwarte and is being extended from the Calar Alto observatory, using HEROS during 62 nights at the 1.23m telescope. The observation plan for 1999 for this task is currently under consideration.

In the previous sections speculations and hypotheses have been presented. Some of them can be tested observationally, while for others the situation might be used as input for closer theoretical examination. Owing to the achieved predictability of outbursts, even scarce observational resources as e.g. satellites can now be used for pointed observations of outbursts.

1. For the rapid decrease of emission strength at the immediate beginning of an outburst either radiative shielding or an decrease of the ionising flux from the star itself has been proposed. Both scenarios can be distinguished in μ Cen due to its intermediate inclination. From UV spectra taken with the International Ultraviolet Explorer it is apparent that the outflow in the equatorial plane does not obscure the star in the line of sight. So extreme UV flux measurements probe the ionising flux emerging directly from the star. If observed during an outburst, the flux variations will decide between both scenarios. Test observations with the Extreme UltraViolet Explorer EUVE were performed on August 6th 1998. They confirmed the detectability of μ Cen with the EUVE instruments. A monitoring of two μ Cen outbursts in early 1999 has been applied for.
2. The rapid V/R variability, if caused by an orbiting cloud, should have an impact on the polarisation of the system. David McDavid, who has unlimited telescope access at the private Limber observatory with his own polarimetric instrument, will contribute polarimetric monitoring to the northern-equatorial multiperiodicity campaign. Furthermore he will apply for a small telescope on the southern hemisphere to observe one of the μ Cen outbursts in detail.
3. To obtain close-up spectroscopic observations of an outburst of μ Cen, about ten days of observing time with the newly built FEROS instrument at the ESO 1.52m telescope will be applied for.
4. Stan Štefl will apply for a simultaneous photometric telescope either at the SAAO or MSO.
5. With the derived periods it seems promising to reanalyse the IUE datasets obtained by Peters (1991) and compare amplitude and phase to the modelled flux variability in the UV.
6. The model of mass ejection by breaking of *nrp* waves has been re-investigated by Osaki (1998), who also proposes an explanation for the observed absorption spikes (Sect. 4.3)
7. Owocki (private communications) plans to investigate the evolution of spatially and temporally localised mass ejections from the central star into a Keplerian disk taking into account hydrodynamical and radiative forces.

8.6 Conclusion

As the major results of this thesis it should be recorded that:

$\Downarrow$ The presumably not too exotic *Be star μ Cen does pulsate nonradially*.

$\Downarrow$ These pulsations do trigger, if not account for, the ejection of mass into the close stellar environment.

$\Rightarrow$ ***Pulsational effects probably are to be identified with the disk forming process, the so called Be phenomenon, in μ Cen***.

Bibliography

Aerts C., De Pauw M., Waelkens C., 1992, A&A 266, 294
Aerts C., Waelkens C., 1993, A&A 273, 135
Baade D., 1982, A&A 105, 65
Baade D., 1984a, A&A 135, 101
Baade D., 1984b, A&A 134, 105
Baade D., 1986, Be Star Newsletter 13, 5
Baade D., 1987a, Inf. Bull. Variable Stars 3124
Baade D., 1987b, Be stars as nonradial pulsators, In: Physics of Be stars, Slettebak A., Snow T. P. (eds.), IAU Coll. No. 92, p. 361, Cambridge Univ. Press, Cambridge
Baade D., 1989a, A&AS 79, 423
Baade D., 1989b, A&A 222, 200
Baade D., 1991, Rapid V/R variability of optical emission lines, In: Rapid variability of OB-Stars: Nature and diagnostic value, Baade D. (ed.), ESO Conf. and Workshop Proc. No. 36, p. 217, ESO, Garching
Baade D., 1998, Pulsation of be stars and of ba supergiants, In: IAU Coll. 169: Variable and Non-spherical Stellar Winds in Luminous Hot Stars, in press
Baade D., Balona L. A., 1994, Periodic variability of Be stars: nonradial pulsation or rotational modulation?, In: Pulsation, Rotation, and Mass Loss in Early-type Stars, Balona L. A., Henrichs H. F., Le Contel J. M. (eds.), IAU Symp. No. 162, p. 311, Kluwer, Dordrecht
Baade D., Dachs J., Weygaert R. van de, Steeman F., 1988, A&A 198, 211
Balona L. A., 1990, MNRAS 245, 92
Balona L. A., 1998, Spectral and photometric variability in pulsating stars, In: A Half Century of Stellar Pulsation Interpretations: A Tribute to Arthur N. Cox, Bradley P. A., Guzik J. A. (eds.), ASP Conf. Ser. No. 135, p. 120
Balona L. A., Henrichs H. F., Le Contel J. M. (eds.), 1994, Pulsation, Rotation, and Mass Loss in Early-type Stars, IAU Symp. No. 162, Dordrecht, Kluwer
Balona L. A., Sterken C., Manfroid J., 1991, MNRAS 252, 93
Baschek B., Holweger H., Traving G., 1966, Abhandlungen der Hamburger Sternwarte 8 1, 26
Bjorkman J. E., Cassinelli J. P., 1993, ApJ 409, 429
Bolton C. T., 1982, A preliminary report on simultaneous UV and optical observations of λ Eri, In: Be stars, Jaschek M., Groth H.-G. (eds.), IAU Coll. No. 98, p. 181, D. Reidel, Dordrecht
Briot D., 1981, A&A 103, 1
Brown A. G. A., Verschueren W., 1997, A&A 319, 811
Clarke D., 1990, A&A 227, 151
Curtiss R. H., 1916, Publications of Michigan Observatory 2, 1
Cuypers J., Balona L. A., Marang F., 1989, A&AS 81, 151
Dachs J., Lemmer U., 1991, Periodic and aperiodic components in photometric variations of active Be stars, In: Rapid variability of OB-Stars: Nature and diagnostic value, Baade D. (ed.), ESO Conf. and Workshop Proc. No. 36, p. 103, ESO, Garching
De Geus E. J., De Zeeuw P. T., Lub J., 1989, A&A 216, 44
Deeming T. J., 1975, A&AS 36, 137
Díaz-Cordovés J., Claret A., Giménez A., 1995, A&AS 110, 329
Doazan V., Selvelli P., Stalio R., Thomas R. N., 1980, $T_{\rm e}$-structure of the wind in γ Cas, In: Proc. Second European IUE Conf., Battrick B., Mort J. (eds.), ESA SP-157, p. 145
Dziembowski W. A., Moskalik P., Pamyatnykh A. A., 1993, MNRAS 265, 588
Eckart C., 1960, Hydrodynamics of Oceans and Atmospheres, Pergamon Press, London
ESO-MIDAS, 1995, User Guide, Vol. B: Data Reduction, ESO, Garching, p. 12-1
Fleming W. P., 1890, Astron. Nachr. 123, 383
Ghosh K. K., Kuppuswamy K., Pukalenthi S., Selvakumar G., 1991, Astron. J. 102, 1191
Gies D. R., 1994, Line profile variations in Be stars, In: Pulsation, Rotation, and Mass Loss in Early-type Stars, Balona L. A., Henrichs H. F., Le Contel J. M. (eds.), IAU Symp. No. 162, p. 89, Kluwer, Dordrecht

Gies D. R., Kullavanijaya A., 1988, ApJ 326, 813
Grady C. A., Bjorkman K. S., Snow T. P., 1987a, ApJ 320, 376
Grady C. A., Sonneborn G., Wu C.-C., Henrichs H. F., 1987b, ApJS 65, 673
Grebel E. K., Richtler T., de Boer K. S., 1992, A&A 254, L5
Guinan E. F., Hayes D. P., 1984, ApJ 287, L39
Gummersbach C. A., Kaufer A., Schäfer D. R., Szeifert T., Wolf B., 1998, A&A, in press
Hanuschik R. W., 1989, Ap&SS 161, 61
Hanuschik R. W., Dachs J., Baudzus M., Thimm G., 1993, A&A 274, 356
Hanuschik R. W., Hummel W., Sutorius E., Dietle O., Thimm G., 1996, A&AS 116, 309
Hanuschik R. W., Vrancken M., 1995, Inf. Bull. Variable Stars 4258, 1
Hanuschik R. W., Vrancken M., 1996, A&A 312, L17
Harmanec P., 1987, Inf. Bull. Variable Stars 3097
Hayes D. P., 1980, PASP 92, 661
Hayes D. P., Guinan E. F., 1984, ApJ 279, 721
Huang S. S., 1972, ApJ 171, 549
Hubeny I., Leitherer C., 1989, PASP 101, 114
Hubert A. M., Floquet M., 1998, A&A 335, 565
Hummel W., 1998, A&A 330, 243
Jaschek M., Groth H.-G. (eds.), 1982, Be stars, IAU Coll. No. 98, Dordrecht, D. Reidel
Kambe E., Ando H., Hirata R., 1993a, A&A 273, 435
Kambe E., Ando H., Hirata R., et al., 1993b, PASP 105, 1222
Kambe E., Hirata R., Ando H., et al., 1997, ApJ 481, 406
Kaufer A., 1998, Variable circumstellar structure of luminous hot stars: the impact of spectroscopic long-term campaigns, In: Rev. in Mod. Astron. No. 11, Schielicke E. (ed.), p. 177
Kaufer A., Stahl O., Wolf B., et al., 1996, A&A 305, 887
Kaufer A., Stahl O., Wolf B., et al., 1997, A&A 320, 273
Kaufer A., Szeifert T., Krenzin R., Baschek B., Wolf B., 1994, A&A 289, 740
Kjeldsen H., Baade D., 1994, Be stars in young LMC clusters, In: Pulsation, Rotation, and Mass Loss in Early-type Stars, Balona L. A., Henrichs H. F., Le Contel J. M. (eds.), IAU Symp. No. 162, p. 271, Kluwer, Dordrecht
Korn A., Wolf B., 1998, NLTE abundances from Magellanic Cloud B stars, Astronomische Gesellschaft Abstract Series No. 14, p. 121
Lamers H. J. G. L. M., Pauldrach A. W. A., 1991, A&A 244, L5
Lawson W. A., Clark M., Cottrell P. L., 1994, MNRAS 266, 740
Lee U., Saio H., 1987a, MNRAS 224, 513
Lee U., Saio H., 1987b, MNRAS 225, 643
Lee U., Saio H., 1990, ApJ 360, 590
Lee U., Saio H., 1997, ApJ 491, 839
Lomb N., 1978, MNRAS 185, 325
Mandel H., 1994, Fiber-linked echelle spectrographs, In: The Impact of Long-Term Monitoring on Variable Star Research, Sterken C., de Groot M. (eds.), NATO ASI Series C 436, p. 303, NATO ARW, Kluwer, Ghent
Marlborough J. M., 1997, A&A 317, L17
McDavid D., Gies D. R., 1988, Be Star Newsletter 19, 13
Osaki Y., 1986, PASP 98, 30
Oudmaijer R. D., Drew J. E., 1997, A&A 318, 198
Owocki S., Cranmer S., Gayley K., 1996, ApJ 472, L115
Pamyatnykh A., 1998, Pulsation instability domains in the upper main sequence, In: A Half Century of Stellar Pulsation Interpretations: A Tribute to Arthur N. Cox, Bradley P. A., Guzik J. A. (eds.), ASP Conf. Ser. No. 135, p. 268
Pavlovski K., Schneider H., 1989, A&A 228, 361
Perryman M. A. C., Høg E., Kovalevski J., Lindgren L., Turon C., 1997, The Hipparcos and Tycho Catalogues, ESA SP-1200
Peters G. J., 1979, ApJS 39, 175
Peters G. J., 1986, ApJ 301, L61
Peters G. J., 1988, ApJ 331, L33
Peters G. J., 1989, Be Star Newsletter 20, 10

Peters G. J., 1990, Be Star Newsletter 22, 19
Peters G. J., 1991, Rapid photospheric variability and circumstellar activity in Be stars, In: Rapid variability of OB-Stars: Nature and diagnostic value, Baade D. (ed.), ESO Conf. and Workshop Proc. No. 36, p. 171, ESO, Garching
Peters G. J., 1995, Observation of prominence or flare-like activity in the B2e star μ Centauri, In: Stellar surface structure, Poster proceedings, Strassmeier K. G. (ed.), IAU Symp. No. 176, p. 212, Vienna
Peters G. J., 1998, ApJ 502, L59
Quirrenbach A., Bjorkman K. S., Bjorkman J. E., et al., 1997, ApJ 479, 477
Rivinius Th., Baade D., Štefl S., et al., 1998a, A&A 333, 125
Rivinius Th., Baade D., Štefl S., et al., 1998b, A&A 336, 177
Rivinius Th., Baade D., Štefl S., et al., 1998c, Multiperiodic line-profile variability and a tentative ephemeris for line emission outbursts of the Be star μ Cen, In: A Half Century of Stellar Pulsation Interpretations: A Tribute to Arthur N. Cox, Bradley P. A., Guzik J. A. (eds.), ASP Conf. Ser. No. 135, p. 343
Rivinius Th., Baade D., Štefl S., et al., 1998d, Predicting the outbursts of the be star μ cen, In: Cyclical variability in stellar winds, Kaper L., Fullerton A. (eds.), ESO Conf. Ser., in press
Rivinius Th., Baade D., Štefl S., Stahl O., Wolf B., Kaufer A., 1997b, Multiperiodic line-profile variability and a tentative ephemeris for line emission outbursts of the Be star μ Cen, Astronomische Gesellschaft Abstract Series No. 13, p. 189
Rivinius Th., Baade D., Štefl S., Stahl O., Wolf B., Kaufer A., 1997a, Short- and medium term variability of emission lines in selected southern be stars, Astronomische Gesellschaft Abstract Series No. 13, p. 36
Rivinius Th., Stahl O., Wolf B., Kaufer A., Gaeng T., Gummersbach C. A., Jankovics I., Kovacs J., Mandel H., Peitz J., Szeifert T., Lamers H. J. G. L. M., 1997c, A&A 318, 819
Rivinius Th., Štefl S., Baade D., et al., 1997d, Be Star Newsletter 32, 14
Rivinius Th., Štefl S., Baade D., et al., 1998e, Be Star Newsletter 33, 15
Rivinius Th., Štefl S., Baade D., Stahl O., Wolf B., Kaufer A., 1998f, Short- and medium term variability of emission lines in selected southern be stars, In: IAU Colloq. 169: Variable and Non-spherical Stellar Winds in Luminous Hot Stars, in press
Scargle J. D., 1982, ApJ 263, 835
Schmutz W., Schweickhardt J., Stahl O., et al., 1997, A&A 328, 219
Schrijvers C., Telting J. H., Aerts C., Ruymaekers E., Henrichs H. F., 1997, A&AS 121, 343
Schwarzenberg-Czerny A., 1989, MNRAS 241, 153
Schwarzenberg-Czerny A., 1993, Analysis of astronomical time series, In: 5th ESO/ST-ECF Data Analysis Workshop, Grosbøl P. J., de Ruijsscher R. C. E. (eds.), ESO Conf. and Workshop Proc. No. 47, p. 149, ESO, Garching
Secchi A., 1867, Astron. Nachr. 68, 63
Slettebak A. (ed.), 1976, Be and shell stars, IAU Symp. No. 70, Dordrecht, D. Reidel
Slettebak A., 1982, ApJS 50, 55
Slettebak A., Snow T. P. (eds.), 1987, Physics of Be stars, IAU Coll. No. 92, Cambridge, Cambridge Univ. Press
Smith M. A., 1985, ApJ 297, 224
Smith M. A., 1989, ApJS 71, 357
Smith M. A., Peters G. J., Grady C. A., 1991, ApJ 367, 302
Sonneborn G., Grady C. A., Wu C.-C., et al., 1988, ApJ 325, 784
Soufi F., Goupil M. J., Dziembowski W. A., 1998, A&A 334, 911
Stahl O., Kaufer A., Wolf B., et al., 1995a, Be Star Newsletter 30, 12
Stahl O., Kaufer A., Wolf B., et al., 1995b, The Journal of Astronomical Data 1, 3, (on CD-ROM)
Stee P., de Araújo F. X., Vakili F., et al., 1995, A&A 300, 219
Štefl S., Aerts C., Balona L. A., 1998a, MNRAS, submitted
Štefl S., Baade D., Balona L. A., Harmanec P., 1995, A&A 294, 135
Štefl S., Baade D., Rivinius Th., et al., 1998b, Circumstellar quasi-periods accompanying stellar periods of Be stars, In: A Half Century of Stellar Pulsation Interpretations: A Tribute to Arthur N. Cox, Bradley P. A., Guzik J. A. (eds.), ASP Conf. Ser. No. 135, p. 348
Štefl S., Balona L. A., 1996, A&A 309, 787
Stellingwerf R. F., 1978, ApJ 224, 953
Sterken C., Jerzykiewicz M., Manfroid J., 1986, A&A 169, 166

Stumpf N., 1992, Spektroskopische Variationen der Be-Sterne κ Dra und θ CrB, Diploma thesis, Ruprecht-Karls-Universität, Heidelberg
Telting J., Schrijvers C., 1997, A&A 723, 579
Townsend R. H. D., 1997a, Non-Radial Pulsation in Early-Type Stars, Ph.D. thesis, University College London
Townsend R. H. D., 1997b, MNRAS 284, 839
Tubbesing S., 1998, Spektroskopische Variationen des Be-Sterns 28 Cygni, Diploma thesis, Ruprecht-Karls-Universität, Heidelberg
Underhill A., Doazan V., 1982, B Stars with and without Emission Lines, p. 279, CNRS/NASA Monogr. Ser. on Nontherm. Phen. in Stell. Atmosph., NASA-SP456
Vogt S. S., Penrod G. D., 1983, ApJ 275, 661
von Zeipel H., 1924, MNRAS 84, 665
Waelkens C., 1991, A&A 246, 453
Waelkens C., Aerts C., Kestens E., Grenon M., Eyer L., 1998, A&A 330, 215
Waters L. B. F. M., Marlborough J. M., 1994, The structue of the circumstellar material in Be stars, In: Pulsation, Rotation, and Mass Loss in Early-type Stars, Balona L. A., Henrichs H. F., Le Contel J. M. (eds.), IAU Symp. No. 162, p. 399, Kluwer, Dordrecht
Y O., 1998, Non-radially pulsating hot stars: Non-radial pulsations and be phenomenon, In: IAU Colloq. 169: Variable and Non-spherical Stellar Winds in Luminous Hot Stars, in press

Acknowledgements

My gratitude goes especially to Bernhard Wolf, Dietrich Baade, Stan Štefl, Otmar Stahl and Andreas Kaufer for all their willingness to join discussions, solve riddles, help up my mind, motivate me, listen to my dumb ideas, help me out of troubles ....
I am grateful to Director of the Landessternwarte, Immo Appenzeller, for all the possibilities at the institute, and also to the staff for not a single day existed, that I would not have liked to go there.
I wish to thank also Luis Balona and Petr Harmanec for their never-ending constructive and stimulating criticism of the time series analysis and the aliasing problem.
This work would not have been possible without Christoph Gummersbach, Thomas Dumm, Thomas Gäng, Josef Kovács, Istvan Jankovics, Holger Lehmann, Holger Mandel, Jochen Peitz, Dominik Schäfer, Werner Schmutz, and Jörg Schweickhardt who carried out part of observations with HEROS.
For their assistance to scrutinise the outburst prediction I thank Conny Aerts, Martin Kürster, and Michelle Thaller, who have taken additional spectra during their observing runs at other telescopes in 1997.
Definitively not at last I will remember all the warmth and collegiality I've encountered on the meetings I've been during my thesis work.
I am grateful to the Deutsche Forschungsgemeinschaft, the Astronomische Gesellschaft and the Czech Academy of Sciences, who have supported my position and my travels, the European Southern Observatory for the generous allocation of observing time, and the kind and open assistance by the ESO local staff at La Silla..
The final words of this thesis however are dedicated to my family and Jutta Schwartzkopff, for not letting astronomy overwhelm me!